Design and Control of a Knee Exoskeleton with Multiple Actuators

A Thesis

Submitted in Partially Fulfillment of the Requirements for the Award of Degree of

Doctor of Philosophy

in

Mechanical Engineering

Submitted by

Prakhar Jain

ROLL NO: 951708005

Under the Supervisions of

Dr. Tarun Kumar Bera
Professor
Mechanical Engineering Department
Thapar Institute of Engineering & Technology, Patiala

Dr. Ashish Singla
Associate Professor
Mechanical Engineering Department
Thapar Institute of Engineering & Technology, Patiala

Dr. Magnus Isaksson
Professor
Department of Electronics, Mathematics and Natural Sciences
University of Gävle, Gävle, Sweden

MECHANICAL ENGINEERING DEPARTMENT
THAPAR INSTITUTE OF ENGINEERING & TECHNOLOGY
PATIALA-147004, INDIA
March, 2025

This thesis is dedicated to

My Parents,

my wife, Siddhali, and

my sister, Prachi

DECLARATION

I hereby certify that:

a. The work presented in this thesis is original and has been conducted by me under the supervision of my advisor.

b. This work has not been submitted to any other institution for any degree or diploma.

c. The thesis has been prepared following the guidelines provided by the Institute.

d. I have adhered to the Institute's Ethical Code of Conduct in all aspects of this work.

e. Where material from external sources has been used—including data, theoretical analyses, figures, or text—appropriate credit has been given through citations within the thesis, with full details provided in the references. Additionally, permissions have been obtained from copyright holders where required.

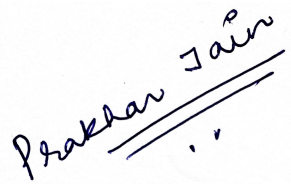

Prakhar Jain

CERTIFICATE

This is to certify that the thesis entitled, '**Design and Control of a Knee Exoskeleton with Multiple Actuators**', submitted by **Mr. Prakhar Jain** to the Thapar Institute of Engineering & Technology, Patiala, India, is a record of bona fide research work carried out under my supervision. The thesis is deemed worthy of consideration for the award of the degree of Doctor of Philosophy of the Institute.

Date: 07/03/25

Dr. Tarun Kumar Bera

Professor and Head

Mechanical Engineering Department

Thapar Institute of Engineering & Technology
(Deemed to be University),

Patiala, India, 147004

Email: tkbera@thapar.edu

Dr. Ashish Singla

Associate Professor

Mechanical Engineering Department

Thapar Institute of Engineering & Technology
(Deemed to be University),

Patiala, India, 147004

Email: ashish.singla@thapar.edu

Dr. Magnus Isaksson

Professor and Dean

Faculty of Health and Occupational Studies

University of Gävle, Gävle, Sweden

Email: magnus.isaksson@hig.se

ACKNOWLEDGEMENT

First and foremost, I would love to express my profound gratitude to **Dr. Tarun Kumar Bera** for his exceptional support and guidance throughout my PhD journey. His unwavering commitment, insightful feedback and patience have been crucial in shaping my research and fostering my academic growth. The journey has required patience, perseverance and resilience. Without his mentorship, this achievement would not have been possible. His guidance has been a constant source of light, helping to navigate the challenges and complexities of this work.

I am profoundly thankful to **Dr. Ashish Singla** for his invaluable contributions and constant encouragement. His belief in my work and his steady motivation have not only enriched this research but have also been a source of strength throughout the journey.

I would also like to express my heartfelt gratitude to my co-supervisor, **Dr. Magnus Isaksson**, Professor at the University of Gävle, Sweden. His trust in me, along with the resources and support he generously provided, made a world of difference in completing this work. His unwavering support has been truly exceptional.

A special note of gratitude goes to my mentor and dear friend, **Dr. Sajid Rafique**, Professor at the University of Gävle, Sweden. His unwavering support in our joint project has been a constant source of strength and motivation throughout this journey.

To my family, I owe a profound debt of gratitude for their enduring love and support. My **parents** have made countless sacrifices to ensure my success, and their belief in me has been a source of immense strength. Their unwavering support and dedication have been the bedrock of my achievements. This journey has been a testament to their sacrifices and the deep love they have shown. My sister, **Prachi**, has been a constant source of inspiration and encouragement. I am also grateful to my cousins, my extended family and my grandmother (**jiji**), whose love and encouragement have been deeply felt and greatly appreciated. My in-laws have shown immense understanding and support, and most of all, my wife, **Siddhali,** whose patience, love, and relentless encouragement have been crucial in overcoming the challenges of this journey. Her unwavering support has been the foundation of my success, and her belief in me has

transformed this challenging path into a shared journey of growth and achievement. I would also like to acknowledge the FIST project to Department of Mechanical Engineering, TIET dated December 20, 2021. FIST Project No.: SR/FST/ET-II/2019/504(C).

I am also deeply thankful for the companionship and support of my friends: **Bhrigu Lahkar**, **Kartik Sharma**, **Ankit Agarwal**, **Ankit Aggarwal**. Each has contributed to this journey in their own unique way. My childhood friends and lab mates **Himanshu**, **Avtar Singh** have been constant sources of camaraderie and encouragement.

I would like to express my sincere gratitude to Thapar Institute of Engineering & Technology, Patiala, and the University of Gävle, Sweden, for providing the essential resources and infrastructure for my research. A special thanks goes to the administrative staff, technical teams, and support personnel at both universities, whose assistance and dedication have been invaluable in enabling the successful completion of this work

Lastly, I am deeply appreciative of the doctoral committee members—**Dr. Tarun Kumar Bera**, **Dr. Ashish Singla**, **Dr. Anant Kumar Singh**, **Dr. Ashish Purohit**, and **Dr. Kulbir Singh**—for their valuable feedback and guidance throughout the evaluation and completion of this thesis. My gratitude also goes to the PhD coordinators, **Dr. Tarun Nanda** and **Dr. Anu Mittal**, for their support and guidance throughout the PhD programme.

Finally, I extend my heartfelt thanks to everyone who contributed, directly or indirectly, to the completion of this research. Your support has been invaluable, and I am truly grateful.

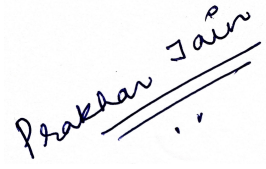

Prakhar Jain

ABSTRACT

This thesis presents the design, modelling and control of a knee exoskeleton aimed at assisting individuals with knee disorders during stand-to-sit-to-stand (STS) motions. The knee exoskeleton is developed by a four-bar mechanism actuated by a linear actuator and is controlled using electromyography (EMG) sensors to detect the user's muscle signals. The system is designed to provide the required knee joint torque and range of motion necessary for smooth transitions between standing and sitting postures. Through detailed simulations, it is demonstrated that the exoskeleton achieves the desired angle of thigh rotation and reduces user effort during STS motions.

A comparative study between linear and rotary actuators reveals that both can provide adequate assistance at the knee joint, with the rotary actuator delivering a higher torque output. This feature allows the exoskeleton to be powered by either or by the actuator depending on the user's needs. To address reliability concerns, the exoskeleton incorporates a fault-tolerant control system using a fault detection, isolation and reconfiguration (FDI) technique. This system enables the exoskeleton to continue functioning even if one of the actuators experiences a fault, ensuring user safety and continuous operation.

The design parameters of the knee exoskeleton are further optimized to enhance user comfort by maximizing the angle of thigh rotation during STS movements. The optimization is performed using the interior point method, implemented in MATLAB environment, to ensure optimal kinematic performance while maintaining mechanical feasibility. The bond graph technique is employed to model and simulate the system dynamics, offering an efficient framework for multi-domain system analysis and control.

Experimental validations confirm the effectiveness of the knee exoskeleton in reducing user effort during STS transitions. The exoskeleton provides up to 60% of the external assistance required, significantly easing the burden on the user. This work contributes to the advancement of knee exoskeletons by providing a robust, fault-tolerant design that can be used in rehabilitation settings or by individuals with mobility impairments. The results of this research pave the way for future developments in assistive devices designed to enhance mobility and independence for users with knee disorders.

Keywords: Knee exoskeleton, four-bar mechanism, linear actuator, rotary actuator, electromyography (EMG) control, stand-to-sit-to-stand (STS) motions, bond graph modelling, experimental validation, fault detection and isolation (FDI), interior point method, optimization.

LIST OF ABBREVIATIONS

ADC	Analog to Digital Converter
ARR	Analytical Redundancy Relation
BG	Bond Graph
CFD	Computational Fluid Dynamics
DC	Direct Current
DPDT	Double Pole Double Throw
EMG	Electromyography
FDI	Fault Detection and Isolation
FSM	Fault Signature Matrix
fmincon	MATLAB’s function for constrained nonlinear optimization
KAFO	Knee Ankle Foot Orthosis
KE	Knee Exoskeleton
MPU	Motion Processing Unit
PAM	Pneumatic Artificial Muscles
STS	Stand-Sit-Stand

NOMENCLATURE

$\alpha_1, \alpha_2, \alpha_3$	Angles of rotation for the thigh link during sit-to-stand transitions
ϕ_1, ϕ_2, ϕ_3	Angles used to calculate joint angles in the four-bar mechanism
ψ_1, ψ_2	Angles related to the orientation of links in the four-bar mechanism
$\theta_1, \theta_2, \theta_3$	Joint angles at different points in the mechanism (rotation of thigh or links)
θ_m	Motor angular position (rotation of the motor shaft)
θ_5	Angular position at the knee joint or link 5 in the four-bar mechanism
θ_n	General angular displacement at various joints, where n refers to the specific joint
C_e	Electrical capacitance in other system components
C_m	Capacitance in the motor's electrical circuit
d_1, d_2, d_3, d_4	Lengths of the four-bar mechanism links
d_5, d_6	Lengths of the knee exoskeleton frame links
d_9	Length of the linear actuator
F	Force generated by the actuator
G	Gravitational acceleration
i_m	Current flowing through the motor's armature circuit
J_G, J_L	Mass moments of inertia for the gear and lead screw, respectively
K_l, K_6	Stiffness constants for the lead screw and gear, respectively
K_p	Proportional constant
L	Load resistance
l_a	Inductance of the motor's electrical circuit
r_a	Armature resistance of the motor
S_e	Source of effort
T	Torque developed at the knee joint
V	Voltage input to the DC motor

W_{exo}	Weight of the knee exoskeleton
W_{ext}	External weight applied on the exoskeleton
X_1, X_2, X_3, ..., X_n	Linear positions or displacements of points in the mechanism

PUBLICATIONS FROM PRESENT WORK

[1] P. Jain, T.K. Bera, S. Rafique, A. Singla, M. Isaksson “Comparative study of knee joint torque estimations for linear and rotary actuators using bond graph approach for stand–sit–stand motions” International Journal of Advanced Robotic Systems, Sage Publishing House September 14, 2020 Accepted, Online October14, 2020, Vol. 17, No. 5, pp.1–13, 2020. IF-1.652, eISSN: 17298814 | ISSN: 17298814.

[2] P. Jain, T. K. Bera, A. Singla, M. Isaksson “Linear Actuator based Knee Exoskeleton for Stand to Sit Motions: A Bond Graph Approach” Simulation International, Sage Publishing House, Accepted on December 21, 2021, Online January 25, 2022, ISSN: 0037-5497. Vol. 98, No. 8, pp.627–644, 2022 IF-1.6

[3] P. Jain, H. Gupta, M. Bhupendra, Y. Dharmendra, V. Aditya, D. Kumar, and T.K. Bera “Design of Knee Exoskeleton using Electromyography Sensor” IEEE Xplore, pp. 1246–1251, 2019.

[4] P. Jain, T. K. Bera, A. Singla, S. Rafique, M. Isaksson “Fault Detection, Isolation and Reconfiguration of Four-Bar Mechanism based Knee Exoskeleton” Sensors, MDPI, Submitted on January 18, 2025, ISSN: 1424-8220 IF-3.4 (Under Review)

LIST OF FIGURES

LIST OF TABLES

TABLE OF CONTENTS

Chapter 1

Introduction

Knee-disorder-incidences are increasing day by day especially for ageing-population and musculoskeletal injuries. These conditions have a major severe life expression and reduce the capacity to perform basic daily tasks including walking, going upstairs, going up and down on seats. Technologies have advanced to overcome these difficulties; knee exoskeletons (KE) have become one of the promising approaches. Knee exoskeletons have been researched, developed and intended to enhance functional independence or reduce discomfort for people with knee pathology.

1.1 Knee Exoskeletons

Knee exoskeletons are complex wearable assistive devices aimed at improving the function of knee joints and assisting people with limited mobility. These devices afford the user both support and the ability to assist in the treatment and management of conditions to include physical therapy, athletic training and disease state.

1.1.1 Classification of Knee Exoskeletons

Based on the functionality, knee exoskeletons can be categorized in to passive, active and hybrid systems. A passive exoskeleton does not need electricity; it utilizes springs and/or levers for support. They are most useful where tasks are light to medium in nature and where the primary need is for inexpensive and easily transportable equipment. They are not so useful, however, where the demands are for dynamic support in activities greater than walking.[1] It has been shown that passive exoskeletons decrease metabolic energy expenditure of walking and increase stability in subjects with knee osteoarthritis.[2]

Dynamic exoskeletons equipped with motors or actuators provide force augmented, mechanical, support and produce torque to enable motion. These devices are designed with feedback control loops which change with the movements of the user in real time.[3] Experimental investigation of active knee exoskeletons has revealed that they aid to stand and walk with less effort for those with severe knee-disorders.[4]

Active exoskeletons are integrated with some properties of passive ones, since otherwise it would have been called an active one. These devices use passive components as the basic

supporting block, adding calculated functional requirements using active components and can be used in various fields.[5] A few studies have indicated that hybrid exoskeletons offer better support as well as flexibility over the skeletal frame – leading to increased comfort and usability.[6]

1.1.2 Advantages of Knee Exoskeletons

Knee exoskeletons offer numerous advantages, including improved mobility, stability and rehabilitation outcomes. These devices help users to perform tasks such as standing up from a seated position or climbing stairs, reducing strain on the knee joint and alleviating pain.[7] In rehabilitation settings, knee exoskeletons enhance the effectiveness of exercises, promoting faster recovery and improved functional outcomes.[8] Advances in control systems, such as the integration of electromyography (EMG) sensors, allow for precise control based on muscle signals, offering a more natural and intuitive experience.[9] Studies indicate that knee exoskeletons can reduce fatigue and increase endurance during rehabilitation activities.[10]

Technological advancements have played a significant role in improving knee exoskeletons. Innovations in actuator technology, control algorithms and materials have led to more effective and reliable devices.[11] For instance, the use of high-performance actuators has enabled exoskeletons to provide more precise and efficient support.[12] Sensor technology improvements have also enhanced the ability of exoskeletons to monitor and respond to user- movements accurately.[13]

1.1.3 Applications of Knee Exoskeletons

Knee exoskeletons have diverse applications. In rehabilitation, they support patients recovering from knee injuries or surgeries by assisting in performing therapeutic exercises.[14] Exoskeletons can also aid post-operative recovery by reducing strain on the knee joint, helping patients regain mobility and strength more quickly.[15]

Enhancement of mobility in knee exoskeletons allows individuals with chronic knee pathologies to perform basic tasks with less difficulty including walking, climbing stairs or getting from a sitting to standing position.[16] Such devices enhance the quality of the lives and extent the independency of a patient who has a condition such as osteoarthritis.[17]

Apart from rehabilitation and improving mobility, knee exoskeletons are employed in industries and military of different countries. They help the workers to perform some tough physical tasks whereby they save their knee moments, enhance the ergonomics and avoid incidences of injuries in industries among them.[18] Recently, knee exoskeletons increase soldiers' stamina in missions by assisting and partly supporting loads carried by the soldiers.[19]

1.2 Associated Developments for Design and Control of Knee Exoskeletons

The knee exoskeleton is currently developed with the aid of recent advancements in robotics, material science and control systems. More recent innovations in materials and manufacturing have brought increases in comfort and strength, largely from the use of carbon fibre composites in knee exoskeletons.[20] There is also a burden which is additional load to people, on mobility when they are carrying lightweight designs.

Advanced structure-design, such as joint adjustment and independent components, has also increased the adaptability of knee exoskeletons to the requirements of different users. The design enhancements make the devices more adaptable and efficient.[21] Actuation technologies have also been developed to the next level of sophistication. Specifically, linear actuators are a great fit for STS motions and deliver accurate direct motion. Rotary actuators that provide rotation, can provide more dynamic help during different types of knee joint movements.[22] These actuator-types could be integrated in a complementary manner to achieve optimal and efficient function of the exoskeleton while addressing the requirement that certain levels of support is to be delivered to the user during distinct phases of movement.

Actuation-control systems are the central element to achieve the needed kinetics and accuracy within knee exoskeletons. EMG sensors are used for real time feedback concerning muscle activity to adapt the assistance provided by the exoskeleton in real time. However, for the purpose of tracking movement and load in addition to EMG, inertial measurement units IMU's and force sensors are incorporated into the system to enhance the response rate.[23]

An understanding of fault detection and isolation techniques has enhanced the safety and reliability of knee exoskeletons. Diagnostic techniques check if actuators and other similar parts are in good working condition or not and if any change is likely to occur that will affect the performance of the component. Contingency strategies maintain the exoskeleton functional and

safe, even where a fault has been identified.[24] These safety measures enhance confidence and comfort to the users, and this makes a significant contribution toward the efficiency of the devices.

1.3 Background and Motivation

The increasing prevalence of knee-disorders has emphasised the need for assistive-technologies that can support individuals in performing daily activities. Conditions such as osteoarthritis and musculoskeletal injuries significantly impact mobility and quality of life. Performing stand-sit-stand (STS) motions which require substantial knee torque, is a common challenge for individuals with these conditions.[25]

Traditional mobility aids like wheelchairs and crutches to offer limited support. Wheelchairs provide mobility but do not assist in the specific biomechanical challenges of STS transitions.[26] Crutches, while useful for offloading weight, require significant upper body strength and fail to offer targeted knee joint support.[27] Lower-body exoskeletons have emerged as a potential solution, yet many focus on broader joint support rather than the specific needs of the knee and they can be bulky, complex and expensive.[28]

This research proposed knee exoskeleton to reduce these problems by installing electromyography (EMG) sensors and linear actuators to perform STS motions. EMG sensors offer the principle of highly selective control based on the activity of muscles, requiring individual assistance from the device. The required knee joint movement and support for STS transitions are provided by linear actuators.[29] This strategy aims at giving a better and workable solution for knee-disorders-patients to enhance their self-reliance and quality of living.

1.4 Contributions of the Thesis

This thesis contributes significantly to the design and control of knee exoskeletons, with the following key advancements:

A knee-exoskeleton comprising of linear actuator based on four-bar mechanism is designed and developed in this work. The proposed exoskeleton helps to provide accurate torque-support to STS motions and increases the effectiveness of such transitions.

Another feature of this knee-exoskeleton is the incorporation of the EMG sensor-based control system that enhances the effectiveness of the developed concepts. This process allows the

exoskeleton to adapt in real-time with muscle activity and improve the skill and efficiency of the aid delivered. The fabricated system is then characterized experimentally in which theoretical predictions are extensively compared with actual results to prove the efficiency of the device.

The thesis also formulates an FDI model, to accomplish the required reliability and safety of operation for the user. This model uses fault detection methods which help to enhance reliability and dependability of the exoskeleton under different environments.

Finally, the design parameters of the knee-exoskeleton are optimised using the interior point method. The optimisation process enhances the design to increase performance of the exoskeleton in supporting STS motions and to decrease user-effort.

1.5 Significance of the Present Work

The design and control of a knee exoskeleton with multiple actuators hold significant potential in addressing the challenges faced by individuals with knee joint disorders, particularly during sit-to-stand (STS) transitions. This work introduces a novel approach by incorporating a four-bar mechanism with both linear and rotary actuators, offering enhanced flexibility and reliability. The proposed exoskeleton not only reduces the effort required by the wearer but also provides a fault-tolerant system capable of detecting, isolating, and reconfiguring in case of actuator failure. By optimizing design parameters and validating through simulations, this research contributes to the development of assistive device that improve mobility particularly, STS motions for patients with knee impairments. The findings pave the way for future advancements, particularly for daily living activities.

1.6 Organisation of the Thesis

The structure of this thesis is designed to provide a comprehensive consideration of knee exoskeleton, from design to practical application. Chapter 1 introduces the subject of knee exoskeletons, detailing their classification, advantages and applications. It also discusses the background and motivation for the research, highlighting the limitations of current technologies and the specific contributions of this thesis. Chapter 2 presents a detailed literature review, examining existing studies and models relevant to knee exoskeletons. It identifies gaps in the current body of knowledge, laying the groundwork for the research presented in the following chapters. Chapter 3 focuses on the dynamic modelling of the proposed knee exoskeleton driven by

both linear and rotary actuators, providing detailed simulations of the device's performance based on mathematical models. Chapter 4 describes the experimental validation of the fabricated exoskeleton. It discusses the implementation of the EMG sensor-based control system and compares theoretical models with practical outcomes. Chapter 5 explores the development of a fault detection and isolation model for the knee exoskeleton, enhancing its reliability and safety. Chapter 6 applies suitable optimisation technique to the design of the exoskeleton, improving its performance in assisting STS motions. Finally, Chapter 7 summarises the findings of the research, discusses their implications and suggests future research directions.

Chapter 2
Literature Review

In this chapter, a comprehensive literature review is presented on knee exoskeletons, covering their design concerns, development, optimization and fault detection. This review is structured to methodically examine the progress made in exoskeleton-technology, relevant obstacles and the development of exoskeleton devices. A solid grasp of this fundamental knowledge is essential for assessing the following studies on enhancing the performance of knee exoskeletons and their real-world uses.

2.1 Early Developments of Exoskeletons

Exoskeletons are wearable mechanical devices specifically engineered to augment or bolster human physical skills. Exoskeleton-technology has gone through substantial development, resulting in a wide range of applications in industrial, military and medical domains.

The year 1960 marked the beginning of designing ground-breaking devices that could potentially be used to enhance human-strength using mechanical and electronic devices. These innovations lead to the origin of the exoskeleton-technology. The early innovation of mechanical devices was the Hardiman exoskeleton, developed in 1960 by General Electric. This device, however, was discontinued soon after its innovation as the hydraulic actuators used in the device to enhance lifting capabilities faced many difficulties such as limitations in weight and movement.[30]

A similar example was the inauguration of the Cybernetic Anthropomorphs Machine (CYBERNETIC) by the US Army in 1980's. This exoskeleton was specifically designed to augment the physical capabilities of soldiers by incorporating servo motors and electronic controllers. However, the device could not withstand its modular architecture leading to several challenges in relation to power consumption and system integration.[31]

In the 1990's too, the Exoskeleton Assistance Device (EAD) was introduced by Daewoo Heavy Industries. The planned purpose of this device was to assist workers in the construction and manufacturing sectors. This device was also discontinued as it faced obstacles pertaining to system integration and costing.[32] The development of the Hybrid Assistive Limb (HAL) by Cyberdyne

Inc., in the late 1990's was a promising achievement. It assisted rehabilitation and augmentative activities and enhanced user-mobility of those with neurological disorders, by integrating bioelectric signals.[33] In early 2000's, the Argo Medical Technologies developed ReWalk exoskeleton using advanced control algorithms to provide mobility-aid for persons suffering from spinal-cord injuries.[34]

2.2 Lower Limb Exoskeletons

Lower limb exoskeletons are used for the rehabilitation assistive living activities and for industrial and military purposes. They are specifically engineered to augment the functionality of the hips and legs.

2.2.1 Applications in Rehabilitation

For the patients who have spinal cord injuries or strokes, the application of the lower limb exoskeletons for rehabilitation purposes were proved to be quite effective. By means of mechanical assistance and promoting proper gait, lower limb exoskeletons thus increase locomotion and consequently, recovery. Another study confirmed that the robotic reinforced rehabilitation was more effective than the traditional methodologies.[35,36] The function of these devices depends on factors including offered support, adaptability to different users and immediate feedback techniques. A novel human-cooperative methodology based on the trajectory control technique for examining the subject related to paediatric gait rehabilitation was presented by Narayan et. al.[37.]

2.2.2 Industrial and Military Applications

To minimize physical injuries and exertions for the lower limbs, exoskeletons are usually used in the industries and in the military. They reduce the likelihood of developing musculoskeletal complaints which include providing support and assistance in lifting burdens and other duties. An example of this would be the exoskeletons used in warehouse settings to decrease the risk of back injuries and to increase productivity. A systematic review and development of such devices being undertaken are being presented by Kalita et. al.[38]

2.3 Knee Exoskeletons

Knee exoskeletons are wearable technologies targeted at the knee joint with the aim of augmenting, rebuilding as well as improving the joint. Some of the reasons for the development of knee exoskeletons include the necessity to come up with an inexpensive means of supporting some knee issues and the dynamic progress in the material science.

2.3.1 Historical Development of Knee Exoskeletons

Knee exoskeletons have been designed to address joint issues for instance osteoarthritis thereby, assisting the knee joint to mitigate pain and enhance mobility.[39] The emergence of knee exoskeletons has been stimulated by two primary drives *i.e.* the availability of cheap assistive technologies and materials science. The initial designs of knee exoskeletons were complex in structure and rather expensive to manufacture. Technological innovations, changes in the choice of the materials used and innovations in the manufacturing process have led to production of effective devices at low costs.[40] The development in material has involved the use of carbon fibres and improved polymers that directed to lighter and stronger exoskeletons that improve comfort and performance.[41,42] There are electrical motors, pneumatic operated actuators and embedded control system as modern manufacturing technologies to support the manufacturing process with high level of precision.[43]

2.3.2 Design Considerations

The engineering of an efficient knee exoskeleton depends on the consideration of many factors. Some of these are biomechanical alignment, control systems, decision on materials, durability and actuation systems. The kinetic and kinematic relations between segments of tibia and femur are decisive for the correct functioning of knee exoskeleton and thus, any discomfort or inefficiency in movements (strained or distorted position, put off stump) influences directly the biomechanical interface and consequently, the overall efficiency of the system.[44]

Systems like electric motor as well as pneumatic actuators are useful in driving the systems. Thus, all types of actuators have the following benefits; pneumatic actuators give better smoothness and responsiveness; bio inspired actuators give extra flexibility.[45] Conducting control systems help in regulating the uses made of the exoskeleton since users are likely to struggle in

adhering to the set timetable. Intelligent control methods and machine learning algorithms are applied in knee exoskeletons where the efficiency is improved with relative simplicity. RISE-based adaptive control system for the EICoSI exoskeleton, aims at assisting knee joint mobility.[46] Another work introduces a control strategy that enhances the functionality of knee rehabilitation exoskeletons.[47] In another work, design and simulation of a leg exoskeleton linkage aims at enhancing human rehabilitation systems.[48] Exoskeleton designed for ankle support is designed especially for rehabilitation.[49]

2.3.3 Applications of Knee Exoskeletons

KE are used in rehabilitation applications, as an aid in normal walking as well as in factory and warfare applications. They help to enhance the local transport and reduce scars and pressures in relation to the rehabilitation processes. They assist in facilitating the users' mobility and promote the natural gait patterns among the users. People who suffer knee injuries, osteoarthritis or neurological disorders get benefited from this device. Next generation models of exoskeleton, including ReWalk, Indego, have opened enhancements in rehabilitation for patients with spinal cord injuries; these improve the efficiency and specificity of the procedures for the users. The use of exoskeletons in rehabilitation can significantly improve the functional recovery of patients by facilitating motor learning and muscle re-education.

Knee exoskeletons aids patients with mobility problems in performing daily life physical activities. These devices assist in everyday tasks such as ascending stairs and shifting from seated to standing posture, beyond facilitating ambulation. The ReWalk exoskeleton significantly improved the quality of life of patients with spinal cord injuries by enabling them to walk.[50] The Indego exoskeleton enhanced the locomotor capabilities of persons with lower limb disabilities and enabled them to perform several vital activities including walking and standing exercises.[51]

Knee exoskeletons reduce physical stress in industrial and military applications and thus, enhance the efficiency of the performance. In the industrial context, EksoVest type of exoskeleton is designed to adequately remedy the challenging working environment by supporting workers in production lines and reducing the stress on the upper body thus, increasing efficiency.[52]

2.3.4 EMG-based Control using Arduino

Electromyography (EMG)-based control systems are incorporated in the knee exoskeletons and add to the knee exoskeletons' performance and usability. To offer an immediate and natural touch to the exoskeleton attachment, the current control strategy hugely relies on the signals generated by muscle contractions. EMG control systems utilize electrodes to detect contraction of muscles and this is translated to signals by the exoskeleton to get optimal movements. This allows for a rapid and adaptable control of the device in synchronising its support to the muscular exertion of the user. Arduino platform is considered one of the most suitable choices for developing such systems considering flexibility, ease of integration and affordability.[53, 54]

There is a gain in functionality of knee exoskeletons when electromyography (EMG)-based control is incorporated. It is possible to have more precise and dynamic corrections that can be made based upon the signals generated by the user's body. This flexibility is particularly fruitful in situations related to rehabilitation since such an approach that is tailored to the requirements of the client is often capable of yielding better effects.[55]

Universally, the control approaches that depend on the EMG signals are preferred to the conventional control approaches that rely on a set of implemented algorithms or external sensors because the former enhances the functionality and comfort of the knee exoskeletons.[56] Certain difficulties that was previously embedded in prior control strategies like the inability to adapt to the changing circumstances of the users and the constant need for fine tuning is addressed with the use of EMG based controls. Having EMG-based systems, the user satisfaction using knee exoskeletons is improved through the provision of immediate response and its dynamism.[57] This development presents the advancement in the knee exoskeleton technology showing a need to incorporate advanced control mechanisms that would enhance the usability of the device.

2.4 Optimising Design Parameters of the Knee Exoskeleton

Further enhancements in the design and control of exoskeletons for the knee joint is crucial as it will enhance the efficiency in the technology that offers therapeutic value. Optimization is vital to decide on the appropriate strategy that will lead to the right design in compliance with the many constraints to achieve certain performance. The present literature review focuses on the number of optimization techniques adopted in the development of knee exoskeletons. The literature evaluates how exactly Interior Point Method (IPM) combined with other methods helps to overcome multiple issues linked to knee exoskeletons.

2.4.1 Optimization Techniques in Mechanical Design

The field of mechanical design optimization is made up of several strategies including clear methods, constructive methods and meta-constructive models. Thus, each category accommodates certain merits depending on the basic structure of the problem, as well as its degree of complexity encountered at certain given stage.

(a) Exact Methods

Interior Point Method (IPM)

The Interior Point Method was first described by Karmarkar in the year 1984. It was found that IPM indeed forms a methodology for solving both linear and non-linear programming. The IPM works for an optimal solution within the feasible zone by using barrier functions to counter the limitations. The robustness and efficiency of IPM in handling complicated constraints were emphasized.[58] In case of knee exoskeletons, the use of IPM becomes crucial for its ability to effectively manage non-linear limitations. IPM was utilised to optimize the configurations of robotic limbs, showing its usefulness in solving complex design problems.[59]

Sequential Quadratic Programming (SQP)

SQP is an accurate method used to solve non-linear optimization problems through the solution of quadratic approximations. It is highly efficient in most cases especially applied on smooth continuous functions in complex situations. In the research conducted in 2020 explained the use of SQP in robotic systems to carry out optimisation in the control of smooth constraints. Nonetheless, it was noticed that IPM often outperformed SQP regarding solving complex and or non-linear constraints because of the better robustness and performance of the method in large-scale problems.[60]

(b) Heuristic Methods

Generative Algorithms (GAs)

The genetic algorithm when propose drew inspiration from natural selection, is valuable for investigating extensive design areas. Like other evolutionary algorithms, genetic algorithm solution development uses operators e.g. selection, crossover and mutation.[61] Genetic algorithms have the flexibility of enhancing the settings of knee exoskeletons. There are some drawbacks

when using GAs in general, mainly because while GAs are good at searching for numerous solutions, they may not necessarily guarantee optimality; something that is important in precision optimization problems, as seen in the design of knee exoskeleton. The efficacy of GAs even more discovered the strength and weakness highlighted to these problems as well.[62.63]

Particle Swarm Optimisation (PSO) algorithm

Particle Swarm Optimization is an algorithm methodology based on the social behaviour that is used in solving optimization problems. For example, PSO application in dynamic optimisation situations is described when solving various robotic engineering problems.[64] In view of this, the PSO algorithm possesses the ability to balance exploration and exploitation making it suitable for dynamic environments. However, it could be problematic when pushed to apply its ingenuity in the complex and diverse constraints that are part of knee exoskeleton systems.

(c) Metaheuristic Methods

Simulated Annealing (SA)

Specifically, the simulated annealing method derived from the metallurgical annealing process probabilistically explores the solutions to avoid trapping in local optima. Another work utilised the Support Vector Machines (SA) in enhancing mechanical parameters in exoskeleton and proving its performance in solving problems with multiple local optima.[65] While it is true that SA is favourable to prevent entrapment in local optima, the direct consideration of complicated constraints by IPM makes the latter more beneficial for the proper tuning of parameters of knee exoskeletons.

Algorithmic Colony Optimization (ACO)

An ant colony optimization model simulates the foraging behaviour of ants to address combinatorial objectives. Another work explored the use of Ant Colony Optimization (ACO) to robotic arm configurations, emphasizing its capacity to address intricate design challenges.[66] The primary advantage of ACO is in its ability to address combinatorial issues. However, when dealing with the continuous and nonlinear aspects of knee exoskeleton optimization, the interior point approach is typically more appropriate. Foundational work on ACO and its applications was provided by Goldberg.[67]

Evolutionary Differentiation (DE)

In the realm of optimization issues, Differential Evolution (DE) has proven to be a highly efficient technique for refining solutions by means of differential vectors. In another work, the study emphasized the efficacy of DE in addressing real-valued problems, particularly in the context of parameter optimisation.[68] However, DE may not consistently manage intricate restrictions as effectively as IPM.

ANNs (Artificial Neural Networks)

In the field of robotic systems optimization, Artificial Neural Networks (ANNs) have been employed to effectively represent intricate and nonlinear interactions. The study investigated artificial neural networks (ANNs) to forecast design parameters and offer informative insights. Although Artificial Neural Networks (ANNs) can provide predictive skills and insights, Integrated Product Management (IPM) is still the preferred approach for directly managing the optimization of design constraints and objectives. Another work established fundamental understanding of neural networks and their use in optimization approaches.[69]

2.4.2 Interior Point Method (IPM): Key Advantages over Alternative Optimization Methods

The Interior Point Method (IPM) is favourable in optimizing knee exoskeleton design. Naturally, there are numerous advantages of using IPM; one of the most important is a high capacity to address complex limitations. As for the kinematic parameter aspect in computational design of knee exoskeletons, strong nonlinear constraints are usually postulated, it is difficult to handle compared with other designs. One of the studies underscore that IPM applies an incredible ability to successfully solve these nonlinear limitations, concluding that the AP complies with all the designed criteria for the optimization algorithm. Correct and reliable design result remains a primary goal in a discipline where constraints are not only arithmetic but involve complex interrelations between individual design elements.[70]

Moreover, the use of IPM demonstrates outstanding results when addressing extensive issue which is given that knee exoskeleton minimization is affected by multiple design factors. Later, in a research work[71], it was shown how the best implementation of the IPM yields optimum solutions for large numbers optimization problems with the best possible quality within the conceivable time

span. The significance of this efficiency is found in the ability to avoid infeasible computational delays that may be encountered when using other approaches which make IPM a practical solution for complex design problems involving multiple variables.

Probabilistic capability of IPM in avoiding local optima is also a very important advantage of the algorithm. Hence, it is challenging to find the global peak with several distinct local optima as the characteristic feature of the optimization environment of knee exoskeleton design. Another work stresses on the fact that IPM possess a strong algorithmic foundation that ensures avoidance of local optima and movements towards the global optimum. It is necessary that this capability is present to ensure that the design achieves the global optimum and not subpar local optimums.[72]

Also, continuity of IPM is another advantage that comes out as follows: Since it can directly respond to impractical and virtually unlimited issues, it develops into a versatile approach for various design cases. The advantage of this approach is the fact that it provides sufficient spectrum of flexibility whereby optimization process may eventually work through difficult design constraints and offer utilization solutions even where the formal methodologies may hit a snag. It is therefore beneficial where constraints could be complex to manage particularly in complex designs. Consequently, the Interior Point Method is characterized by its capability to deal with complex constraints, problem solving capabilities of large-scale problem, non-incurrence to the problem of local optima and universality. The synergy of all these advantages offer rationale for pursuing the application of this approach in the context of the design parameters in knee exoskeleton to effectively and efficiently tackle the multifaceted issue on the optimisation of design.

Nevertheless, it is possible to point out imperfections of the current state of knowledge about optimization strategies for knee exoskeletons. One serious area of weakness is in the failure to incorporate some of the optimization techniques to harness their strengths. Combining of the IPM in heuristic or metaheuristic structures in the hybrid modelling have sense to increase the performance when the global search ability is going to be controlled with local optimization.[73] The study suggested that use of hybrid optimization techniques could improve the solutions and computational cost.

Furthermore, many of this research focuses on simulation-based optimization without adequate real world empirical testing. To fill this gap, it is important to carry out a practical validation of optimized designs as far as their usability is concerned. The fine-tuning of optimization algorithms and the verification of their applicability are closely connected with the integration of the real-world testing and user feedback. Therefore, in the present work, the selection of the interior point approach for optimization is done due to its ability to deal with complex constraints, solve problems of large scale and to avoid local optima.

2.4.3 Applied Optimization Techniques and Comparative Insights

(a) Optimization of a Four-Bar Mechanism

Bianchi et. al. applied the genetic algorithms (GAs) to the optimal design parameters of the knee exoskeleton and its four-bar mechanism.[74] This agrees with the results of the study that Genetic Algorithms (GAs) are effective in handling performance as well as design constraints at the same time. Genetic algorithm (GAs) based on natural selections have also proved themselves capable of exploring large area of design space and can find solutions that can adapt to different performance criterion. However, the study also revealed limitations in achieving optimality compared with other more accurate methods, including the Interior Point Method (IPM). This basic randomness in Genetic Algorithms (GAs) has the capability to fail in reaching the expected global optimum consistently. This makes a major drawback for matters that require accurate solutions.

(b) Application of Particle Swarm Optimization

The work done by Zhang et. al. proved the efficiency of PSO applied to the kinematic parameters of the robotic systems in dynamic optimization.[75] One of the benefits of the PSO method that mimics a social system to solve optimization problems was realised in the freedom offered in probing the design space as well as in the ability to adapt to changes in key parameters. Finally, the research focused on the ability of PSO in dealing with complex and dynamic environments and gave good indications toward optimisation. However, while admitting that PSO is useful to maintain flexibility between exploration and exploitation, the focus of the work is on how the IPM allows for the direct control of complex constraints. Due to the deterministic nature, IPM can

approach a design problem systematically and it is most appropriate where accuracy of the optimization task is of paramount importance in the design of knee exoskeleton.

(c) Use of Simulated Annealing for Mechanical Parameter Optimization

In a current study by Bianchi et al. (2018), they used SA in determining optimal mechanical performance factors in knee exoskeletons.[76] Thus, like special kind of metallurgical process called 'annealing', simulated annealing method also provides flexibility and robustness for the search of global optima. This is advantageous in complex optimization problems since this approach searches the solution space probabilistically to avoid being trapped by the local optima. However, the research suggests that there is a lot of advantages offered by Interactive Product Modelling (IPM) as it deals with complex constraint design difficulties. For this reason, the capability of IPM in handling non-linear constraining and yielding of high accurate solution reiterate the strength of the method when precise managing of constraints is crucial.

Hence, the above-discussed case studies depict results of various optimization techniques like genetic algorithms, particle swarm optimization, simulated annealing in various scenarios. Each of the four methods has its own benefits, however, the extraordinary capacity of IPM to recognize complex limitations and secure the perfect solution makes it perfect for the stringent and precise optimization called for in the design of the knee exoskeleton.

2.5 Fault Detection and Isolation (FDI)

FDI is crucial for rapid detection and identification of faults in different complicated systems and sub-systems like knee exoskeleton and it is used to make the system reliable and safe. The next section analyze the method and challenge associated with FDI, particularly for the application of knee exoskeleton with the help of bond graph theory.

2.5.1 Overview of Fault Detection and Isolation

The FDI methods are generally divided into two groups which are the model-based and data-based approaches. In model-based approach, the usual behaviour of the system is predicted by using mathematical models of the system and the detecting of defects are done while in data driven approach, statistical models and machine learning techniques are used to detect defects using the

data available in real-time basis. Combined with the approaches of the methodologies themselves, they take advantage of to provide deeper defect detection. A particular work, stress upon the advantages and limitations of these schemes, close attention to the exact models and the flexibility of the data-driven methods for adapting to change.[77]

2.5.2 Model-Based FDI Methods

The mathematical model-based finite difference in performance approaches rely on expected and actual performance models. The residuals that are a measure of the deviation between observed and predicted values are useful to find defect identification. Residual analysis and observer-based methods are employed to identify anomalies. These approaches have proven efficient in knee exoskeletons because of their capability of addressing complex interactions between the system parts. Another work has shown that the residues and observers help to detect deviations in mechanical and control systems.[78,79]

2.5.3 Data-Driven FDI Methods

Among the Data driven FDI approaches, it is apparent that defects are diagnosed without the specification of an analytical system model. In these methodologies, there are usually statistical measures and application of machine learning algorithms. Acquisition of knowledge of patterns in the data is done by machine learning, complemented with statistical values and the major goal is to identify the existence of a defect through analysis of past data.[80] Although both approaches offer great benefits in terms of flexibility and adaptability, their accuracy comes as the result of large datasets.

2.5.4 Hybrid FDI Approaches

Hybrid techniques of FDI combine model-based and data-driven methods for the increased accuracy of failure identification. Use of composite solutions, through incorporation of different approaches provide a more robust solution in dealing with the specific measures considered as constraints by separate solutions. The study conducted by Chen et al. shows that there is increase in fidelity of fault diagnosis skills when model-based predictions are cascaded with real-time data analytics.[81]

2.5.5 FDI in Knee Exoskeletons

It is necessary to have fully differentiated input to ensure that the knee exoskeletons are dependable and safe. These systems involve many interlinked components presenting unique challenges given their astonishing complexity. Another work examined FDI approaches applied to exoskeleton systems, focusing on the importance of accurate and efficient identification of faults to promote user's safe interaction with the device and to enhance the exoskeleton performance.[82]

Residual analysis and observer-based approaches are model-based approach which is used for the diagnosis of problems in mechanical and control systems. The effectiveness of these methods helps to diagnose the defects in the electric actuators and sensors that are used in the automotive manufacturing systems. Analyzing real-time data through other advanced IT methods including machine learning enhances defective part identification. In other work, Hwang et al. discussed the application of machine learning techniques with reference to fault detection in knee exoskeletons.[83]

2.5.6 FDI using Bond Graph Theory

One of the theories that have been postulated in modelling systems is the bond graph theory developed.[84] This approach is the graphical model used to represent the system parts and their connections so that energy flow may be evaluated. Techniques like causal bond graphs as well as bond graph residuals are used in enhancing the process of defect diagnosis. Therefore, it is seen that the bond graph theory is useful for the functional fault identification and isolation.

It is worth pointing out that techniques applied to describe these phenomena include the use of bond graph theory for modelling and analysis of interactions between the mechanical, electrical and hydraulic systems in the control of knee exoskeletons. A bond graph model aids the engineers in presenting the flow of energy in a system and in assessing the abnormalities which may indicate issues. By the incorporation of ARRs and FSM in this architecture, it is easy to identify and isolate the faults. This work shows how bond graph technique can facilitate improvements to the existing FDI to improve diagnostic skills for defects.[85,86] A detailed case study demonstrates the application of bond graph theory for FDI in a real-world scenario. This case study provides a robust example

of how bond graph modelling can be applied to detect and isolate faults in complex systems, offering valuable insights into its applicability for exoskeleton systems.[87]

2.5.7 Application to Current Work

This work extends the application of FDI for knee exoskeletons for the first time by integrating bond graph theory with modern fault detection approaches. The main goal is to ensure the primary and redundant actuators of a knee exoskeleton perform at their best during STS movements. This study involves applying Analytical Redundancy Relations (ARRs) as a way of arriving at residuals which are tracked with a view of detecting the defects. The coherence vector method is used to identify abnormal behaviour or trends from normal patterns while the fault signature matrix is used for the purpose of fault identification.

In practical applications or when there is a failure such as a fault in the rotary motor, the system is designed to ensure that the standby actuators can adequately deliver the necessary torque and reach the desired angle of rotation for the sit to stand (STS) motion. A fault simulation is made by disconnecting the power supply of the rotary actuator and examining the residuals to check the capacity of the backup actuators to perform the function. The bond graph model, when used in conjunction with ARRs and FSM, helps to establish a robust structure to isolate, categorise and re-allocate any fault and ensure the dependable performance and safety of the exoskeleton for the user. The aim of this study is to apply these methods in the enhancement of the dependability and efficiency of knee exoskeletons. This will assist in preventing or at least neutralizing any imperfections and will ensure that there is maximum performance during the critical movements.

2.6 Bond Graph Modelling

Bond graph modelling is an enhanced form of analytical tool used for visualising as well as studying complex systems through defining energy couplings of its constituents. Such methodology provides a sound and integrated approach to depict multiple physical realities which include mechanical, electrical, hydraulic and thermal systems using the same graphical notation. The advantage of this approach is mainly realized in its efficiency in simplifying the representation of interactions and energy exchange in each system.[88] Bond graph modelling employs a few simple basic elements to represent some components as well as their interconnections in a system. The

elements encompass capacitors, inductors, resistors and sources, each characteristic of unique forms of energy storage or dissipation.

• Capacitors (C): These components act as a storage systems of energy in for instance the spring systems or the elastic assets. The ability of their compliance to store potential energy depending on the voltage and the current produced.

• Inductors (I) are elements that mimic the storage components like mass or inertial components and thus, helping to show that kinetic energy can be stored. They can be characterized by their fixed shunt and the relationships between electricity and voltage.

• Resistances (R) is a symbol for the resistive components which depict energy losses due to resistance in the form of heat owing to electrical resistance. These are distinguished by their electric resistances as well as the dissipation of powers.

Inputs or energy inputs coming from outside the system are known as source (S). Sources are classified into two categories: In the first category or effort sources, it may be voltage sources in electrical systems or force sources in mechanical systems while in the second category or flow sources, there may be current sources in electrical systems or velocity sources in mechanical systems.

2.6.1 Bond Graph Elements and Causality

The components of bond graph are used to model the energy aspects and the interconnection among the elements of a particular system. The element of most importance in the construction of bond graph models is the completeness as well as correctness in the determination of input-output links which is referred to as causality. Consequently, it ensures that the model represents the physical behaviour of a system and retains the accuracy of the model's predictions, when attributing causality can be done with very high precision.[89]

In bond graph, causality defines the direction of energy flow as well as the relationship between input and output of the system. For example, in a capacitor case, causality is the interaction between output voltage and input current while in inductor case, it is the connection between output current and input voltage. It is essential to accurately identify the causality for the assignment so that there is no misrepresentation of the real system in recreating with the help of the model and ensure that the subsequent solution mimics the real-life performances of the

system.[90] BG modelling technique have been proven to predict remaining useful life in addition to fault diagnosis.[91,92]

2.6.2 Application of BG to Knee Exoskeletons

In the area of knee exoskeletons, bond graph modelling is extremely useful since it allows the understanding and modelling of complex relationships between multiple components consisting of actuators-sensors and the mechanical elements. It is possible to develop a detailed model of the dynamic characteristic of the knee exoskeleton and its possible behaviour during various operation modes using bond graph approach. By applying bond graph modelling in the design of knee exoskeleton, it is possible to analyse the system behaviour and the effects of the faults. Thus, it helps in defining the critical elements of the design and their interactions and hence, in providing necessary provisions for the improvement of the design such that effective FDI schemes can be developed.

Thus, it can be stated that bond graph modelling has a great potential and is suitable for elucidation of complex systems. Due to the accuracy in expressing energy exchanges and dependency, it is a critical tool in enhancing the capacity of a system, as well as the reliability of design and control strategies in the development of knee exoskeletons.

2.7 Observations from Literature Review

The analysis of existing research on knee exoskeletons revealed many significant deficiencies and difficulties that directed the goals of the current study. The knee joint plays a vital role in everyday movements such as stand-sit-stand (STS) motions and is significantly susceptible to injuries because of its intricate structure and the strain it experiences. Despite the occurrence of knee-related mobility problems among individuals, current remedies such as knee-ankle-foot orthoses (KAFOs), wheelchairs and crutches have not completely reinstated natural movement or offered absolute autonomy.

Contemporary lower-body exoskeletons have demonstrated potential, especially in the field of gait rehabilitation, by providing more controlled and efficient training in comparison to conventional physical therapy. Nevertheless, obstacles like as the weight of the devices, intricate designs, challenging user interfaces and restricted battery life persistently impede their extensive adoption.

One notable gap recognised in the existing body of research is the absence of adaptable and energy-efficient knee exoskeletons capable of accommodating diverse users. In addition, although previous studies have investigated different actuators and mechanisms, there is a scarcity of research that compares the performance of linear and rotational actuators in knee exoskeletons, particularly in terms of their capacity to deliver the required assistive torque during STS movements.

One further area is the absence of consideration of bond graph (BG) modelling approaches in knee exoskeletons' analysis. Despite the advantages of BG modelling that is mostly connected with its ability to depict complicated systems and meet the requirements of FDI its use in this context is still rather limited.

Based on these observations, the aim of the present work is to design and develop a KE with multiple actuators. The KE is operated using both linear and rotary actuators based on the four-bar mechanism with FDI system. This design also seeks to optimize the exoskeleton mainly in performance and reliability to support the individuals regardless of the failed actuator. To fill the gaps and to improve the utility of knee exoskeleton for mobility-impaired individuals, this work attempts to incorporate BG modelling with FDI technique.

2.8 Critical Analysis of Existing Exoskeletons

While numerous studies have explored the design and control of knee exoskeletons, a critical analysis reveals significant limitations in their applicability to sit-to-stand (STS) transitions. For instance, conventional exoskeletons often fail to address the asymmetry in knee torques between paretic and non-paretic limbs, a key challenge for hemiparetic patients.[93] Additionally, many designs rely on single-actuator systems, which lack redundancy and fault tolerance, posing risks in real-world applications.[94] These limitations highlight the need for a more robust and adaptive exoskeleton design.

2.8.1 EMG-Controlled Systems

Electromyography (EMG)-controlled exoskeletons have been proposed for adaptive motion assistance. However, existing systems often lack integration with mechanical frameworks like the four-bar mechanism, which is crucial for achieving a wide range of motion during STS transitions.[95] Furthermore, the literature lacks detailed studies on the real-time responsiveness of

EMG signals in dynamic environments, raising questions about their reliability in practical applications. This gap underscores the importance of developing an EMG-controlled system that is both mechanically and computationally robust.

2.8.2 Comparative Analysis of Actuator Systems

Linear and rotary actuators have been widely used in exoskeleton designs, but their performance in STS transitions has not been thoroughly compared. Linear actuators, while compact and self-locking, often struggle to provide sufficient torque for heavier users. In contrast, rotary actuators offer higher torque at lower speeds but may introduce mechanical complexity. A critical evaluation of these trade-offs is essential to determine the optimal actuator configuration for knee exoskeleton

2.8.3 Fault Detection and Isolation (FDI) in Exoskeletons

The literature reveals a significant gap in fault-tolerant systems for exoskeletons. While bond graph modelling has been used for FDI in other domains, its application in exoskeletons remains underexplored.[96] Existing systems often lack the ability to detect and isolate faults in real-time, which is critical for ensuring user safety and system reliability. This gap highlights the need for a robust FDI framework that can seamlessly switch between primary and backup actuators in case of failure.

The identified gaps in the literature directly inform the objectives of this research. For instance, the lack of fault-tolerant systems motivates the development of a dual-actuator exoskeleton with an FDI framework. Similarly, the absence of EMG-controlled four-bar mechanisms underscores the need for an integrated design that combines mechanical robustness with adaptive control. By addressing these gaps, this research aims to advance the state-of-the-art in knee exoskeleton design and control.

2.9 Challenges of Existing Exoskeletons

The following subsections critically examine the challenges and limitations of existing knee exoskeleton systems, focusing on their design, control, and practical applicability. These challenges highlight the need for the solutions that address the shortcomings of current technologies, particularly in the context of sit-to-stand (STS) transitions and fault tolerance. By identifying these gaps, the aim to overcome these limitations and enhance user experience.

2.9.1 Limitation of Existing Exoskeletons

Conventional exoskeletons often fail to provide balanced support for hemiparetic patients during sit-to-stand (STS) transitions, and single-actuator systems lack redundancy, posing risks in real-world applications. These limitations underscore the need for a more robust and adaptive exoskeleton design.

2.9.2 Gaps in EMG-Controlled Systems

Existing systems often lack real-time responsiveness in dynamic environments, raising concerns about their reliability. This gap emphasizes the importance of developing an EMG-controlled system that is both mechanically and computationally robust.

2.9.3 Comparative Analysis of Actuator Systems

An evaluation of linear and rotary actuators has been included to compare their performance in STS transitions. While linear actuators are compact and self-locking, they often struggle to provide sufficient torque for heavier users. In contrast, rotary actuators offer higher torque but may introduce mechanical complexity. This analysis is essential for determining the optimal actuator configuration for knee exoskeletons.

2.9.4 Fault Detection and Isolation (FDI) in Exoskeletons

The discussion on FDI highlight the lack of fault-tolerant systems in exoskeletons. While bond graph modelling has been applied in other domains, its use in exoskeletons remains underexplored. The proposed research addresses this gap by developing a robust FDI framework capable of detecting and isolating faults in real-time, ensuring system reliability and user safety.

The observations identified are linked to fault-tolerant systems motivates the development of a dual-actuator exoskeleton with an FDI framework, while the absence of EMG-controlled four-bar mechanisms underscores the need for an integrated design that combines mechanical robustness with adaptive control.

2.9.5 Optimisation of Design Parameters

The literature lacks studies on optimizing exoskeleton design parameters to maximize joint range of motion and user comfort. [97] This gap has been linked to the research objective of optimizing link lengths and actuator configurations using suitable optimization technique.

2.10 Objectives of the Present Work

The focus of the present work is to design and implement a knee exoskeleton that provides desired support for impaired mobility during STS movements. The objectives of the present work are:

1. To model the dynamics of the human knee exoskeleton system
2. To fabricate and control the knee exoskeleton
3. To study torque estimation using linear vs. rotary actuators for the STS motion:
4. To perform fault detection, isolation, and reconfiguration of the knee exoskeleton
5. To optimize the design parameters of the knee exoskeleton

The thesis is organized into six chapters, commencing with an introductory section on the dissertation subject in Chapter 1. In Chapter 2, an extensive literature review is presented, followed by the formal definition of the research objectives. A detailed analysis of the dynamic modelling of the proposed knee exoskeleton is presented in Chapter 3. Chapter 4 verifies the theoretical conclusions by comparing experimental data collected from the fabricated system, which includes the use of an EMG sensor-based controller for motion control system (STS). An analysis of the fault detection and isolation model of the exoskeleton is presented in Chapter 5. At last, Chapter 6 is dedicated to the optimization of the design parameters, while Chapter 7 serves as the conclusions of the work.

Chapter 3

Dynamic Modelling of Knee Exoskeleton

3.1 Introduction

Human knee joints have significant importance in performing activities of daily living (ADL) such as running, walking and stand-sit-stand (STS) motions. With the growing number of lifestyle diseases, several people suffer from knee disorders like muscle paleness, pain, paralysis and gait impairments. Due to this, they often find it difficult to perform common mobility tasks, particularly, stand-sit-stand motions as the high knee torques are required to perform these motions.

A four-bar mechanism driven knee exoskeleton (KE) combined with a linear actuator controlled by electromyography (EMG) sensor for assistance during STS transfer for elderly is still the need of the hour as per the literature and to the best of author's knowledge, no work has been found where a four-bar driven EMG controlled knee exoskeleton is developed that could be used to assist people having knee disorders to perform STS motion. Therefore, in this work, efforts have been made to develop the full. Furthermore, as per the author's knowledge, the bond graph (BG) modelling technique remains a lesser explored area to model the dynamics of exoskeleton systems and specially, for the knee joint as this technique offers multiple advantages over classical dynamic modelling techniques which are discussed in the subsequent paragraph. In this work, the actuator and the motor lie in the electrical domain, whereas the gearbox, lead screw, and four-bar mechanism stay in the mechanical domain. Such multi-domain systems can easily be modelled using BG and the present work shows useful application of this technique.

Thus, the proposed knee exoskeleton is modelled and fabricated specially for assistance during STS motions in this article. It is an EMG sensor-based planar four-bar mechanism actuated by a linear DC motor. The exoskeleton is mounted upon an artificial limb to check the design efficacy. The modelling and simulation studies of the complete system at different loads are performed using the bond graph technique. The prototype is fabricated, and the experiments are performed to validate the desired torque produced by the actuator at the knee joint for performing the STS motion. Furthermore, the actuator characteristics for the entire cycle of the desired activity

have also been shown in this work. Additionally, with the help of dynamic simulation and experimental results, it has been shown that the actuator force varies throughout the desired activity rather than staying constant. Furthermore, the EMG sensor proved to be helpful to identify the user intention during the STS motion. Thus, the assistive torque developed by the actuator at the knee joint of the exoskeleton is found to be suitable to assist the wearer. As a result, little effort is required by the wearer for performing the stand-sit-stand motions. Furthermore, the BG approach to model multidisciplinary systems like KE proved effective as it conveniently models the system containing various elements in different energy domains.

The organization of this chapter is as follows: At the beginning, the CAD model for a KE is discussed. The dynamic model of the KE is established in BG environment and is simulated during STS motion. Thereafter, the torque estimation is done for the KE with linear vs. rotary actuators during STS motion. The bond graph representation of KE is also detailed using *SYMBOLS Shakti* software. Finally, the performance comparison on assistive torque and angle of rotation are done using the same model.

3.2 Dynamic Modelling of Knee Exoskeleton during Stand to Sit Motion

The cycle for stand-sit-stand motion is shown in Fig. 3.1. The process starts when the thigh is at the angle (α_3) of 1.7° away from the axis of shank (+ve y-axis) in the clockwise direction. For the sit position, the thigh rotates through an angle (α_2) of 83.3° in a counter clockwise direction from the positive y-axis. While in the sitting posture, the thigh still makes an angle (α_1) of 6.7° with respect to the negative x-axis. Figure 3.1 shows the angle (α_3) between the thigh (femur) and the extension of the shank (tibia) of the human body in the frontal plane. This value is the angle between the tibia and the femur of the human knee joint, which is approximately 6° to the femur's anatomic axis (perpendicular to the mechanical axis). The value of α_1 and α_2 depends on the height of the chair and the height of the subject. However, the value of α_3 is subjected to individuals' physiological behaviour or posture and is independent of the chair's height and subject size. For the case, when the chair's height is fixed, α_1 decreases and α_2 increases if the height of the subject increases, as these angles are complementary to each other ($\alpha_1 + \alpha_2 = 90°$). Similarly, the value of α_1 increases, and α_2 decreases with the decrease in the subject's height. When subject height is fixed, α_1 decreases, and α_2 increases due to the rise of chair height. Similarly, as chair height is lowered, α_1 increases, and α_2 decreases during the fixed size of the subject.

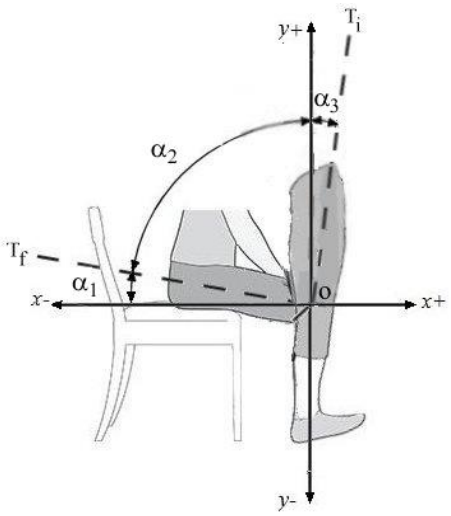

Fig. 3.1 Proposed stand to sit motion

Figure 3.2 shows the knee exoskeleton developed by the authors at the Systems and Control research lab at TIET, Patiala, India. The proposed knee exoskeleton mounted on the artificial limb for performing the desired motion is depicted in Fig. 3.2(a), whereas, Fig. 3.2(b) shows the subject wearing the prototype on the limbs.

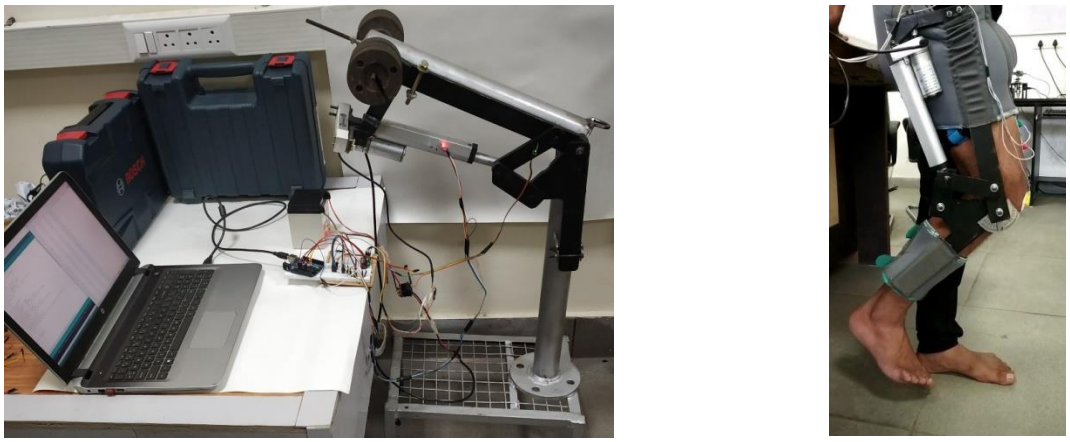

(a) (b)

Fig. 3.2 Knee exoskeleton mounted on (a) Artificial limb and (b) Human leg

3.2.1 CAD Model

The CAD model of the knee exoskeleton is developed in SolidWorks 2019, as shown in Fig. 3.3. This design is inspired by the work of Kim et al.[97]. The front and isometric views of the CAD model are depicted in Fig. 3.3(a) and Fig. 3.3(b), respectively. The kinematic parameters of the proposed knee exoskeleton are shown in Fig. 3.3(c). The proposed design is based on the planar

four-bar mechanism, actuated by a linear DC motor for the necessary actuation. The four-rigid links d_1, d_2, d_3 and d_4 (fixed) connected in the form of a quadrilateral by four-pin joints constitute the four-bar mechanism. In the present mechanism, the sum of the shortest (d_3) and the longest link (d_4) is less than the sum of the other two links (d_1+d_2). The link (d_4) adjacent to the shortest link (d_3) is kept fixed during STS motion. Therefore, according to Grashof's criteria, it is a crank-rocker mechanism, where the shortest link (d_3) acts as a crank, while the link adjacent to the fixed link acts as a rocker (d_1). The top end of the actuator relates to link d_5 (extension of the same link d_3) at pin joint 6, whereas the piston end is connected to the link d_2 at joint 2. d_9 represents the instantaneous length of the actuator. There are five-pin joints, i.e., 1, 2, 4, 5, and 6 in the exoskeleton. The lengths of two bars (d_2 and d_3) of the four-bar mechanism (Fig.3(c)) are assumed. The lengths of the other two bars (d_1 and d_4) of the four-bar mechanism are designed based on the actuator length (d_9) in the compressed (0.242 m) and the expanded position (0.379 m), the lengths d_5 and d_6 of the KE frame and initial angle $\theta_i = (90 - \alpha_3)°$ and final angle $\theta_f = (90 + \alpha_2)°$ of rotation of link d_3. The lengths of the link d_1 and d_4 are calculated using the relations: $\psi_1 = \tan^{-1}\frac{d_5}{d_6}, \psi_2 = \cos^{-1}\left(\frac{d_7^2+d_2^2-d_9^2}{2d_7d_2}\right), d_7 = ({d_5}^2 + {d_6}^2)^{\frac{1}{2}}, d_8 = ({d_2}^2 + {d_3}^2 - 2d_2d_3\cos(180 - \psi_1 - \psi_2))^{\frac{1}{2}}, \phi_1 = \cos^{-1}\left(\frac{{d_8}^2+{d_3}^2-{d_2}^2}{2d_8d_3}\right), \phi_2 = \cos^{-1}\left(\frac{{d_8}^2+{d_4}^2-{d_1}^2}{2d_8d_4}\right), \phi_3 = \tan^{-1}\left(\frac{x_5-x_1}{y_5-y_1}\right)$ and $\theta = (180 + \alpha_3) - (\phi_1 + \phi_2 + \phi_3)$. The proposed knee exoskeleton is a generalized design as it could be worn by the wearer irrespective of leg length. The joint 5 of the exoskeleton is positioned at the knee joint of the wearer. The shank length of the exoskeleton could be adjusted according to the wearer's calf length though the dimensions of the four-bar mechanism of the KE remain unchanged. In the present work, linear actuator (LA) is preferred over BLDC motor owing to its ease of installation and low cost. Furthermore, when a LA is combined with four-bar mechanism, it offers high torque whereas light weight BLDC motors which provide high torque are much expensive in comparison to that of LA.

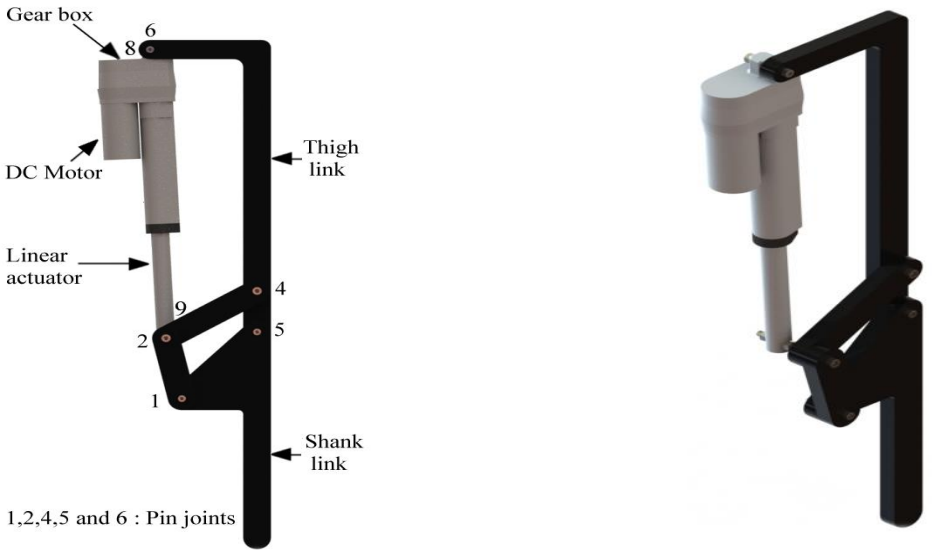

(a) (b)

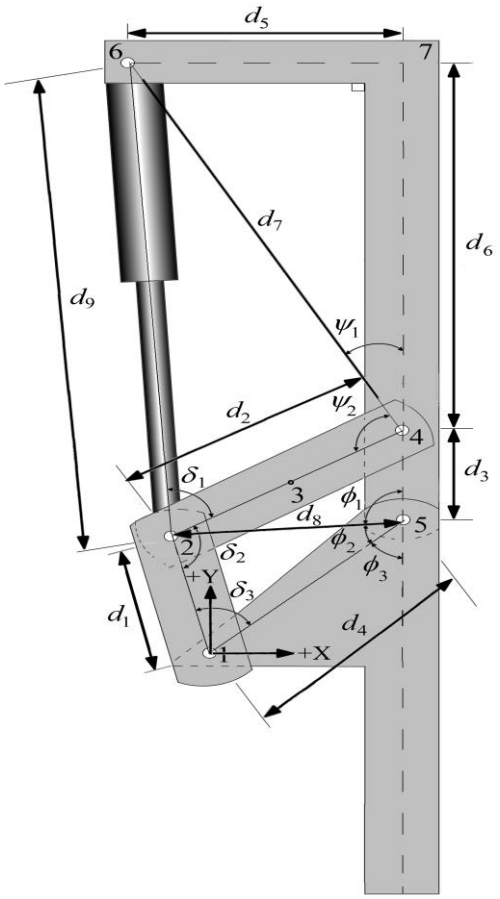

(c)

Fig. 3.3 Different views of KE: (a) Front view, (b) Isometric view and (c) Kinematic model

3.2.2 Bond Graph Model

The modelling of the knee exoskeleton is developed using the bond graph (BG) technique. Few assumptions are made before modelling through this multi-physics modelling tool. All the five joints of the knee exoskeleton are considered pin joints. The modelling of the knee and the corresponding friction between solid-fluid interfaces are not considered in this work. Though the shank part of the leg moves during STS motion in the actual scenario, in this work, the shank always lies in a vertical position. The masses and the mass moment of inertia are considered at the joints only. All the links are considered rigid. Bond graph (BG) is a system modelling approach that is based on the conservation of power. This technique finds its importance when the various components of the system lie in different energy domains. The significant advantage of using this technique is that only the kinematic equations are required for modelling any system. The dynamic equations can be automatically developed from the BG model.[88] The modelling of the current KE is crucial to understand the nature and the magnitude of the forces generated by the actuator and the estimation of joint angle and knee torque at any instant acting at the knee joint of the exoskeleton. These parameters are significant for better understanding the degree of assistance that the current exoskeleton could provide to the user for the intended motion. In the present case, the BG technique has been adopted as the linear motor lies in the electrical domain, whereas the gearbox, lead screw and four-bar mechanism lie in the mechanical field. A multi-domain system like this could be easily modelled using the BG technique.

A word BG for the present exoskeleton is shown in Fig. 3.4. The effort signal in the form of voltage is supplied to the DC motor that generates angular velocity, a flow input to the gear box. Lumped flexibilities are added to avoid differential causalities, and these are also known as coupling capacitor or pad element. These pads are represented in the (1-C-R) bond structure at the intermediate 0-junction between the gearbox and lead screw or between the lead screw and the four-bar mechanism.

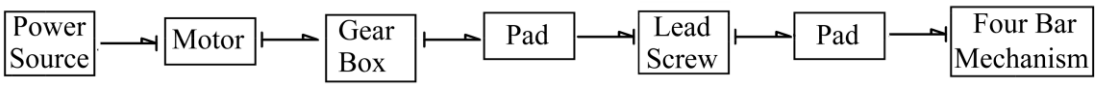

Fig. 3.4 Word bond graph

(a) Bond graph model of the four-bar mechanism

The detailed BG model of the four-bar mechanism is depicted in Fig. 3.5. The input at joint 2 of the KE is the actuator force, whereas the output of the knee exoskeleton (Fig. 3.5) at joint 6 relates to the cylinder end of the actuator (Fig. 3.7). The input to the actuator (Fig. 3.7) is the force imparted by the lead screw (Fig. 3.6). This may happen due to the problem of fonts during the uploading of the manuscript. $\dot{X}_1$and $\dot{Y}_1$ represent the linear velocities of the joint 1 along *X* and *Y*-direction, respectively. Similarly, $\dot{\theta}_1$, $\dot{\theta}_3$and $\dot{\theta}_5$ represents the angular velocities of the joint 1, 3, and 5, respectively. The linear velocities of joint 2 along *X* and *Y*-direction are given by $\dot{X}_2 = \dot{X}_1 + \dot{\theta}_1 u_1$ and $\dot{Y}_2 = \dot{Y}_1 + \dot{\theta}_1 u_1$, respectively, where $u_1 = -d_1 sin\theta_1$ and $u_2 = d_1 cos\theta_1$. Similarly, kinematic equations for other points can be obtained in the similar fashion. The moduli used for finding out the velocities at different points are given by $\mu_3 = \frac{2}{d_2 \sin\theta_3}$, $\mu_4 = -\frac{2}{d_2 \cos\theta_3}$, $\mu_5 = -\frac{d_2 \sin\theta_3}{2}$, $\mu_6 = \frac{d_2 \cos\theta_3}{2}$, $\mu_7 = -\frac{1}{d_3 \sin\theta_5}$, $\mu_8 = \frac{1}{d_3 \cos\theta_5}$, $\mu_9 = -0.39 d_3 \cos(\theta_5 - 1.23)$, $\mu_{10} = -0.39 d_3 \sin(\theta_5 - 1.23)$.

The linear and angular velocities of all the joints are represented by 1-junction through which the inertial elements (I) are connected. These elements represent the masses in the case of linear motion and mass moment of inertias in the case of rotary motion. The flow detector (Df) senses the linear and angular velocities of these joints. As joints 1 and 5 have no movement with respect to the inertial frame, the zero sources of flow (Sf) are attached at the 1-junctions through the coupling capacitor. To avoid differential causalities, the coupling capacitors are added at the corresponding 0-junctions. K_P and R_P, are the capacitive and resistive elements, respectively and these are connected in series at 1-junction. The sources of effort (Se) representing weight (W_{exo}) of the exoskeleton and the external weights (W_{ext}) are connected at 1-junction representing the velocities of the joint 6. The linear and angular velocities of the joint 5 (knee joint) are measured using the flow detector (Df) connected at corresponding the 1-junction. The knee joint torque is obtained, which is the torque acting at joint 5 of the KE. The forces acting at joint 1 are measured by the effort detectors (De) and normal component (with respect to the link d_4) of the force acting at the same point is calculated based on the force components and the angular position of the link d_4. Finally, the torque acting at the knee joint (joint 5) is calculated based on the data obtained from the BG model.

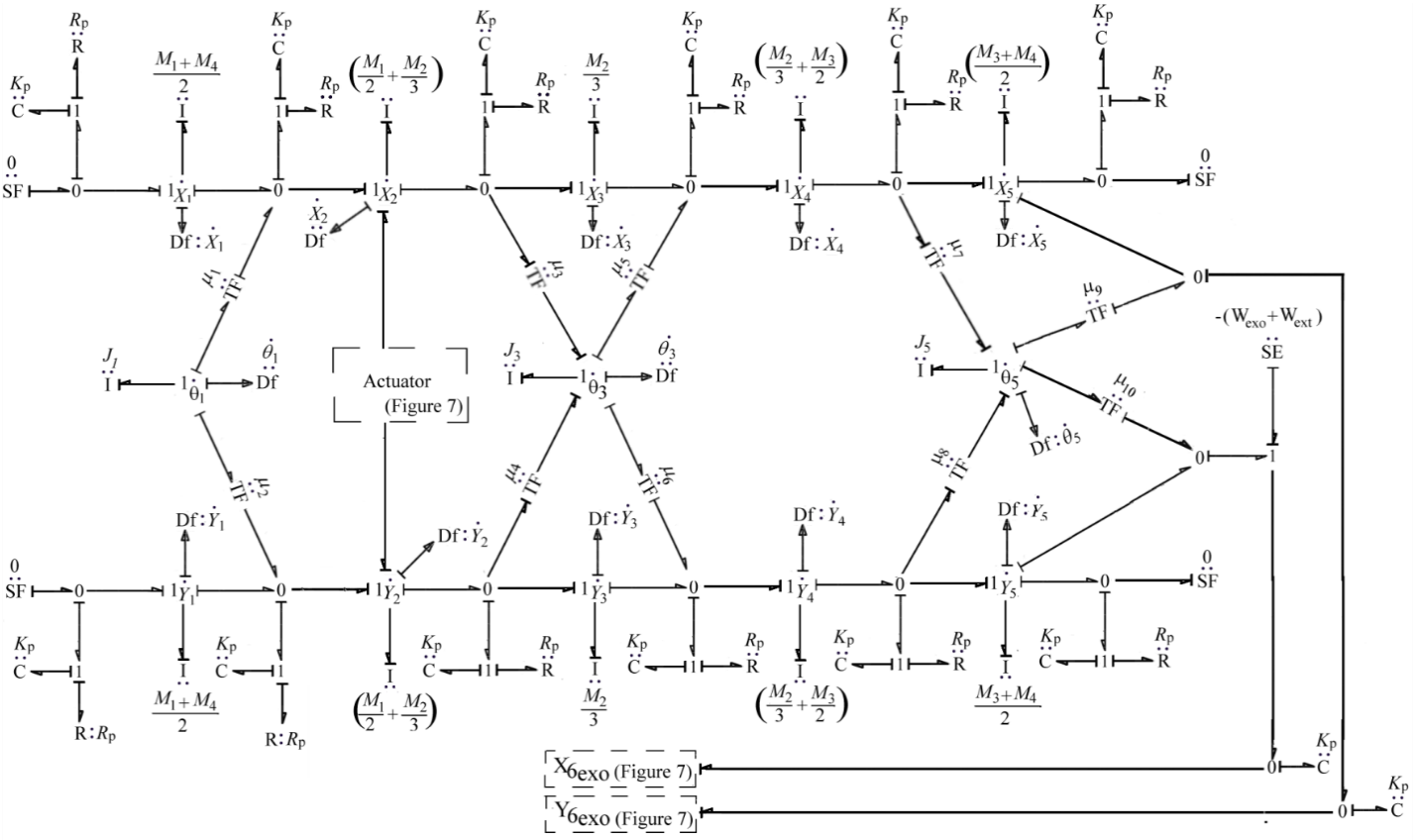

Fig. 3.5 Bond graph model of the knee exoskeleton

(b) Bond graph model of the motor with the lead screw

Figure 3.6 illustrates the BG model of the motor and the lead screw. A DC motor is used as the source of power. The voltage (v) is supplied as an input power source and is represented by the element, source of effort (Se), connected at 1-junction. The armature inductance (L_a) and armature resistance (R_a) are represented by inertial element (I) and resistive element (R), respectively. These are connected at the 1-junction, as the current remains the same (due to series circuit) for all the elements of the input electric circuit of the DC motor. The current (i) in the armature circuit is sensed by the current sensor, represented by the flow detector (Df). The modulus of the gyrator μ_M is the motor characteristic constant. The viscous damping (R_V) and mass moment of inertia of the gear (J_G) are represented by R and I-element, respectively, and are connected at the same 1-junction. The gear ratio (μ_G) is represented by the transformer element (TF). This is considered as unity as a set of gear-pinion is required to transfer the motion from one axis to the other. Since there is no speed reduction in this scenario, therefore, there occurs no problem of slipping and jerk. K_G connected at 0-junction denotes the torsional stiffness of the gear. The damping (R_L) and the

mass moment of inertia of the lead screw (J_L) are connected at 1-junction. K_L connected at 0-junction denotes the stiffness of the lead screw. $\mu_V = \frac{\text{Lead}}{2\pi}$ represents the transformer modulus of the lead screw. Finally, the change of position of the nut of the lead screw ($\dot{L}_L$) is sensed by the velocity sensor (Df) connected at 1-junction. The motor is connected to a lead screw which is connected to the actuator through a transformer element representing the clutch with modulus $\mu_c = 1$ and $\mu_c = 0$ when the clutch is in the engaged and the disengaged positions, respectively. No clutching and declutching arrangement have been used in the hardware for the experimentation. This arrangement has only been used in the BG simulation only ($\mu_c = 1$). However, in the future work, a secondary actuator will be used in the current design for the fault detection, isolation (FDI) and reconfiguration purpose. Then, clutching arrangement will be used in the experimental setup also.

(c) Bond graph model of the linear actuator

The input to the actuator is the force imparted by the lead screw, as depicted in Fig. 3.6. The coordinates of the centroid of the cylindrical part of the actuator and of the piston rod are (X_C, Y_C) and (X_P, Y_P), respectively. J_C and J_P are the mass moment of inertia of the cylindrical component and that of piston rod, respectively and are represented by inertial element (I) connected to the respective 1-junctions. Figure 3.7 depicts the BG model of the linear actuator.

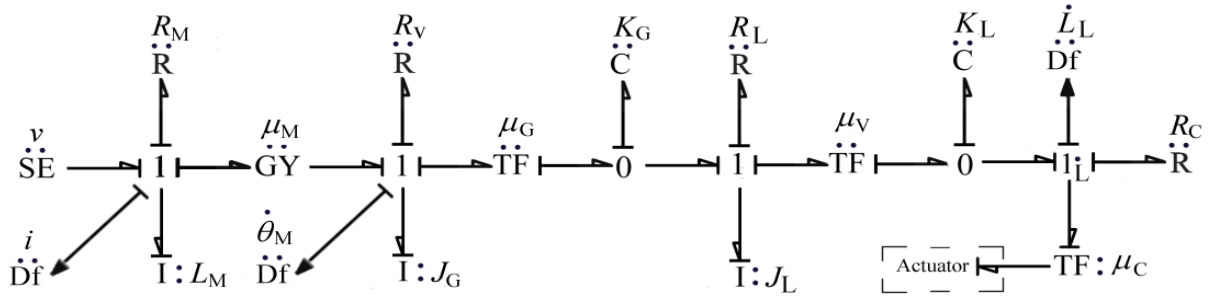

Fig. 3.6 Bond graph model of the motor along with lead screw

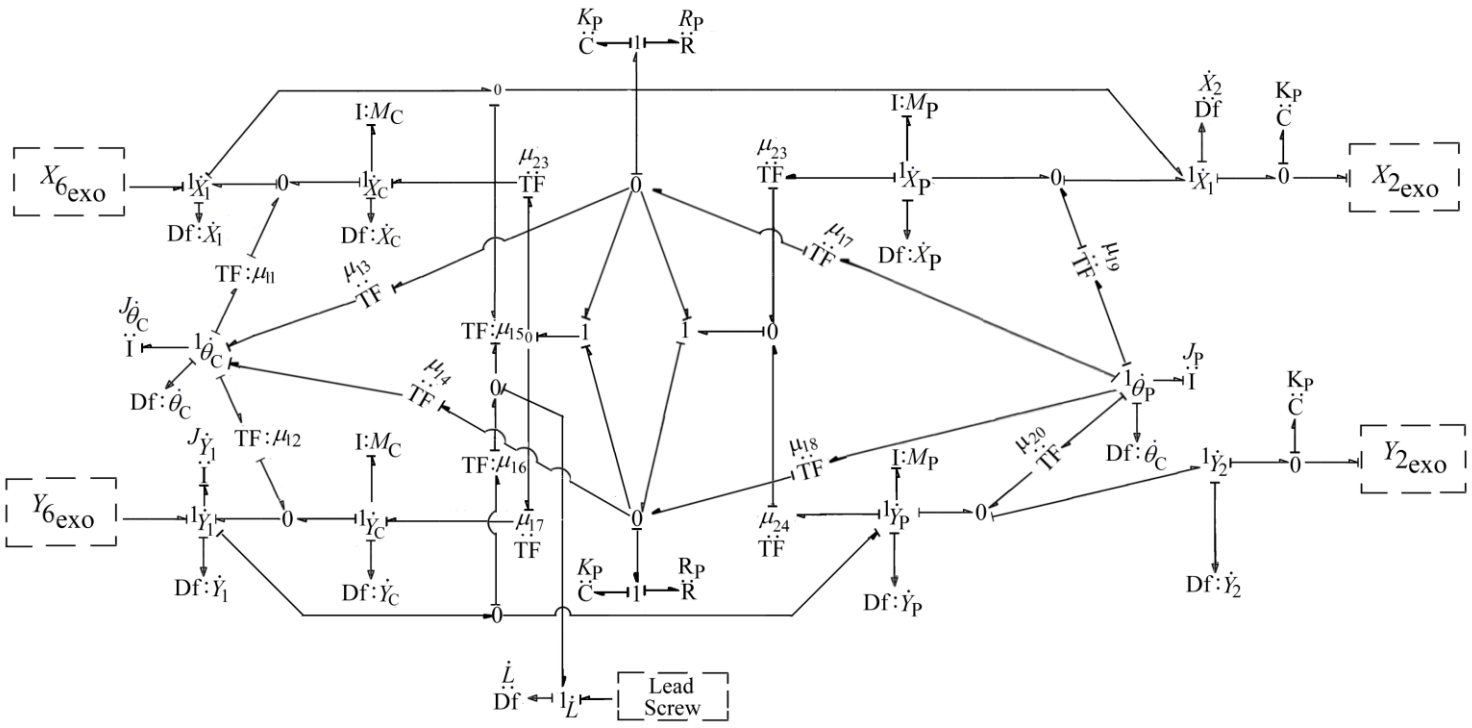

Fig. 3.7 Bond graph model of the linear actuator

3.3 Simulation Results and Discussions during Stand to Sit Motion

The bond graph modelling and simulation of the exoskeleton consisting of linear actuator, motor, and the lead screw are performed using *SYMBOLS Shakti* software for four different load cycles. The algorithms can be established quickly by assigning causalities to the BG elements, and the response of the system could be easily obtained. The state-space equations in terms of first-order differential equations of the system are generated once the model is finalised. The numbers of equations are equal to the numbers of energy storing elements with integral causality present in the system.

3.3.1 Parameters Values for Simulations

The time duration for each stand-sit-stand cycle for different loads is observed approximately as 10.3 s. The system parameters used for simulations and their values are specified in Table 3.1. Few parameters (of four-bar mechanism) are measured, while others (parameters of the actuator) are either taken from the manufacturer's catalogue or the product's specifications.

Table 3.1 Parameter values for simulations

Parameters	**Values**
Exoskeleton parameters	
Mass of cylinder part (M_C)	0.5 kg
Mass of piston (M_P)	0.1 kg
Mass moment of inertia of cylinder part (J_C)	0.05 kg m^2
Mass moment of inertia of piston and piston rod (J_P)	0.02 kg m^2
Contact stiffness (K_P)	10^8 N/m
Contact damping (R_P)	10 Ns/m
Distance of centroid of the cylinder from the cylinder end (l_C)	0.050 m
Distance of centroid of piston assembly from piston end (l_P)	0.080 m
Distance of centroid of the piston from piston end (l_{P1})	0.090 m
Width of the piston (d)	0.020 m
Voltage (v)	12 V
Motor constant (μ_M)	1 Nm/A
Motor armature resistance (R_M)	0.1 Ω
Motor inductance (L_M)	0.5 H
Gear constant (μ_G)	1
Torsional stiffness for gear (K_G)	10^7 N/m
Mass moment of inertia of lead screw (J_L)	0.1 kg m^2
Damping of lead screw (R_L)	0.1 Ns/m
Lead of lead screw (L)	0.0146 m
Stiffness of lead screw (K_L)	10^7 N/m
Mass of Link$_1$ (M_1)	0.104 kg
Mass of Link$_2$ (M_2)	0.149 kg
Mass of Link$_3$ (M_3)	0.069 kg
Mass of Link$_4$ (M_4)	0.316 kg
Length of Link$_1$ (d_1)	0.080 m
Length of Link$_2$ (d_2)	0.115 m
Length of Link$_3$ (d_3)	0.053 m
Length of Link$_4$ (d_4)	0.117 m
Effective weight of thigh, exoskeleton and sensor (W_{exo})	28.86 N

3.3.2 Motor Characteristics for Stand-Sit Position

The simulations are performed using a knee exoskeleton mounted on an artificial limb for the stand-sit-stand transfer for different weights. These weights are $W_{exo,}$ (W_{exo} +20) N, (W_{exo} +40) N, and (W_{exo} + 60) N, where W_{exo}=28.86 N represents the weight of the upper limb of the proposed knee exoskeleton.

Figure 3.8 depicts the change in motor current and motor torque values with time for the stand-sit transfer. It can be noted from Fig. 3.8(a) that there is a spike in the motor current at the

start of the cycle, at time t=0.55 s, which further drops sharply, close to the initial value, at 1.55 s of the cycle time. The spike in the graph is caused as the motor is initially at rest and presents a high torque. This current is equivalent to the motor's stall current, which would continuously decrease as the motor creates its back electromotive force (emf). Further, as the cycle time increases, the current reaches 4.3 A at the mid of the stand-sit phase at time t=2.57 s, before dropping down to 3.8 A, at the sitting position i.e. at 5.15 s. The marginal increase in the value of motor current is observed in each case with an increase in the weight. This is because the motor draws more stator current to counter the mechanical load rise, which further makes motor to reduce its back emf. The similar trend is observed for motor torque assuming the motor constant to be 1 Nm/A, as shown in Fig. 3.8(b).

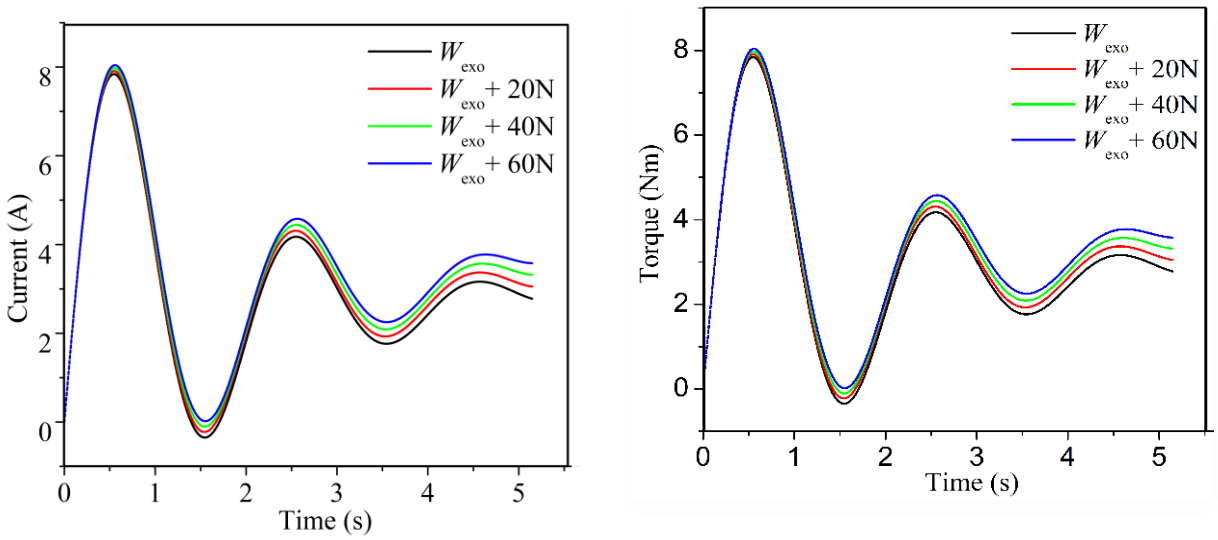

(a) (b)

Fig. 3.8 Motor characteristics for stand -sit position (a) Current *vs* time and (b) Torque *vs* time

3.3.3 Actuator Characteristics

Figure 3.9(a) shows the change of actuator length for the duration of one cycle of stand-sit-stand transfer. At the beginning of the cycle, the length of the actuator (d_9) is approximately 0.379 m, which is the position where the actuator is at the maximum extended position. With an increase in the cycle time, the actuator length first decreases to the minimum value of 0.24 m at 5.15 s (sit position). It then increases back to its initial maximum value. As observed, the graphs are the same for all the load cycles as the rate of change of actuator length is independent of the mechanical load. There is a slight change in the length of the actuator for the different loads at the starting of sit position.

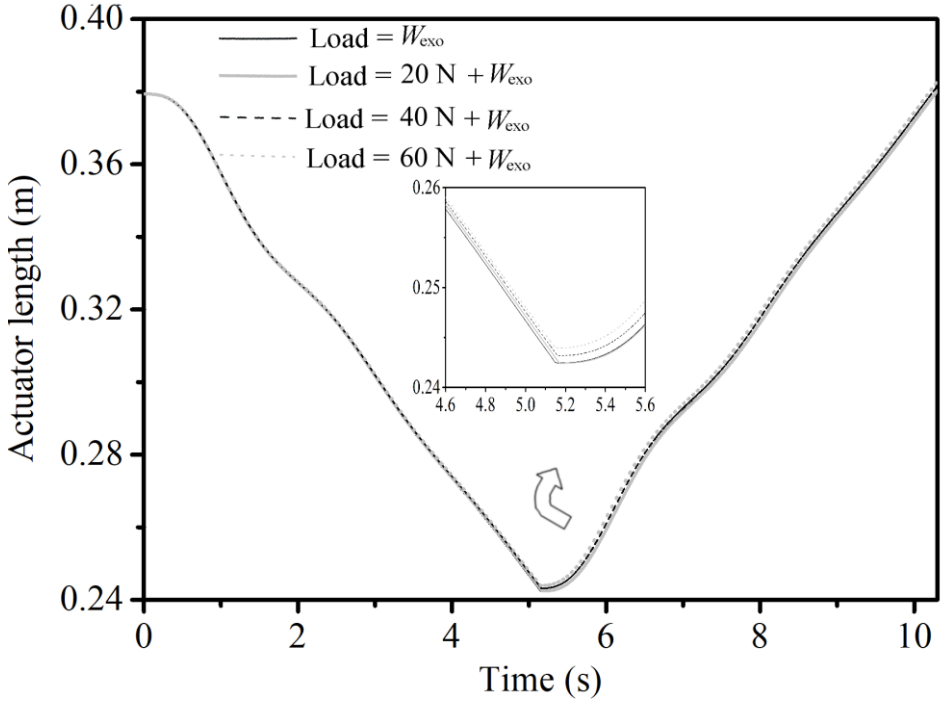
Load = W_{exo}
Load = 20 N + W_{exo}
Load = 40 N + W_{exo}
Load = 60 N + W_{exo}
Actuator length (m)
Time (s)
0.40
0.36
0.32
0.28
0.24
0
2
4
6
8
10
0.26
0.25
0.24
4.6
4.8
5.0
5.2
5.4
5.6

(a)

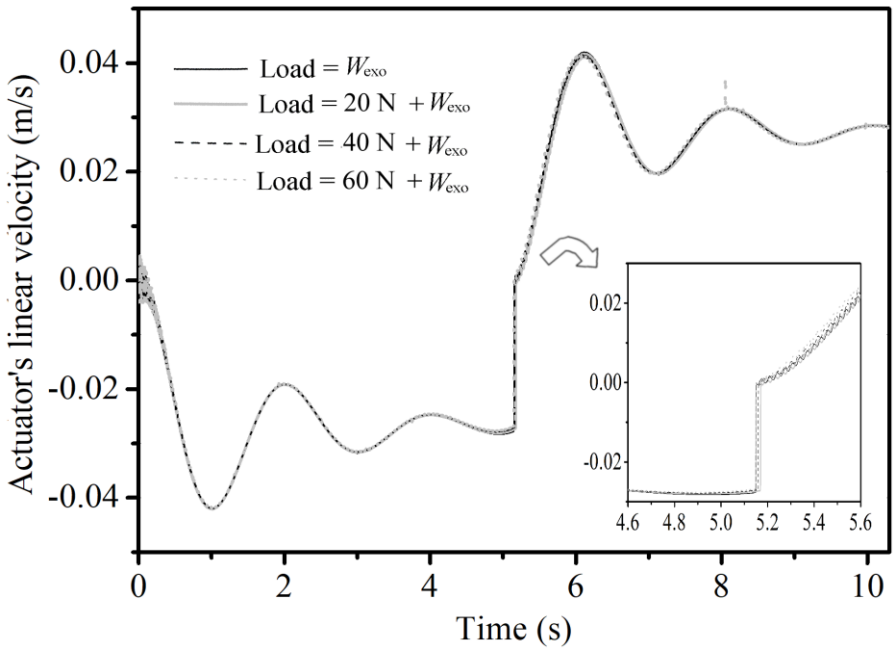
Load = W_{exo}
Load = 20 N + W_{exo}
Load = 40 N + W_{exo}
Load = 60 N + W_{exo}
Actuator's linear velocity (m/s)
Time (s)
0.04
0.02
0.00
-0.02
-0.04
0
2
4
6
8
10
0.02
0.00
-0.02
4.6
4.8
5.0
5.2
5.4
5.6

(b)

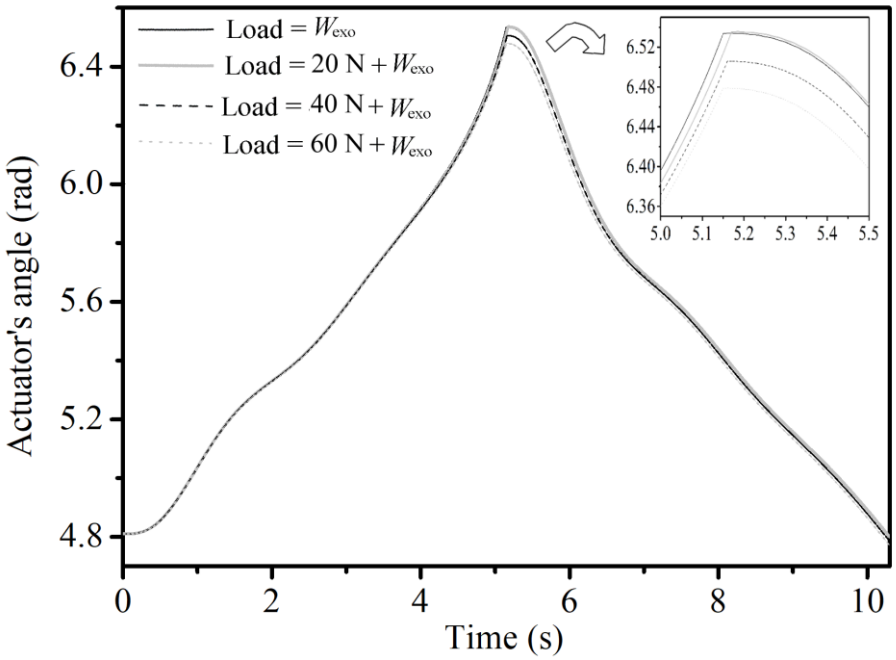

(c)

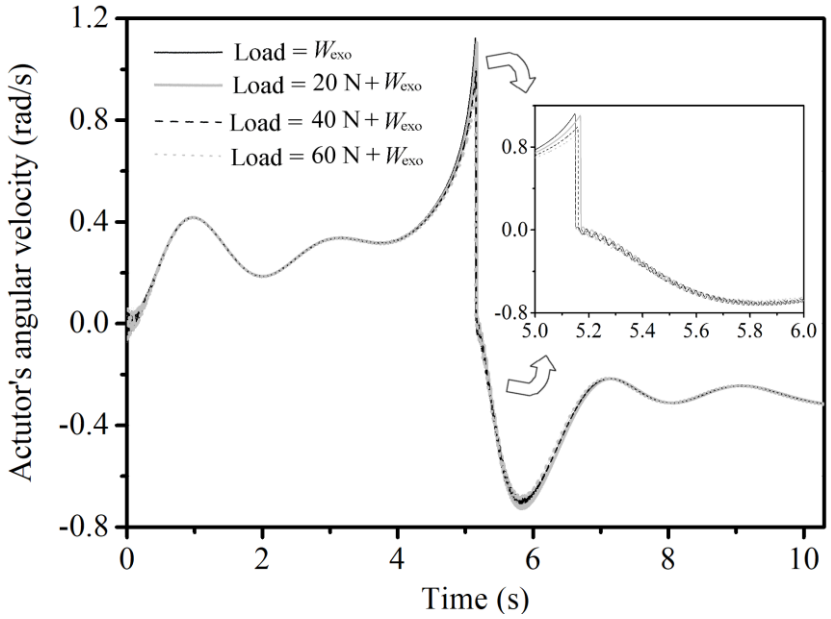

(d)

Fig. 3.9 Actuator's characteristics (a) Change of actuator's length, (b) Actuator's linear velocity, (c) Actuator's angle and (d) Actuator's angular velocity

The linear velocity of the actuator sharply falls to -0.04 m/s (negative sign indicates contraction of the actuator) just at the start of the cycle (t=1s) for the load $W_{exo,}$ which is similar with other

loads of (W_{exo} +20) N, (W_{exo} +40) N and (W_{exo} + 60) N. The steady-state velocity is approximately -0.028 m/s at the end of the half-cycle where the exoskeleton lies in sitting phase. Similarly, the steady-state velocity of the actuator during the expansion or sit-stand phase is about 0.0284 m/s (positive value indicates the expansion of the actuator), as shown in Fig. 3.9(b). Fig. 3.9(c) depicts the change of actuators angle with respect to the positive *X*-axis. At the start of the cycle, the actuator angle is 4.81 rad (275.55°), which further increases as time increases. The actuator angle peaks at 6.50 rad (372.70°) in 5.15 s (sit position) for all the weights. The graph follows the reverse trend when the time further increases. Towards the end of the process (10.30 s), the actuator returns to its initial extended position. As the time increases, the angular velocity increases sharply and reaches a maximum value of 1.13 rad/s (positive sign indicates the rotation of the actuator about the perpendicular Z-axis in CCW direction) as shown in Fig. 3.9(d). The actuator starts rotating in the clockwise direction; the angular velocity reaches the steady-state value of -0.32 rad/s. It could also be noted that the trend for the angular velocity is similar for all the load cycles. However, the angular velocity of the actuator decreases marginally at the mid-cycle with the increase in the mechanical load.

3.3.4 Angle of Rotation of Link 1, Link 2 And Link 3

Figure 3.10(a) shows the plot for the force developed by the actuator during stand-sit (half cycle) motion with respect to the angle of the rotation of link 3. It can be observed from cases A, B, C and D that the force developed by the actuator increases with the angle of rotation of link 3 (joint angle) for each load cycle. This is because, as the wearer takes a stand -sit transfer, the joint angle increases, leading to a rise in the moment arm. As a result, the knee torque increases, and to counterbalance the enhanced knee torque, the force developed by the actuator increases. The maximum actuator force for cases A, B, C and D are 336.1 N, 538.9 N, 667.5 N, 790.2 N, respectively, for the joint angle of approximately 3.07 rad (175.89°). It is observed that there is a decrease in the stroke length with an increase in the value of the angle of rotation of the third link. The stroke length for each load cycle is approximately 0.379 m at an angle of 1.541 rad (88.29°), and it reduces to 0.242 m at an angle of 3.078 rad (176.35°). As expected, the stroke length is found to be independent of the load carried by the actuator. The position trajectories of joint-2, centroid-3, and joint-4 of the exoskeleton are shown in Fig. 3.10(b). 'S' and 'E' indicate starting and ending positions of the joints, respectively, during the stand to sit position. The joint-2 moves in a circular path as point-1 is a fixed point. The joint-4 fixed with the thigh also moves in the

circular path as the shank is assumed to be fixed vertically during the motion. Figure 3.10(c) depicts the angle of the knee joint of the exoskeleton. The initial angle at the standing position is 181.7º, and the angle at the sitting position is 96.7º. Figure 3.10(d) depicts the power developed by the actuator with the cycle time for different weights. The maximum power developed by the actuator is 21 W,18 W, 14 W and 9 W for the loads of W_{exo}, W_{exo}+20 N, W_{exo}+40 N and W_{exo}+60 N, respectively for the one-cycle of stand-sit-stand motion.

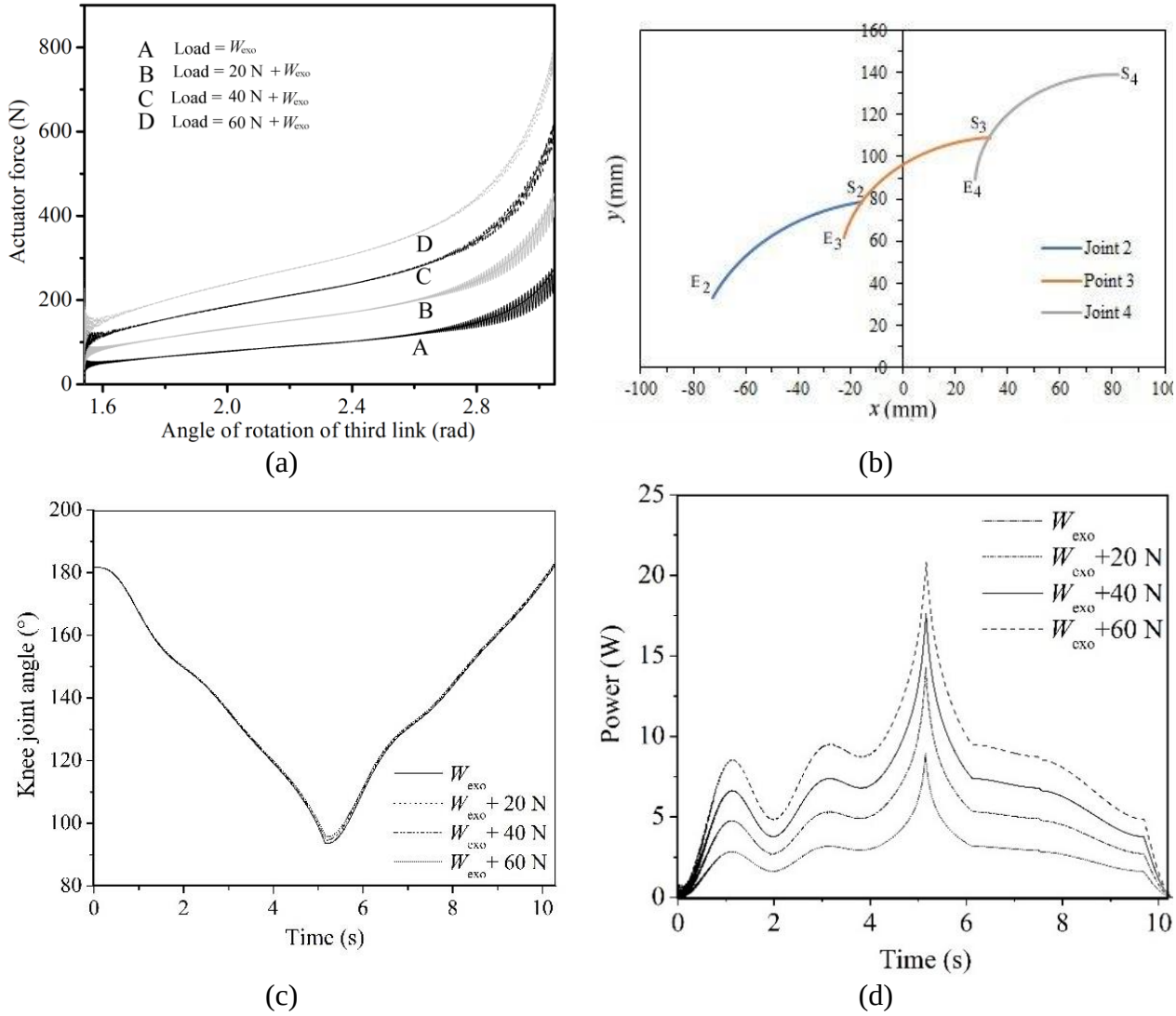

Fig. 3.10 (a) Actuator force vs. angle of rotation of third link, (b) Position trajectories of the joint-2, point-3 and joint-4 of the knee exoskeleton, (c) Knee joint angle of the knee exoskeleton and (d) Actuator power with cycle time

Figures 3.11(a) and 3.11(b) show the angle of rotation of Link 1, 2 and 3 with respect to the cycle time of stand-sit-stand motion for the applied loads of W_{exo} and (W_{exo}+20) N, respectively.

As depicted in Fig. 3.11(a), the initial angles of rotation of Link 1 and Link 3 for the load of W_{exo} at the start of the cycle are 1.77 rad (101.4°) and 1.54 rad (88.2°), respectively. As time increases, the angle turned by Link 1 and 3 first increases to the maximum peak value of 2.71 rad (155.3°) and 3.08 rad (176.5°), respectively at 5.15 s and then drops to 1.75 rad (100.3°) and 1.53 rad (87.7°) and at the end of the cycle at 10.3 s. However, a marginal change in the angle of rotation of Link 2 with respect to cycle time is observed. The angles of Link 2 at the start and mid of the cycle are 3.70 rad (211.9°) and 3.74 rad (214.3°), respectively. The variations of the angle for other loads (Fig. 3.11(b)) are almost like Fig. 3.11(a).

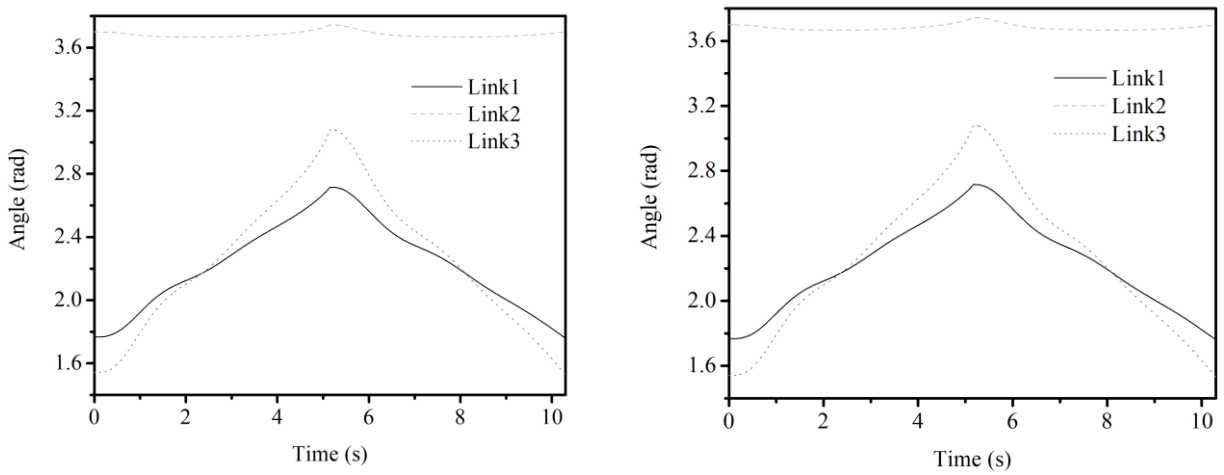

(a) (b)

Fig. 3.11 Angle of rotation of Link 1, Link 2 and Link 3 for (a) W_{exo} and (b) (W_{exo} +20) N

3.3.5 Knee Torque vs Time

The torque developed at the knee joint of the exoskeleton for different weights with respect to cycle time is depicted in Fig. 3.12. The knee torque values are plotted for the entire cycle of stand-sit-stand transfer for each load cycle corresponding to loads of $W_{exo,}$ (W_{exo} +20) N, (W_{exo} +40) N, and (W_{exo} + 60) N. As seen from the graph, the initial values (at 0.002 s) of the torque developed by the actuator at the knee joint (joint 5) of the `exoskeleton for the case A, B, C and D just are 3.05 Nm, 5.29 Nm, 6.25 Nm, and 9.20 Nm, respectively. The knee torque first increases and then reaches its maximum value at 5.15s before dropping to the initial values during the second half of the cycle time. The maximum values of knee torque for the cases A, B, C, and D are 10.93 Nm, 23.8 Nm, 31.24 Nm, and 39.7 Nm at 5.15s, respectively. The change in the knee joint torque is attributed to the difference in the arm length.

The torque developed by the exoskeleton at the knee joint is adequate to substantially assist the user for the desired stand-sit-stand operation by limiting the user's effort to minimal. The torque required to enable the wearer without human effort is approximately 67.2 Nm.[92] Therefore, the presented exoskeleton can substantially assist the patients suffering from knee disorder as it provides an external assistance of 40 Nm. Hence, the proposed knee exoskeleton can provide 60% of the external assistance during the STS motion, limiting the human effort by 40 %. When combined with a four-bar mechanism, the linear actuator allowed a good range of motion for the desired STS transfer.

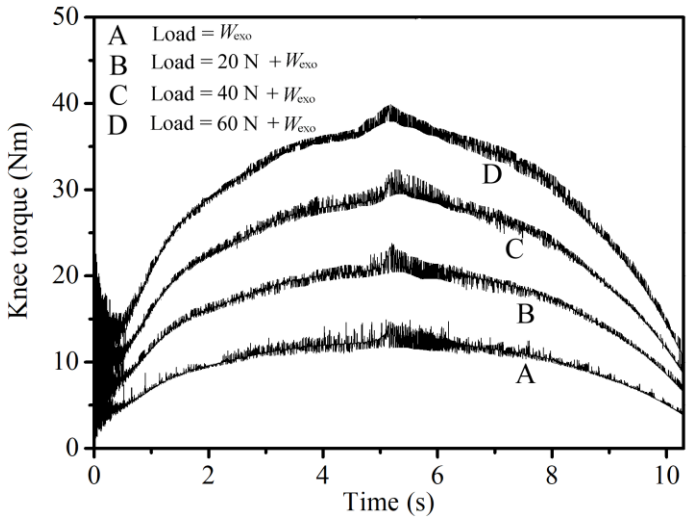

Fig. 3.12 Knee torque *vs* time

3.4 Torque Estimation using Linear *vs* Rotary Actuators during Sit-to-Stand Motion

3.4.1 Challenges faced by Individuals with Knee Joint Disorders

Stand-sit-stand motions (STS) are most frequently performed activities in daily life. This movement causes extensive stress on the knee joint. People suffering from knee joint disorders face difficulties in performing the stand-sit-stand motions (STS). The compact knee exoskeleton (KE) has been found to be realistic, less mechanistic and less expensive than the current entire lower, upper, and full body exoskeletons.

3.4.2 Need for Compact Knee Exoskeleton (KE) with Backup Actuator

There are risks of technical failures of the actuator of KE with growing number of technical glitches and finite battery life problems that are potentially dangerous for the vulnerable users. To

address this issue, it is necessary to design and integrate a spare actuator into KE, which will be able to assist during movement, if the primary one fails. Furthermore, no literature has been found regarding performance comparison between linear and rotary actuators based on their ability to provide assistive torque at the knee joint during stand-sit-stand motions of four-bar mechanism. This comparison is crucial to design a knee exoskeleton that accommodates both these actuators for the case when primary actuator ceases to work due to shorter battery life or owing to sudden fault. The idea of incorporating a secondary actuator is important as majority of the end users of the KEs are vulnerable persons and having a backup actuator will enhances its reliability and safety aspects. In this scenario, the secondary or the backup actuator must not only be able to provide the necessary rotation to the thigh link, but also, it should be able to provide sufficient torque to the knee joint of the exoskeleton to complete the desired STS motion.

3.4.3 Comparative Study of Linear vs. Rotary Actuator for STS Motion

Here, dynamic modelling of two types of knee exoskeletons (KE) actuated by linear and rotary means is done. The modelling and simulation of both the KE driven by four-bar mechanism, the one powered by linear actuator and the other by rotary actuator have been performed. The bond graph (BG) technique and SYMBOLS Shakti software, respectively, have been used for the modelling and simulation. The presented comparisons have been made for the assistive torque by each of these actuators at the knee joint of the KE. In addition, the current study has calculated the position angles of the links of the four-bar mechanism and the required angle for the rotation of thigh to achieve the desired STS motion and a comparison has been made. Thus, the present work itself verifies that both the actuators are self-capable to extend the necessary support to the wearer for the STS motion. Besides, the application of BG approach to model the multidisciplinary systems like KE was proved to be effective as through it the system containing various elements in different energy domains is conveniently modelled.

In the present work, the cycle of stand-sit-stand motion starts when the thigh lies in the first quadrant and makes an angle of θ_3 (1.7°) with the y^+ axis which is the standing position (T_i), as shown in Fig. 3.13. The thigh then rotates at an angle of θ_2 (85°) in counterclockwise direction to attain the sitting position. This is the position when the thigh rests in the second quadrant at an angle of θ_1 (6.7°) from *x*-axis (T_f). However, these values greatly depend on the size of the chair as well as the height of the wearer. Thus, in this work, one cycle of stand-sit-stand motion is said

to have been completed when the thigh returns to its initial standing position θ_3. The entire STS cycle takes place in the sagittal plane as shown in Fig. 3.13(a) and Fig. 3.13(b).

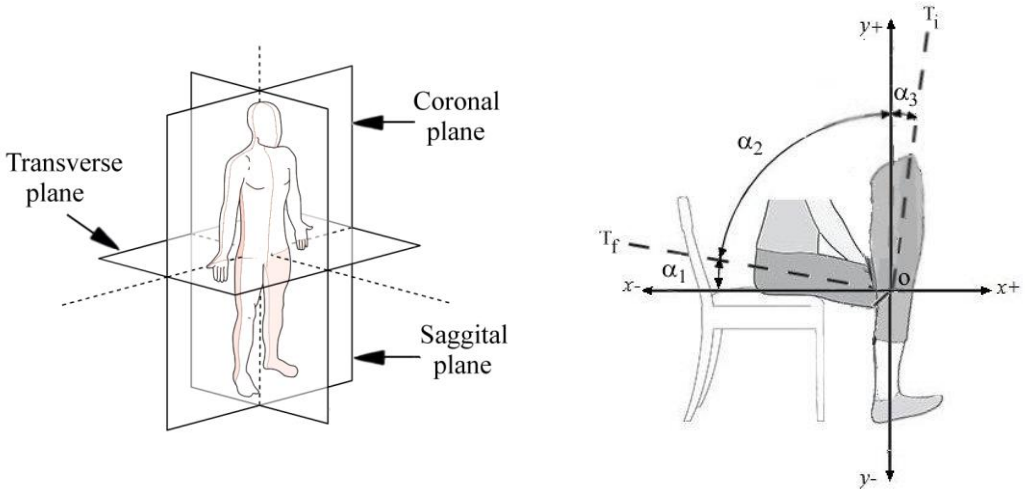

Fig. 3.13 (a) Anatomical planes and (b) Proposed stand to sit motion

The linear and rotary knee exoskeleton actuators are depicted in Fig. 3.14(a) and Fig. 3.14(b), respectively. The four-bar mechanism consists of links d_1, d_2, d_3 and d_4 constituting the four bars of the mechanism. In this mechanism, it is observed that the combined length of shortest link and the longest link is less than the combined length of other two links that is (d_3+d_4). Therefore, as per Grashof's law, it is a case of crank rocker mechanism. In this the links d_3 and d_1 act as crank and rocker, respectively. For stand-sit-stand motion (STS) in the sagittal plane, the link d_3 which is the thigh link rotates the human thigh whereas the link d_4 is connected to calf which remains fixed. The four-bar mechanism is formed by the arrangement of four links escalating through pin joints 1, 2, 4 and 5. The coordinate axis is shown in the Fig. 3.14 at joint 1. The joint 5 is the knee joint of the exoskeleton whose orientation in the coronal plane is parallel to the user's knee joint orientation.

In the KE shown in Fig. 3.14(a), the linear actuator which has a DC tubular motor contains a displacement limit switch and has a self-locking feature. The circuit breaks when the telescopic bar runs to the top or to the bottom, thereby disconnecting the electric current automatically. The DC motor containing a lead screw drive propels the push rod. The telescopic rod can only be retracted without rotation. If the positive electrode is stretched and the negative electrode is shrunk, the telescopic direction of the rod can be changed by changing the polarities. The joint 2 and joint

6 of the KE connect the piston rod end and cylinder end of the actuator, respectively. The actuator's length is represented by d_9. Point 3 is the centroid of the link d_2. The linear velocities of joint 2 and 4 lying on d_2 are calculated with respect to the linear and angular velocities of point 3. The point 7 is not a joint, rather it represents the point where the external load is assumed to be concentrated. Also, d_5 denotes the length of the link connecting the point 6 and point 7. The knee exoskeleton based on rotary actuator which is a planetary geared DC motor is shown in Fig. 3.14(b). It allows the maximum rated torque at lower speeds along with perfect position which is difficult to achieve with conventional DC motors where if motor speed decreases the output power gets reduced. The axis of the motor shaft is coaxial with joint 5 of the KE. Furthermore, the motor which is connected at point 8 of the exoskeleton drives the shaft with a belt-pulley mounted at joint 1 as shown in Fig. 3.14(b). This design is inspired from the work of Kim et al.[24] However, in the present work, the link lengths of the mechanism is designed on the basis of the actuator length in the compressed and expanded position, the angle of rotation of the link d_3 and the knee torque requirement at the joint 5 of the exoskeleton for the desired STS motion.

3.4.4 Modelling of KE with Rotary Actuator

The BG model of the DC motor (rotary actuator) is illustrated in Fig. 3.15 while that of the knee exoskeleton integrated with a rotary act is illustrated in Fig. 3.16. The angular velocities of joints 1, 4 and 5 are denoted as $\dot{\theta}_1$, $\dot{\theta}_4$ and $\dot{\theta}_5$, respectively. The motor torque is delivered to rotate the link d_1 which is connected to the link q through the belt pulley system at joint 1.

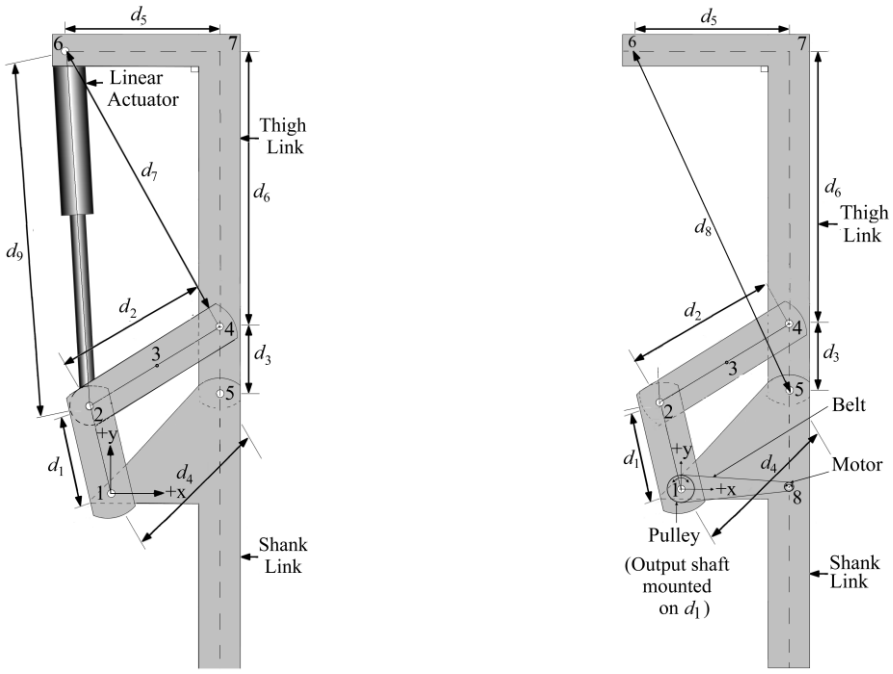

(a) (b)

Fig. 3.14 Knee exoskeleton with (a) Linear actuator and (b) Rotary actuator

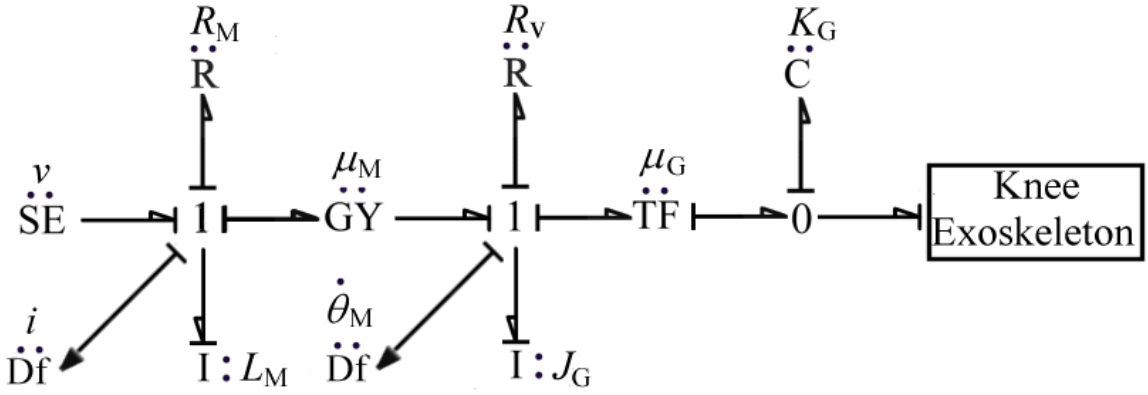

Fig. 3.15 BG model of DC motor

s

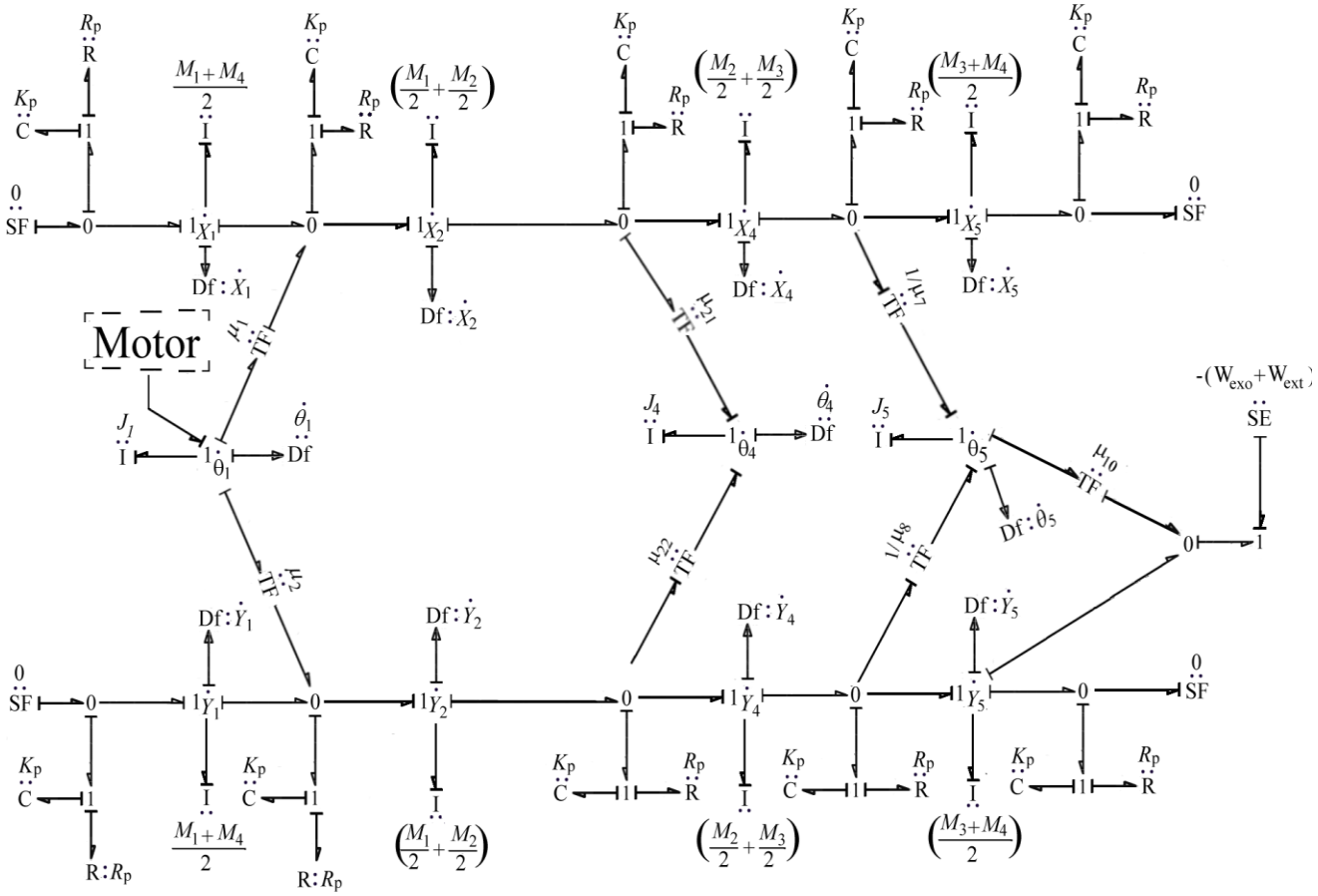

Fig. 3.16 BG model of the knee exoskelton driven by rotary actuator

3.4.5 Performance Comparison

The knee exoskeletons actuated by linear and rotary actuators are simulated for the stand -sit - stand in a specialised BG simulation software Symbols Shakti. Different external loads $W_{exo,}$ (W_{exo} + 20 N), (W_{exo} + 40 N) and (W_{exo} + 60 N) are added at the point 7 of the knee exoskeletons to check the efficacy of the current design to meet the minimum and maximum torques requirement for the STS motion, where, W_{exo} = 28.86 N is the weight of exoskeleton and additional weight with W_{exo} is the effective weight of the upper part of the user wearing KE. The major advantage of using BG technique is that it is easy to model the system containing different elements in different energy domains and only kinematic equations are required to develop dynamic model of the system. The dynamic equations can easily be derived using software. The simulation time for a sand-sit-stand cycle is approximately 10.3 s. The parameters used for BG simulation of the knee exoskeletons systems are specified in Table 3.2. Few parameters (of four bar mechanism) are measured while

others (parameters of the actuator) are either taken from the manufacturer's catalogue or from the product's specifications. Table 3.3 represents the initial position for the exoskeleton.

Table 3.2 Values of parameters used in BG models of KE

Parameters	Values
Knee Exoskeleton	
Mass of d_1(M_1)	0.104 kg
Mass of d_2 (M_2)	0.149 kg
Mass of d_3 (M_3)	0.069 kg
Mass of d_4 (M_4)	0.316 kg
Length of d_1	0.080 m
Length of d_2	0.115 m
Length of d_3	0.053 m
Length of d_4	0.117 m
Effective weight of the exoskeleton (W_{exo})	28.86 N
Distance of centroid of piston from piston end (l_{P1})	0.09 m
Width of piston (d)	0.02 m
Linear Actuator	
Voltage (v)	12 V
Motor constant (μ_M)	1 Nm/A
Motor armature resistance (R_M)	0.1 Ω
Motor inductance (L_M)	0.5 H
Torsional stiffness for gear (K_G)	10^7 N/m
Mass moment of inertia of lead screw (J_L)	0.1 kgm^2
Damping of lead screw (R_L, R_C)	0.1 Ns/m
Lead of lead screw (L)	0.115 m
Stiffness of lead screw (K_L)	10^7 N/m
Rotary Actuator	
Voltage (v)	18 V
Gear ratio(μ_G)	0.0895
Motor constant (μ_M)	1.5 Nm/A
Contact damping (R_P)	300 Ns/m
Contact stiffness (K_P)	10^8 N/m

Motor armature resistance (R_M)	1.0 Ω
Motor inductance (L_M)	0.1 H

Table 3.3 Initial position for the exoskeleton's simulations

Point	**Angle/Length**	***x* (m)**	***y* (m)**
Point 1 on d_4 and d_1	-	0	0
Point 2 on d_1 and d_2	-	-0.016	0.078
Point 3 on d_2	-	0.033	0.108
Point 4 on d_2 and d_3	-	0.082	0.139
Point 5 on d_3 and d_4	-	0.080	0.086
Point 6 on piston's end and on d_3	-	-0.053	0.456
Piston end on d_1 and d_2	-	-0.016	0.078
Actuator's length (d_9)	0.379 m	-	-
Actuator angle from X^+axis	275.6°	-	-

(a) Motor characteristics

Figure 3.17(a) and 3.17(b) show characteristics of current for linear and rotary actuators during stand-sit motion simulations for different loads. Just at the start of the stand-sit motion, an initial spike in the motor current is observed for each load. The current in the motor peaks at 8A and then drops to zero in 1.5s. As the time increases, the current drawn by the motor starts to increase again and reaches 4.8A, before settling down to 3.8A, in 5.15s, for all the loads as depicted in Fig. 3.17(a). For the case of rotary actuator, there is a sudden surge in the current. The current reaches the maximum value of approximately 15.4A and then becomes constant for the entire duration of the stand-sit transfer.

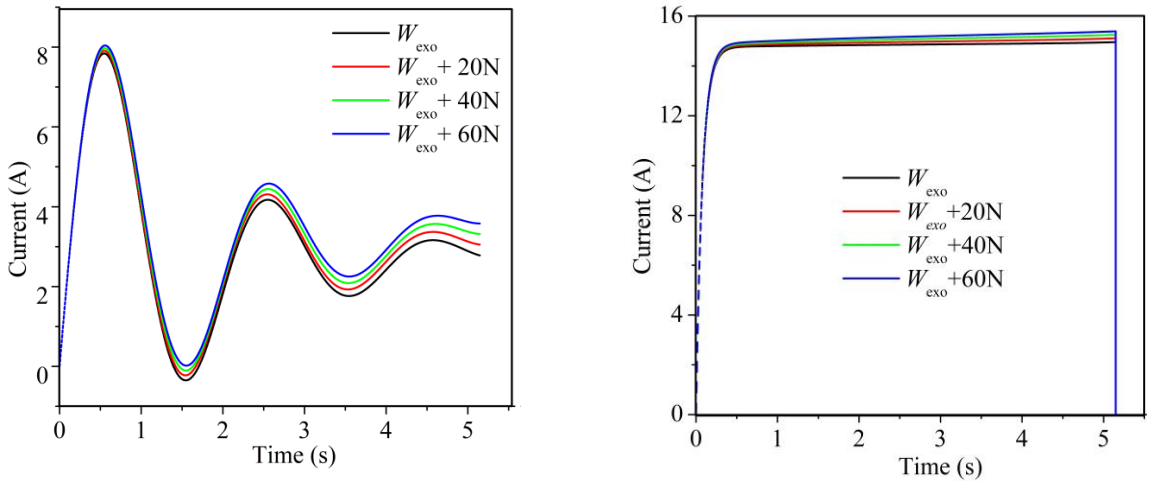

(a) (b)

Fig. 3.17 Motor characteristics (current) for stand to sit position (a) Linear actuator and (b) Rotary actuator

The initial current spike in the motor's current as shown in Fig. 3.17(a) and 3.17(b) is caused by the fact that the motor draws larger stator current to counter the increase in the mechanical load which causes conductors of armature to move slowly through the electromagnetic field. Thus, the back electromotive force (emf) is reduced. The reduced back emf allows a larger current to flow through the armature and these larger current increases driving torque. A slight increase in the motor current is observed for each load. Furthermore, the motor constant in the case of rotary actuator is 1.5 Nm/A and thus the value of the motor torque is 1.5 times the motor current unlike the case of linear actuator where the motor constant is 1 Nm/A as shown in Fig. 3.18(a) and 3.18(b).

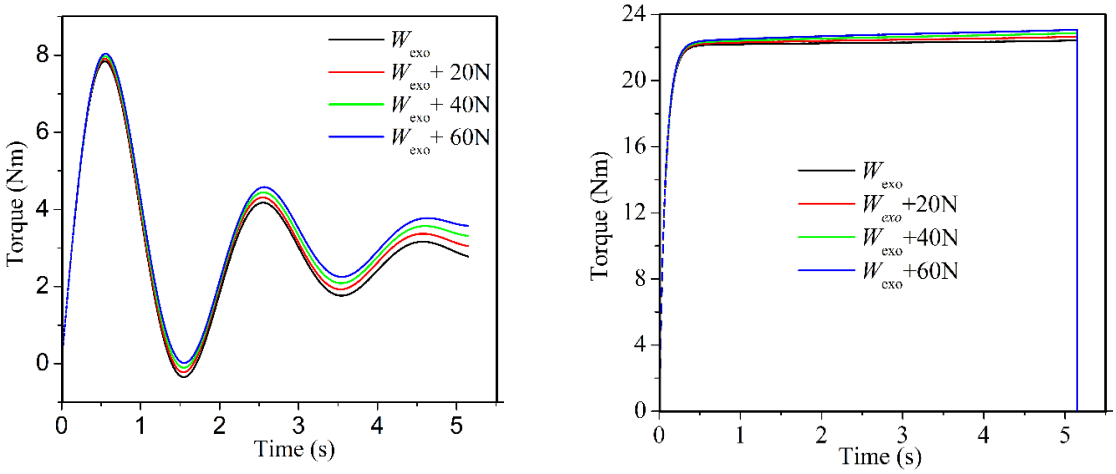

(a) (b)

Fig. 3.18 Motor characteristics for stand to sit position i.e. torque for (a) Linear actuator and (b) Rotary actuator

(b) Comparison of angle of rotation during STS motion

The values of the angle of rotation of the links of the four-bar mechanism in the KE when it is actuated by the linear and rotary actuator are determined. Figure 3.20(a) and 3.20(b) represents the angle of rotation of d_1, d_2 and d_3 of four bar mechanisms for linear and rotary actuator during a cycle of stand-sit-stand motion where 10.3 s is required for the loads of W_{exo} and W_{exo} +20 N. Meanwhile, d_1 and d_3 are initially at 1.77 rad (101.4°) and 1.54 rad (88.2°) with respect to the positive direction of x-axis which is considered as the stand position of the rotor. With increase in the cycle time, the angle achieved by the links increases and reaches to the maximum value of 2.71 rad (155.3°) and 3.08 rad (176.5°), respectively at 5.15 s. Thus, the value of angles, by the links d_1 and d_3, to attain sit position are 53.9° and 88.3°, respectively. At 10.3 s the locations of the links at the end of the cycle have the following values 1.75 rad (100.3°) for link 1 and 1.53 rad (87.7°) for link 2. Consequently, the total angles achieved by the links d_1 and d_3 during the complete STS cycle into 10.3 s are only 107.8° and 176.6° as mentioned above. The link d_3 is the thigh link which is used to rotate the human thigh during STS motion in the sagittal- plane and the angle developed by it is known as the joint angle. A very little difference is seen with the STS motion in the change in the angle turned by the link d_2. It is found that d_2 gets a total angle of 3.3° during the stand-sit-stand motion.

For rotary actuator-based KE, the angles achieved by the link d_1, d_2 and d_3 during the entire stand-sit-stand cycle are 108.6°, 3.72° and 176.78°, respectively. It is important to note that angles achieved by the d_1, d_2, and d_3 with respect to cycle time are approximately the same for the loads W_{exo} and W_{exo}+20 N. This shows that both the linear and rotary actuator can provide the necessary range of rotations to the thigh link for the desired STS motion. Furthermore, when the KE is driven either by the rotary or by the linear actuator, the total angle achieved by the thigh link with respect to time remains same. Thus, it is found that both proposed actuators can provide the desired rotation of the thigh link needed for the STS motions. Furthermore, simulations are carried out to estimate the desired knee joint torque which is the torque developed by the actuator at joint 5 of the exoskeletons for the STS motion. Figure 3.19 shows the body postures of the wearer during the STS operation using the KE. It shows the angle of rotation of the thigh link (d_3) when the wearer performs the STS motion.

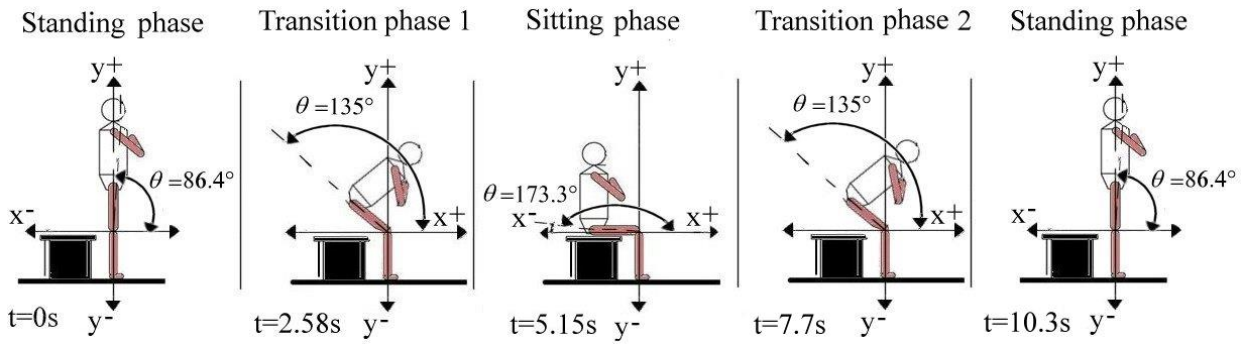

Fig. 3.19 Body postures during the stand-sit-stand cycle with KE

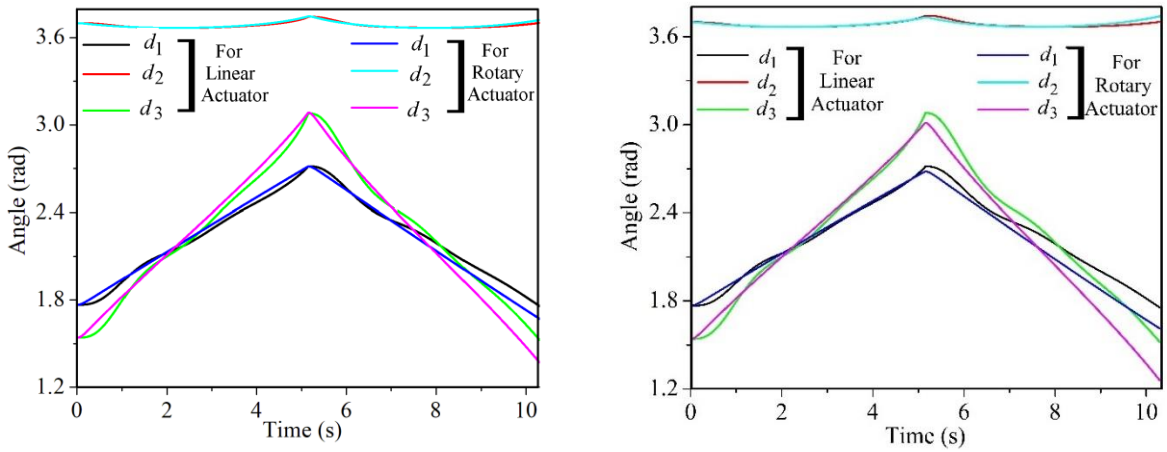

(a) (b)

Fig. 3.20 Angle of rotation of the links for linear and rotary actuator with weights of (a) W_{exo} and (b) W_{exo}+ 20 N

3.4.6 Simulation for Effectiveness of Design under Various External Loads

Figure 3.21(a) and 3.21(b) show the knee joint torques developed by linear and rotary actuator, respectively at different loads for the complete stand-sit-stand cycle of 10.3 s during simulation. As the cycle starts, an increase in joint torque is observed as time increases and reaches the maximum value at 5.15 s which is the sit position. The torque value starts to decrease as time progresses and reaches to the minimum at the stand position at 10.3 s. With increase in the load, the maximum torque developed by the actuator at joint 5 increases. This is due to the fact that as the transition from stand to sit takes place, the moment arm increases which results in the increase in the torque developed at the joint 5 (knee joint) of the exoskeleton. The maximum values of the knee torques when the exoskeleton is driven by linear actuator are found at 10.93 Nm, 23.8 Nm, 31.24 and 39.7 Nm for W_{exo} , W_{exo}+20N, W_{exo}+40N and W_{exo}+ 60N, respectively at sit position at

5.15 s. Similarly, for the case of rotary actuator, the corresponding maximum knee torque values for different loads W_{exo}, W_{exo}+20N, W_{exo}+40N and W_{exo}+ 60N are found as 20.17 Nm, 31.47 Nm, 44.25 Nm and 57.21 Nm, respectively. To facilitate better comparison, the recorded knee torque at joint 5 is plotted against the cycle time with different weightage. These weights are selected to verify the current KE design of using two actuators to meet the different torque demands.

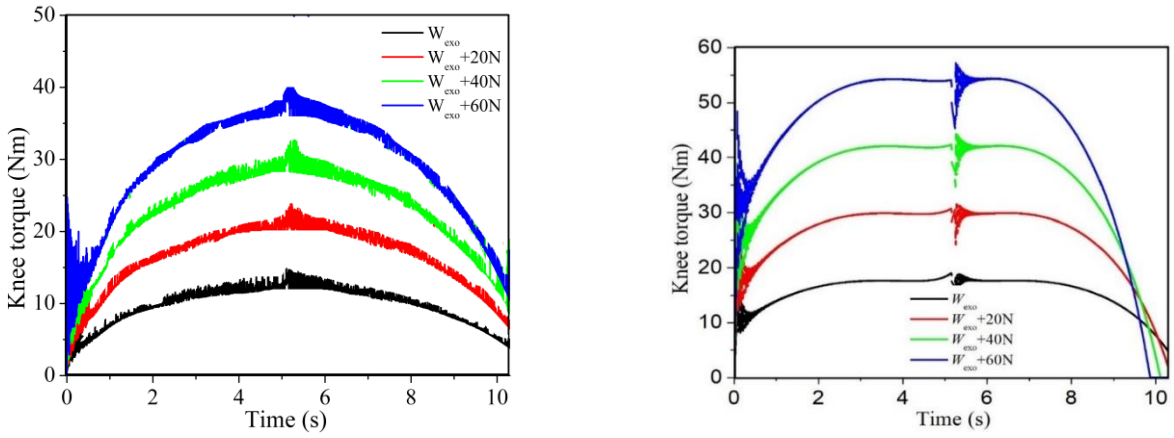

Fig. 3.21 Knee torque *vs* time for different weights using (a) Linear actuator and (b) Rotary actuator

Figure 3.22(a) and 3.22(b) represent the plots for the knee torque values with respect to the angle achieved by d_3 for linear and rotary actuator, respectively for stand-sit motion. The time required for stand to sit position is 5.15 s and the total time required for stand-sit-stand is about 10.3 s. Due to the uniformity of the graph in the second part, only the first part of the cycle is shown in Figure 13. It could be seen that the maximum torque is developed by the actuator at the sit position when the link d_3 (thigh link) has achieved a total angle of 88.3° from its initial stand position. The position of the link d_3 at the sit position is 173.3° from $+x$ axis as shown in the Fig. 3.22. The maximum torque developed by the linear and rotary actuator are approximately 40 Nm and 57 Nm, respectively. An initial spike in the knee torque is observed for stand-sit motion. This is because the motor exerts greater amount of torque to overcome the inertia of the link d_3 to be rotated as seen from the Fig. 3.22(a) and 3.22(b), respectively.

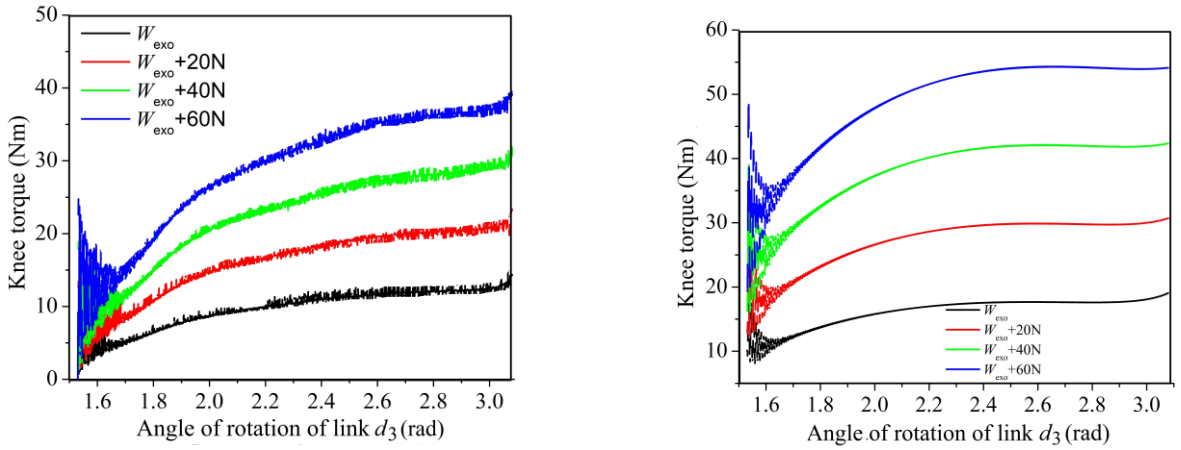

Fig. 3.22 Knee torque *vs* angle of rotation of d_3 for different weights for (a) Linear actuator and (b) Rotary actuator

It can be noted that the torque developed by the linear and rotary actuator at the knee joint is suitable to provide significant assistance to the user for performing stand-sit-stand motions. The maximum torque required for STS motion as per the literature for a healthy male of height 178 cm and mass 80 kg free from any musculoskeletal and neurological injuries is 67.2 Nm.[97]

The KE based on linear and rotary actuator can deliver the maximum knee torques of 40 Nm and 57.21 Nm, respectively, thus providing approximately 60 % and 85 % of the external assistive torque required at the knee joint for the stand-sit-stand motion, thereby, limiting the user efforts to only 40 % and 15 % respectively. However, the rotary actuator limits the user effort to minimal. Thus, either of the linear or rotary actuator are effectively capable to provide the required torque for STS motions in the proposed KE based on four-bar mechanism. Therefore, a knee exoskeleton for the purpose of reconfiguration is possible when powered by these two actuators.

3.5 Conclusions

A knee exoskeleton based on four-bar mechanism consisting of a linear actuator has been designed, modelled, and fabricated in this work. The modelling and simulation have been performed using the bond graph technique. The modelling performed using the bond graph technique was useful to identify the characteristics of the linear actuator and the amount of knee torque that the exoskeleton can develop before fabrication of the actual exoskeleton. The torque developed by the actuator at the knee joint is sufficient to assist the wearer in performing the desired motion. As a result, the user needs to apply minimal effort while using the proposed device. The range of joint angle values

obtained from the design is also in line with the literature. Thus, the design of the knee exoskeleton is well suited to assist the wearer during the desired stand-to-sit motion or vice versa.

The dynamic modelling of the knee exoskeletons based on linear and rotary actuators have also been studied in this work for STS motion using BG technique in a specialised simulation software. The results are obtained for motor current and torque, angles of rotation of the links of the four-bar mechanism and knee joint torque developed by the linear and rotary actuator when combined in a KE. It is found that both actuators provide same degree of rotation of the links of the four-bar mechanism with respect to the cycle time for stand-sit-stand motion. This proves that the present knee exoskeleton, when combined either with linear or rotary actuator is capable to provide the required range of motions to the thigh link for STS motions. Furthermore, the found maximum torque developed by the linear and rotary actuators at the knee joint of the exoskeleton prove that the device may significantly assist the users during the STS transfer. However, the rotary actuator was found to limit the wearer's effort to the minimal in comparison to that of linear actuator in the present design of KE. Therefore, for performing STS motion, the current four-bar mechanism is well suited to accommodate both the linear and rotary actuator. The work provides a useful foundation to design a KE for the cases when the primary actuator ceases to work due to a sudden fault or battery discharge. In such scenarios, the secondary actuator must be able to provide the necessary actuation required for the desired STS motion. The BG approach to model the system proved to be quite useful as only the kinematic equations were required to model this multi-domain exoskeleton system. The dynamic equations are automatically derived from the simulation software.

In the subsequent chapters the focus is on the development of the exoskeleton prototype. The fault detection, isolation, and reconfiguration (FDI) are implemented where the secondary actuator would be provided along with the present linear actuator in the proposed exoskeleton. The research would also be focused on optimizing the exoskeleton's design parameters to achieve a greater joint range of motion and knee joint torque for different activities of daily living.

Chapter 4

Fabrication of Knee Exoskeleton and Experimental Validations for STS Motions

4.1 Introduction

The development and fabrication of knee exoskeletons mark a significant advancement in wearable robotics, aimed at improving mobility and restoring functional abilities for individuals with lower limb impairments. This chapter explores the intricate process of designing, fabricating, and integrating key components essential for a knee exoskeleton tailored specifically for Sit-to-Stand (STS) motions.

Critical to the fabrication of any exoskeleton is the careful selection of materials and design considerations to ensure functionality and user comfort. Lightweight yet durable aluminium alloys play a crucial role in maintaining structural integrity while minimizing overall weight, thereby optimizing usability, and reducing user fatigue during extended use. Advanced Computer-Aided Design (CAD) software enables precise modelling and simulation of the exoskeleton's structural framework, joints, and linkages, ensuring seamless interaction and compatibility between moving parts.

At the core of the knee exoskeleton lies the primary actuator, pivotal for generating motion and assisting with joint movements during STS transitions. Chosen for its high load capacity and efficient power consumption, the actuator is meticulously integrated into the exoskeleton's framework. Enhancing the functionality and responsiveness of the knee exoskeleton are advanced sensor technologies and feedback systems. Gyroscopes and accelerometers, like the GY 521 MPU 6050 modules, provide real-time measurement of angular velocities and accelerations crucial for monitoring joint movements. Integrated with the exoskeleton's microcontroller, these sensors enable precise data acquisition and analysis, forming the basis for future closed-loop control strategies aimed at enhancing operational efficiency.

A load cell further augments the exoskeleton's capabilities by measuring forces exerted during STS motions. Utilizing strain gauge technology within a Wheatstone bridge configuration, the load cell converts mechanical forces into electrical signals. Analog-to-Digital Conversion (ADC) facilitates accurate measurement and calibration of force readings, providing essential

feedback for optimizing actuator performance and ensuring safe operation under varying user loads and conditions.

The knee exoskeleton's operational infrastructure is supported by efficient power supply and control electronics. A robust 12 V battery system, complemented by voltage regulators and protective circuitry, ensures stable power distribution to critical components such as actuators and microcontrollers. Control electronics, centred around an Arduino UNO R3 microcontroller, orchestrate the exoskeleton's operation by interpreting sensor data, executing control algorithms, and managing communication protocols. This integration of hardware and software facilitates seamless interaction between user inputs and desired mechanical outputs, highlighting the exoskeleton's adaptability and user-centric design.

In this chapter, the knee exoskeleton is tested to validate its functionality during Sit-to-Stand (STS) motions. Essential equipment is employed for fabricating and controlling the exoskeleton in an open-loop configuration, confirming its capability to perform effectively. The actuator, operating at 12 V with a robust load capacity of 900 N and constructed from lightweight aluminium alloy, incorporates safety features such as travel limit switches and a self-locking mechanism to prevent potential damage and ensure secure positioning. The actuator force and knee torque are measured and compared with the simulation results to verify the efficacy of the developed knee exoskeleton.

4.2 Development and Integration of Components of the Knee Exoskeleton

The knee exoskeleton serves as a critical device in assisting sit-to-stand (STS) motions, enhancing mobility, and reducing effort for users. This section details the fabrication and testing of the knee exoskeleton in an open-loop configuration specifically designed for STS movements. Key equipment essential for controlling and monitoring the exoskeleton's performance is outlined in Table 4.1. The experimental validation focuses on assessing the exoskeleton's functionality under various conditions, including load variations and integration with electromyography (EMG) sensors for muscle activity monitoring.

Table 4.1 Equipment specifications

Equipment	Quantity	Specifications and features
Arduino UNO R3	2	Microcontroller ATmega328P, operating voltage 5 V
Linear Actuator	1	DC 12V, Banggood Stroke Tubular Motor (JS-TGZ-UI), Maximum load current 3A, No-load current < 1A, 900N force capacity, 10% duty cycle, 20-30W rated power
GY 521 MPU 6050	2	3-axis analog gyro sensors + 3-axis accelerometer module, I2C communication, compatible with Arduino UNO
Load Cell	1	150 kg weighing load cell sensor, Dimensions: 130 mm x 40 mm x 22 mm, Integrated with 24-bit ADC converter for precise force measurement
EMG Sensor	1	RKI-2401 EMG Muscle Sensor V3, Dual power supply: +9 V and +3.5 V, Amplification factor of 500, Analog output
Relays	1	5 V, Double Pole Double Throw (DPDT) relay for controlling higher voltage circuits
Batteries	2	9 V Zinc Carbon Battery, Power supply for sensors and low-power electronics

4.2.1 Actuator Specifications and Safety Features

The actuator used in the exoskeleton operates at 12 V with a robust load capacity of 900 N, constructed from lightweight aluminium alloy. Each side of the actuator features a push bar equipped with a travel limit switch. This safety feature ensures that if the telescopic bar extends to its maximum length, it automatically cuts off power to the motor, preventing any potential damage. Additionally, the actuator includes a self-locking mechanism that allows it to hold its position securely even when power is not supplied.

4.2.2 Integration of EMG Sensors with Control Electronics

Figure 4.1 provides a detailed depiction of the interconnected components within the knee exoskeleton system. Central to this setup are the electromyography (EMG) sensor electrodes, crucial for sensing and recording the wearer's muscle activity, particularly during movements such as sitting or standing. These electrodes detect electrical signals generated by muscle contractions,

with the amplitude of the recorded voltage directly reflecting the intensity and number of engaged muscles.

To effectively capture and process these signals, the EMG sensor electrodes transmit the electrical data to an integrated EMG muscle sensor circuit. This sensor unit operates using two 9V batteries to power its functions. Initially, the raw EMG signals picked up by the electrodes are relatively weak and high-frequency in nature. To ensure accurate measurement and effective signal processing, the sensor unit amplifies these signals by a factor of 500. This amplification significantly boosts the signal strength. This makes it more suitable for subsequent stages of processing.

Once amplified, the EMG signals undergo further processing within the sensor module. This includes rectification and smoothing procedures to convert the oscillatory EMG signals into a stable format suitable for digital processing. The processed voltage signals are then transmitted to an Arduino UNO microcontroller, a critical component in the control and coordination of the entire exoskeleton system. However, the actuator responsible for driving the knee exoskeleton operates at a higher voltage range of 12 V to 24 V, which exceeds the operational capability of the Arduino UNO directly. To bridge this voltage disparity, a 5 V relay is incorporated into the system architecture. The Arduino UNO microcontroller outputs 5 V control signals to the relay, which acts as a switch to regulate the higher voltage supply (12 V or 24 V) required by the actuator. This relay mechanism ensures that the actuator receives the appropriate power to perform its intended functions based on the input from the EMG signals.

Powering this intricate setup is a robust 12 V, 2.5 A battery, strategically chosen to supply sufficient electrical energy to both the Arduino microcontroller and the actuator. This battery serves as the primary power source, ensuring continuous and reliable operation of the knee exoskeleton system during use.

Once activated, the actuator drives a four-bar mechanism integrated into the exoskeleton structure. This mechanism is meticulously designed to mimic and support natural human movements, facilitating smooth transitions between sitting and standing positions. By leveraging mechanical assistance from the exoskeleton, the wearer experiences enhanced mobility and support in performing everyday activities with reduced effort and strain.

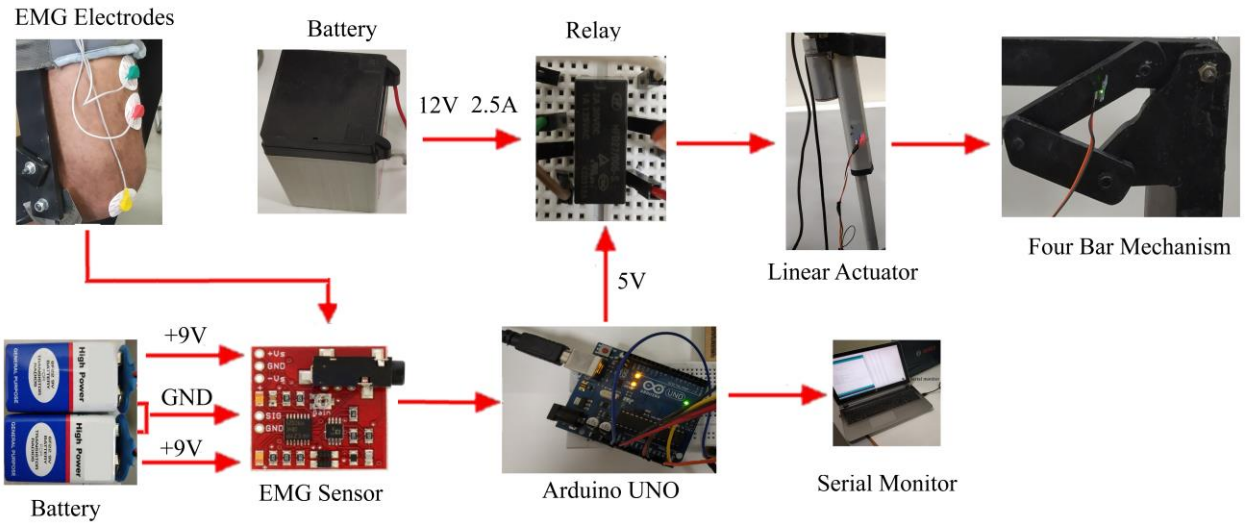

Fig. 4.1 Configuration of components in the knee exoskeleton

4.2.3 System Integration and Sensor Connectivity

The interfacing and connectivity of sensors with the microcontroller are illustrated in Fig. 4.2. Figure 4.2(a) displays how the Motion Processing Units (MPUs) and the load cell are integrated with the Arduino UNO. The MPU-6050 communicates with the Arduino via an I2C serial connection, facilitated by the Arduino wire library. This communication protocol uses two lines: SDA (Data) and SCL (Clock). On the Arduino UNO board, the SDA line corresponds to analog port A4, while the SCL line is connected to A5.

In this work, two MPUs are utilized: one is fixed at the front end of the actuator, and the other is fixed at the front end of link d_2. Calibration of the MPU involves placing it along a reference line on a flat surface and rotating it through various angles. A manual goniometer is employed to verify these angles against actual rotations measured by the MPU, establishing a calibrated scale. The Arduino program adjusts for offsets to ensure accurate readings across different rotational positions. The first MPU provides the actuator angle (δ_1), while the second MPU provides the angle of link d_2 with respect to the ground (x-axis), enabling calculation of δ_1 by finding the difference between the two angles.

A load cell, serving as a transducer, measures the force exerted by the actuator during experiments. This load cell employs four strain gauges in a Wheatstone bridge configuration to detect force. When the actuator generates force, it deforms these strain gauges, translating the force into electrical signals. These signals are processed by an Arduino board equipped with a 24-bit

Analog to Digital Converter (ADC). Connections involve wiring the load cell's power, ground, data transmission (DT), and serial clock (SCK) wires to the Arduino UNO's VCC, GND, A1, and A6 pins, respectively. The output signals are observed via a serial monitor and calibrated for accuracy.

During experimental trials, the actuator's forces during stand-sit-stand motions are recorded using the load cell. Forces peak at specific times, influenced by both the exoskeleton's own weight and additional weights applied at designated points. These force measurements are crucial for calculating the torque exerted at joint 5 of the knee exoskeletons (KE), providing insight into the mechanical performance under different loads.

Calibration of the load cell involves setting it up as a cantilever beam, securely mounting one end and noting its readings under no-load conditions. A calibration factor is applied to zero the current readings, ensuring accurate measurements. Subsequent tests involve hanging known weights on the load cell to verify its linear response and repeatability.

The Electromyography (EMG) electrodes interface directly with the Arduino UNO via an amplifier powered by two 9V batteries connected in series. The electrodes capture muscle movement signals, which are amplified 500 times to enhance sensitivity. Raw EMG signals are high-frequency and oscillatory, requiring rectification and smoothing before being sent to the Arduino for further processing. These processed signals inform the Arduino of muscle activity, facilitating real-time adjustments in the exoskeleton's operation.

In this work, motion control does not employ a sensor feedback loop; instead, a Double Pole Double Throw (DPDT) relay configuration (Fig. 4.2(c)) is used to control the actuator during stand-to-sit motions. Node A connects to the Arduino's +5 V pin, enabling the relay to manage higher voltages (12–24 V) necessary for actuator control.

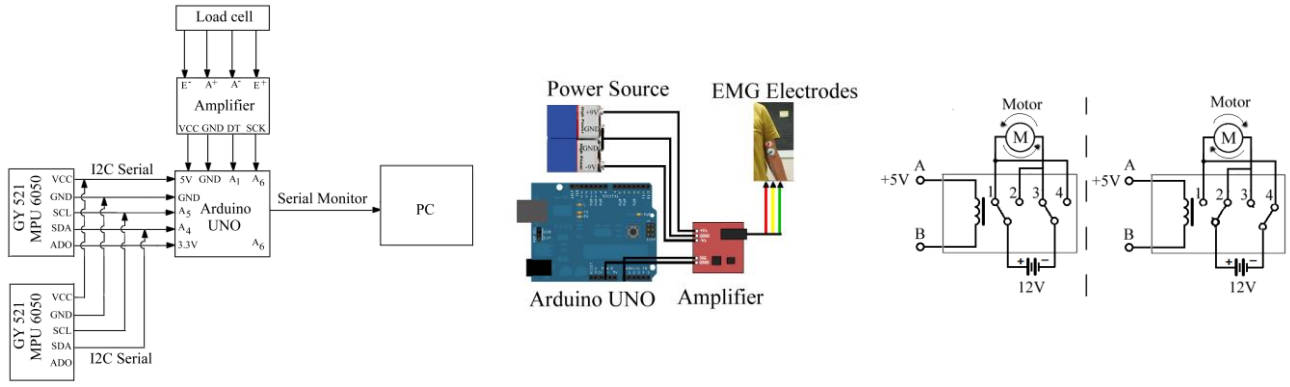

(a) (b) (c)

Fig. 4.2 Schematic of sensor integration in the knee exoskeleton

4.2.4 Experimental Methodology and Data Acquisition

Experimentation involves testing of an artificial limb equipped with a custom-designed knee exoskeleton to validate simulated outcomes and demonstrate practical functionality. This specialized exoskeleton is tailored for seamless integration with artificial limbs, facilitating precise execution of targeted movements. The experimental setup meticulously replicates real-world conditions to accurately evaluate the exoskeleton's performance.

Figures 4.3(a)–4.3(d) showcase diverse perspectives of the experimental arrangement, illustrating how the knee exoskeleton interfaces with the artificial limb from various angles. These visuals capture detailed insights into the exoskeleton's adaptation and ergonomic design, essential for comprehensive functional assessment.

Figures 4.3(e)–4.3(h) outlines the individual components comprising the current iteration of the knee exoskeleton. Each component plays a vital role in enhancing limb mobility and facilitating smooth execution of intended motions. Figure 4.3 depicts the key elements contributing to the exoskeleton's operational efficacy during experimental trials.

Through thorough experimentation, the fabricated knee exoskeleton undergoes validation against simulated scenarios. This process not only verifies the accuracy of initial simulations but also affirms the exoskeleton's practical utility in real-world applications.

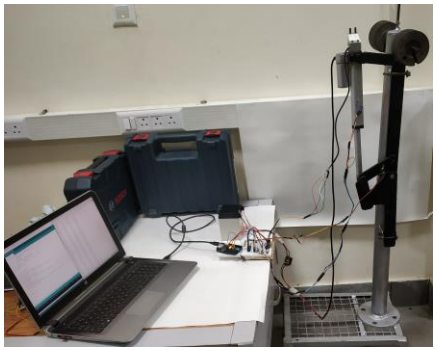

(a)

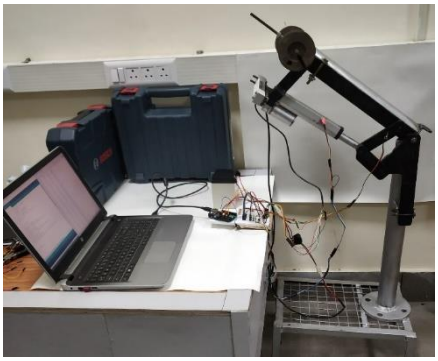

(b)

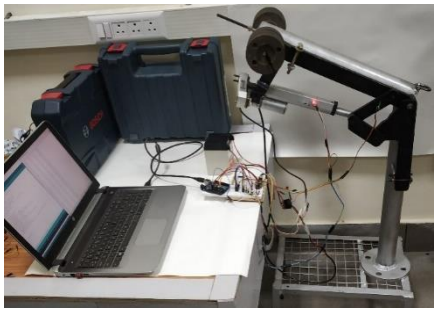

(c)

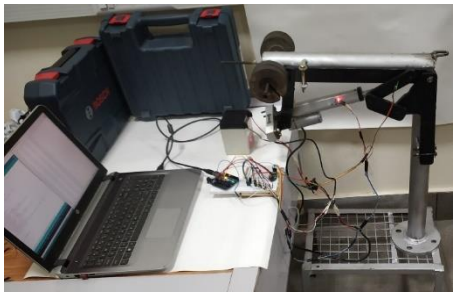

(d)

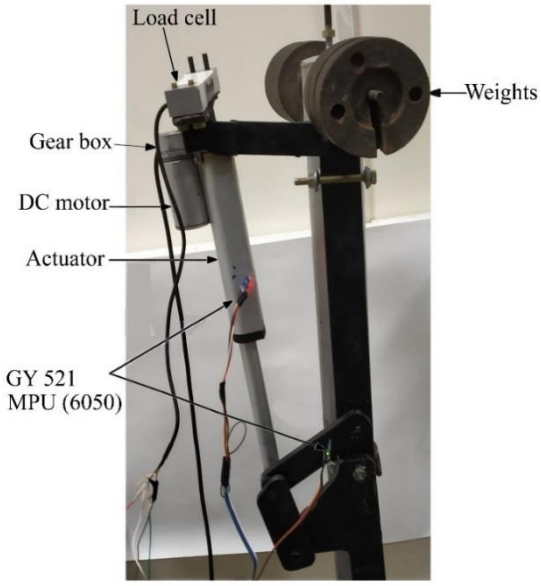
Load cell
Weights
Gear box
DC motor
Actuator
GY 521
MPU (6050)

(e)

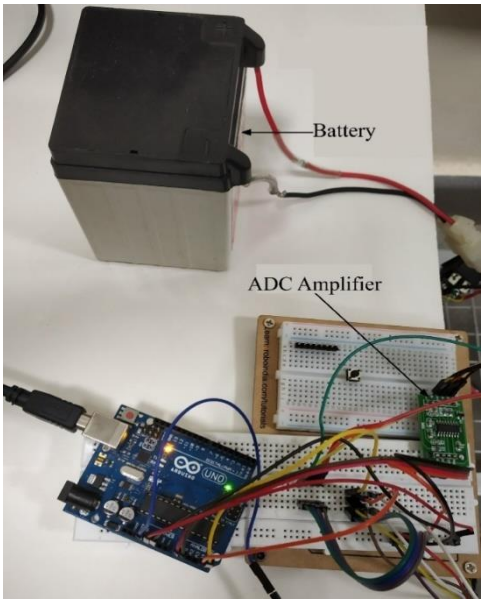
Battery
ADC Amplifier

(f)

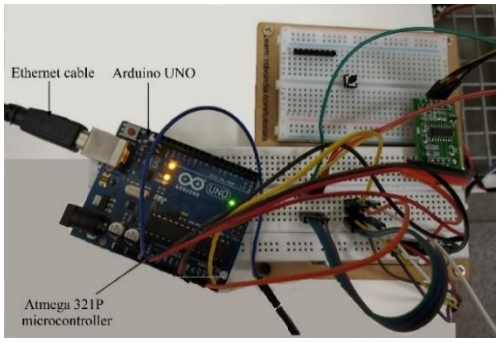

(g)

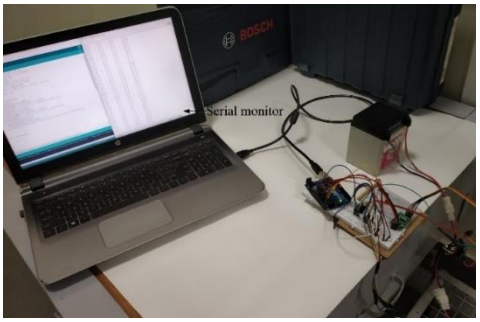

(h)

Fig. 4.3 Multi-angle perspectives of the experimental configuration

The experiments focused on testing a complete cycle of stand-sit-stand motion using the fabricated knee exoskeleton under varying loads. These loads included scenarios with no external weight and additional weights of 20 N, 40 N, and 60 N, which simulate different wearer body weights to assess the exoskeleton's performance across realistic conditions. It's important to note that these specific weights are not typically required during actual use by a wearer.

4.3 Actuator during Sit-to-Stand Motions

In this section, the experimental findings concerning the dynamics of actuator force and joint angle variations in the knee exoskeleton during Sit-to-Stand (STS) motions are presented. It includes a detailed analysis of how the actuator force dynamically changes throughout the motion cycle, alongside variations in the joint angle *(θ).* Furthermore, the experimental results with simulations are compared to assess the accuracy and performance of the exoskeleton under different load conditions.

4.3.1 Experimental Findings on Actuator Force Dynamics and Comparison with Simulation

Figure 4.4 presents the experimental findings related to the actuator force (F) and the angle *(θ)* between the actuator and d_2 over the duration of the STS motion cycle, which lasted approximately 10.3 seconds. During this cycle, the actuator force exhibited distinct behaviour: it initially increased and peaked at specific intervals. For instance, the force peaked at 311.32 N (due solely to the exoskeleton's self-weight of 28.86 N), 474.62 N, 605 N, and 660.48 N (including the self-weight and an additional 60 N external load) within the first 5.15 seconds. Subsequently, there was a noticeable decline in force values until 5.25 s, followed by stabilization towards the end of the

10.3-second cycle, which marked the completion of the stand-sit-stand motion as depicted in Fig. 4.4(a).

This fluctuation in actuator force directly correlates with the joint angle *(θ)* over time, as depicted in Fig. 4.4(b). Initially, θ values were measured at 60.61°, 61.5°, 61°, and 61.83° for different load conditions. As the STS cycle progressed, these angles increased significantly, peaking at 156.51°, 166.21°, 162.96°, and 168.21° respectively at 5.15 seconds. This increase is attributed to the rising joint angle during the stand-to-sit transition, which elongates the moment arm and consequently increases knee torque. To counteract this increased torque, the actuator force (*F*) correspondingly increased. As the actuator approached its maximum extension, θ gradually returned to its initial values towards the end of the cycle. These experimental results not only validate the exoskeleton's capability to support STS movements under varying loads but also provide valuable insights into its performance dynamics throughout the motion cycle.

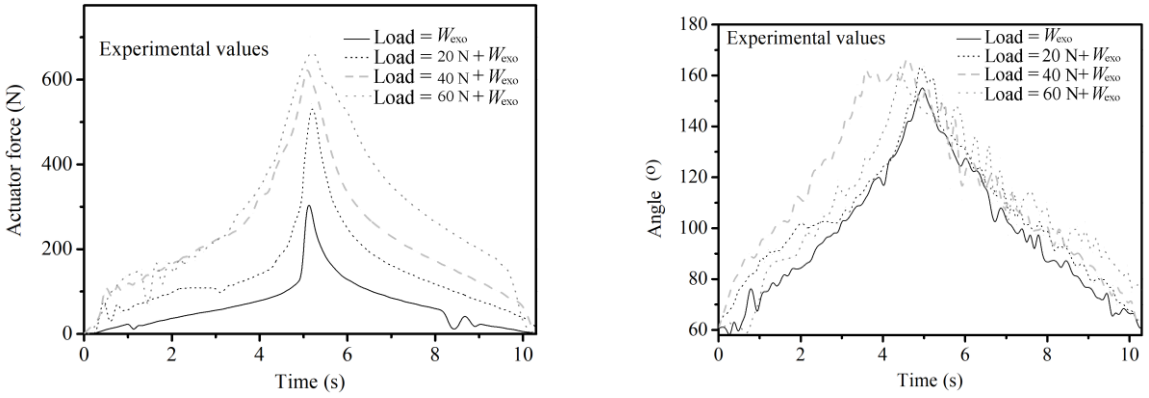

(a) (b)

Fig. 4.4 Experimental analysis for (a) actuator force and (b) angle between Link 2 and the actuator

Figure 4.5 provides a comparison between the experimental and simulated values of the actuator force over time under various load conditions. Throughout the duration of each load cycle, the simulated actuator force consistently shows a slight increment compared to the experimental values. This marginal difference primarily stems from the slower response of the affordable controller used with the load cell during the experimental trials.

Furthermore, Fig. 4.5(a), 4.5(b) and 4.5(d) reveal a minor variance in the peak actuator force between the experimental and simulated data.

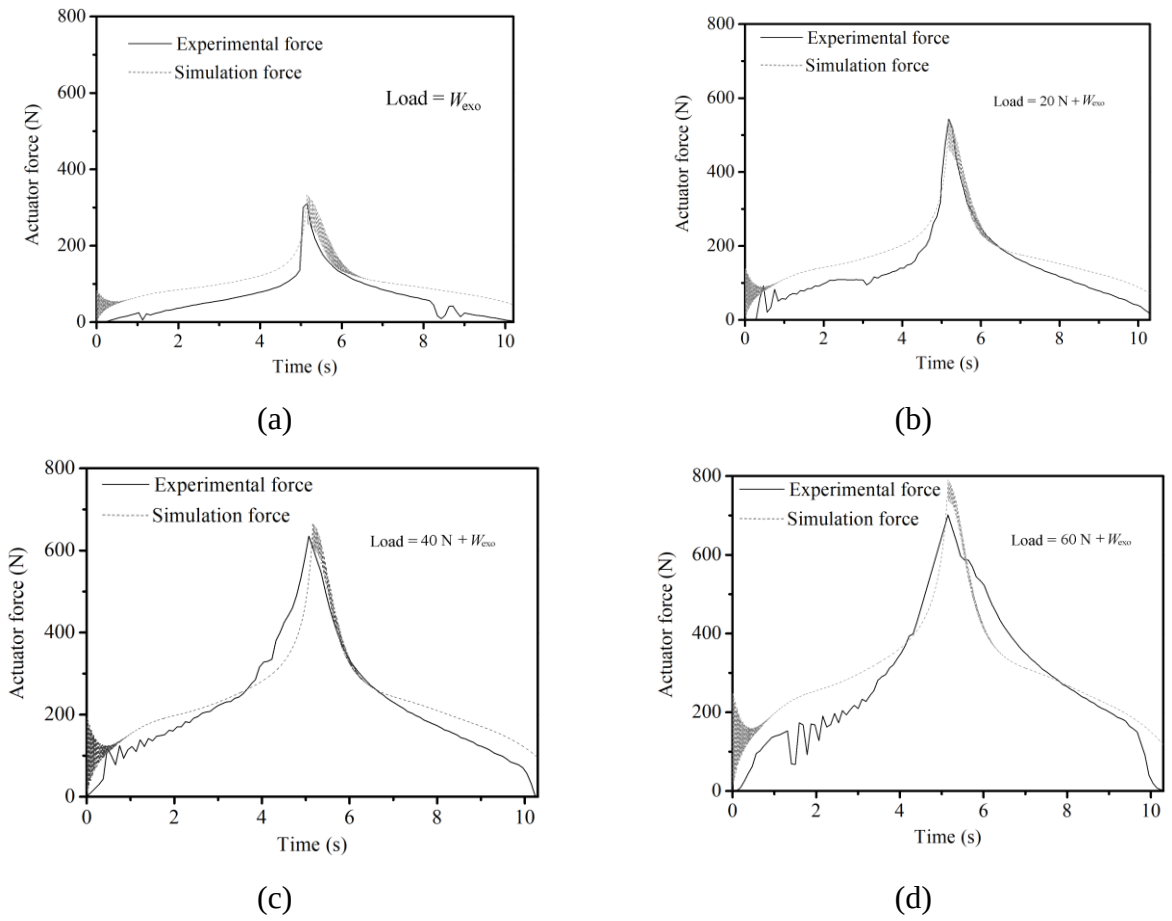

Fig. 4.5 Actuator force comparison: Experimental vs. simulated loads

4.3.2 Integration of EMG Sensor for Motion Detection

The experimentation involved not only utilizing a DPDT relay for open-loop control but also integrating an electromyography (EMG) sensor to facilitate a complete cycle of stand-sit motion. The EMG sensor's primary function was to detect the wearer's intention to change motion states, eliminating the need for manual control switches. With the Arduino board already equipped with a pull-down resistor, no external resistor was necessary. The EMG output voltages, ranging from 0 to 3.25 V, were linearly mapped to match the Arduino's operating voltage range of 0 to 5 V. A threshold voltage of 1.225 V was empirically determined by averaging EMG signals during muscle inactivity, indicating the user's intention to initiate arm movement.

Figure 4.6(a) illustrates the voltage plot over the cycle time of the stand-sit motion. Meanwhile, Fig. 4.6(b) compares the experimental and simulated values of the torque exerted at

the knee joint (joint 5 of Fig. 3.3) of the knee exoskeleton (KE) under different loads. Simulation values were obtained using BG simulation software (SYMBOLS Shakti) for the models as shown in Fig. 3.5–Fig. 3.7. The knee joint torque progressively increases with cycle time for each load cycle, reaching its maximum approximately halfway through before declining to zero at the end of the stand-sit-stand motion, as observed in both experimental and theoretical scenarios.

For load scenarios A, B, C, and D, the experimental maximum knee joint torque values were measured at 11.02 Nm, 24.87 Nm, 31.07 Nm, and 40.63 Nm, respectively, while theoretical values stood at 10.93 Nm, 23.8 Nm, 31.24 Nm, and 39.7 Nm. The comparison reveals that experimental and theoretical torque values generally align within an acceptable range. However, slight deviations in peak experimental values from theoretical predictions were noted in cycles B and C, potentially attributed to unaccounted dynamics of the actuator during expansion or contraction phases.

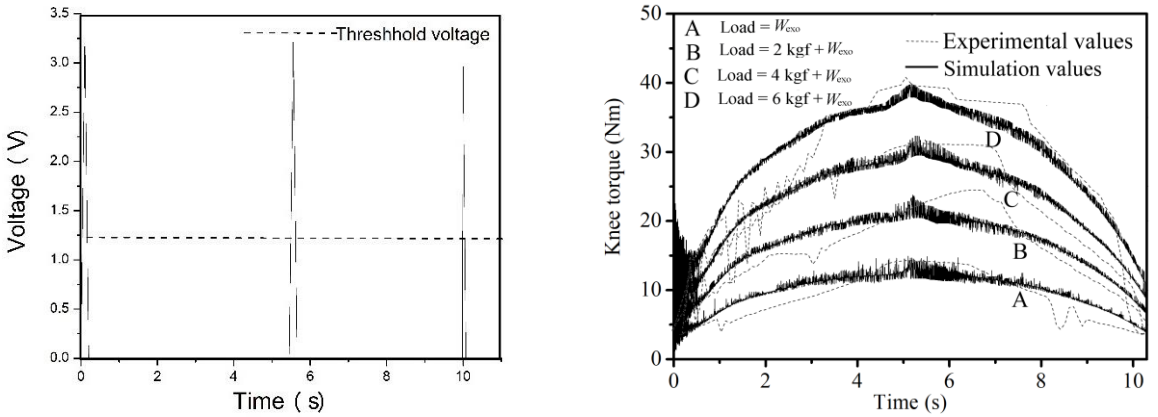

(a) (b)

Fig. 4.6 (a) Voltage plot and (b) knee torque comparison

According to the literature, the upper body comprises approximately 60% of the total body weight for both males and females, while healthy males of specific height and weight typically require a maximum average torque of 67.2 Nm or 0.84 Nm.[98] The current exoskeleton design provides a maximum torque capacity of up to 40 Nm, effectively assisting with 60% of the external torque during the STS motion, thereby reducing human effort by 40%. Integrated with the four-bar mechanism, the linear actuator ensures the desired rotation of the thigh link (d_3 as shown in Fig. 3.3(c)) necessary for facilitating the stand-sit-stand transfer.

4.4 Conclusions

Thus, this chapter details the development and testing of a knee exoskeleton specifically designed for Sit-to-Stand (STS) movements, aimed at improving mobility for individuals with knee impairments. The exoskeleton was constructed using lightweight yet strong materials like aluminium to ensure comfort and reduce fatigue. The core of the exoskeleton is the linear actuator, functioning akin to a DC motor to facilitate joint movements during STS motions. Sensors such as gyroscopes, accelerometers, and a load cell were utilized to measure movement and provide feedback, assessing the exoskeleton's performance across different conditions.

Experimental tests confirmed the exoskeleton's ability to effectively execute STS movements. Measurements of forces and torques under varied loads demonstrated the efficacy of the KE Integration of EMG sensors enabled intuitive control of the exoskeleton based on user muscle signals, eliminating the need for manual switches.

Scaling the fabricated design presented in this work for mass production necessitates a careful evaluation of cost-effectiveness and material availability. Modular designs with standardized components could reduce production costs while maintaining design flexibility. The exploration of lightweight and cost-efficient materials, such as advanced composites or reinforced plastics, could further support scalability without compromising performance. Collaboration with industrial partners would provide valuable insights into manufacturing processes and supply chain optimization, streamlining the transition from prototype to mass production. Additionally, lifecycle cost analyses could ensure economic viability and sustainability.

By addressing these considerations, the proposed knee exoskeleton system can evolve into a scalable, user-friendly, and efficient solution tailored for a diverse range of users and operating environments. These future explorations would not only enhance the technical robustness of the system but also broaden its practical applicability. In conclusion, this chapter details the design, fabrication, and validation of a knee exoskeleton tailored for STS motions. The outcomes substantiate its functional efficacy, laying a foundation for future advancements in wearable robotics to enhance user mobility and quality of life.

In the next chapter, the fault detection, isolation, and reconfiguration (FDI) would be discussed where the rotary actuator would be incorporated along with the linear actuator in the proposed exoskeleton.

Chapter 5

Fault Detection, Isolation and Reconfiguration of Knee Exoskeleton

5.1 Introduction

Knee exoskeletons represent a pivotal advancement at the intersection of robotics, biomechanics, and healthcare. Initially conceptualized for military applications to augment soldiers' strength and endurance; exoskeleton technology has rapidly evolved into versatile devices with profound implications for rehabilitation, assistive care and industrial applications. The evolution of materials science, advancements in robotics and a deeper understanding of human biomechanics have collectively propelled the development of exoskeletons from bulky prototypes to sleek, functional devices that seamlessly integrate with human anatomy.

When it comes to medical rehabilitation, knee exoskeletons have become essential equipment when it comes to increased mobility and better quality of life for patients with lower limb disorders. These devices assist users in performing activities such as walking, standing, sitting and climbing stairs, thereby reducing physical strain and facilitating earlier rehabilitation progress. Moreover, in industrial settings, exoskeletons augment human capabilities, enabling workers to perform physically demanding tasks with reduced fatigue and lower risk of musculoskeletal injuries.

5.1.1 Challenges in Fault Management and System Reliability

Knee exoskeletons face significant challenges regarding reliability and fault management due to the integration of complex mechanical, electrical and electronic components. These vulnerabilities can compromise device functionality, with common failures including mechanical wear in actuators, inaccurate sensor feedback and unexpected environmental or user interaction issues. Such failures not only disrupt operations but also pose risks to the users' safety, potentially leading to falls or worsening physical conditions. In industrial settings, equipment downtime from failures can disrupt workflow efficiency and result in substantial economic losses.

5.1.2 Role of Fault Detection, Isolation and Reconfiguration

Effective fault detection, isolation (FDI) and reconfiguration strategies are essential for mitigating risks associated with failures of knee exoskeleton and improving overall system-reliability. FDI systems continuously monitor exoskeleton's health and promptly detect deviations from expected performance and autonomously initiate corrective actions to maintain operational integrity. These strategies employ advanced sensing technologies, resilient control algorithms and adaptive reconfiguration mechanisms to monitor sensor-data and actuator-responses in real-time. By pinpointing faults through analytical redundancy techniques and fault signature analysis, they adjust control parameters or activate redundant actuators to minimize downtime and optimize performance across diverse conditions.

5.1.3 Overview of Knee Exoskeletons and Applications

Knee exoskeletons have a significant advancement in biomedical engineering and are designed to assist individuals with lower limb impairments by enhancing mobility and functionality. These devices support natural knee joint movements, aiding in daily activities and rehabilitation exercises with improved safety and reduced effort.

Applications span medical rehabilitation, assistive technology for disabilities and industrial support. In medical contexts, exoskeletons aid recovery from injuries or conditions affecting lower limb function, promoting muscle strength and joint flexibility. They also empower users with disabilities to engage actively in social and occupational activities, enhancing independence and quality of life. In industries, these devices mitigate physical strain, reducing risks of injuries and fatigue among workers while improving productivity.

Despite transformative potential, challenges persist in reliability, adaptability and safety. Integration of complex components necessitates robust fault management systems, crucial for addressing operational disruptions and maintaining user-safety in real-world applications.

5.1.4 Fault Detection and Isolation (FDI)

Fault Detection and Isolation (FDI) is critical for ensuring knee exoskeleton's reliability during dynamic motions like Sit-to-Stand (STS). This section explores methodologies and principles tailored for enhancing performance and minimizing risks in these advanced devices. FDI strategies

monitor, identify and mitigate potential faults, ensuring reliability throughout dynamic movements.

(a) Analytical Redundancy Relations (ARRs) in Exoskeleton Control

ARRs are the fundamentals in FDI strategies for knee exoskeletons during STS motion. Derived from dynamic models and sensor data, ARRs compare desired with actual system responses, detecting anomalies indicating faults in actuators, sensors or control algorithms. They monitor joint angles, torques and forces during transitions, ensuring deviations from expected behaviours those are promptly addressed.

(b) Integration of Sensors for Fault Detection

Effective fault detection relies on sensors providing real-time feedback on joint angles, forces and user interactions. Encoders, IMUs and load cells placed strategically to capture critical data during STS motions. Signal processing analyses sensor readings, identifying abnormal patterns signalling potential faults for immediate response.

(c) Mathematical Modelling for FDI in Knee Exoskeletons

Mathematical models predict exoskeleton behaviour under normal and faulty conditions, facilitating fault isolation. Residual signals from model predictions and sensor data pinpoint faults, enabling timely interventions to maintain operational integrity.

(d) System Behaviour Analysis and Simulation Techniques

Simulation software evaluates FDI algorithms and exoskeleton performance during STS motions. Researchers replicate movements, manipulate parameters and simulate faults to validate strategies before practical use. Detailed analysis optimizes robustness and effectiveness, ensuring reliable performance in diverse applications.

5.1.5 Methodology

This chapter details the approach used to develop fault detection, isolation and reconfiguration strategies specifically tailored for a knee exoskeleton designed to facilitate stand-sit-stand motions within a simulated environment. The work begins with the design of the knee exoskeleton's mechanical architecture, focusing on selecting actuators, sensors and control components suitable

for integration into the exoskeleton's framework. Special attention is given to ensure compatibility with human knee biomechanics and adherence to safety standards for assistive devices. Sensor integration and simulation involve inertial measurement units (IMUs) for precise measurement of joint angles, force/torque sensors to accurately capture interaction forces and position sensors for tracking limb movement-dynamics during simulated STS motions. Simulation procedures are meticulously developed to ensure realistic data acquisition and validation within the simulated environment.

Mathematical modelling, utilizing the bond graph technique, plays a pivotal role in simulating the dynamic behaviour of the knee exoskeleton. These models derive essential motion equations and torque requirements, forming the foundation for developing robust control algorithms tailored to the unique biomechanical characteristics of knee joints. Simulation processes validate the dynamic model across a range of STS scenarios, enabling the optimization of control strategies specifically tailored for fault detection, isolation and reconfiguration within the knee exoskeleton's operational parameters.

Analytical redundancy relations (ARRs) are employed to monitor sensor data and actuator responses in real-time during simulation. This approach facilitates the early detection of anomalies and enables the autonomous reconfiguration of control parameters to maintain uninterrupted functionality during STS motions within the simulated environment.

5.1.6 Fault Detection Process

Detecting faults in knee exoskeletons involves a systematic approach aimed at monitoring, analysing and identifying anomalies those may impact the device's performance during STS motions. Residuals are generated using analytical redundancy relations (ARRs) which compare expected sensor outputs and actuator responses with actual measurements. These residuals serve as early indicators of deviations from normal operation, facilitating timely detection of potential faults and ensuring continuous device functionality. Coherence vector analysis plays a pivotal role in fault identification by examining residual patterns against predefined thresholds or expected values. A non-zero coherence vector signifies deviations that require further investigation, aiding in the precise diagnosis of specific fault types or component failures. The development of a fault signature matrix (FSM) organizes fault patterns identified through residual analysis into a

structured framework. Each fault signature correlates with distinct fault types or component malfunctions, enabling efficient diagnosis and implementation of appropriate corrective actions.

These methodologies ensure robust fault detection and management in knee exoskeletons, enhancing reliability and operational integrity during dynamic STS motions and diverse operational scenarios. Reconfiguration strategies utilize adaptive control algorithms and redundant actuators to maintain functionality and performance integrity in the presence of faults. Autonomous reconfiguration methods dynamically adjust control parameters and activate backup actuators based on real-time fault detection and isolation outcomes, ensuring uninterrupted operation during STS motions.

5.1.7 Integration of Backup Actuators

Secondary actuators are incorporated into the designs of knee exoskeleton to ensure continuous functionality in critical tasks such as torque generation and joint motion, enhancing system reliability and user safety even in the event of component failures or anomalies. Effective fault isolation and reconfiguration strategies are crucial for optimizing knee exoskeleton reliability and performance. This work focuses on enhancing fault detection, isolation (FDI) and reconfiguration strategies tailored specifically for knee exoskeletons designed for STS motions. In the scenarios where one of the actuators experiences a fault during motion, the backup actuator seamlessly takes over to maintain uninterrupted operation and achieve the necessary angle of rotation for STS motions.

The approach involves systematic fault detection, isolation and reconfiguration using quantitative methodologies based on mathematical models. Analytical redundancy relations (ARRs) play a pivotal role by comparing expected system behaviour with actual sensor data and actuator responses, identifying discrepancies called residuals. Each residual serves as a unique indicator of system health, showing sensitivity to specific faults while remaining insensitive to others under normal conditions. Coherence vector analysis further enhances fault detection by evaluating residual deviations from nominal values or thresholds. A non-null coherence vector indicates the presence of a fault, prompting further investigation into the specific fault signature associated with the affected component. To effectively isolate faults, a fault signature matrix (FSM) organizes predefined fault signatures derived from models or empirical data. This structured approach ensures each fault scenario which can be identified and matched to its

corresponding fault signature within the FSM, facilitating targeted isolation of the faulty component.

In practical terms, if a fault affects the knee exoskeleton's rotary motor, the system must adjust to maintain both required torque and angle of rotation for seamless STS transitions. This requires integrating multiple actuators, including linear and rotary types, to ensure sufficient torque at the knee joint and to enable smooth, controlled movements crucial for user functionality during STS motions.

5.2 Modelling of Knee exoskeleton with multiple actuators

The knee exoskeleton proposed in Fig. 5.1 incorporates multiple actuators to achieve the desired STS motions. This proposed KE is powered both by a linear actuator and two rotary actuators, denoted as RA-1 and RA-2, providing combined functionality. The rotary actuators are mounted at Joint 1 of the KE and positioned on both sides of the triangular element d_4. During standard operating scenario, both actuators work in the tandem to produce the required motions, ensuring a smooth and efficient assistive motion for the user. This collaborative operation enhances the exoskeleton's ability to support stand-sit-stand transitions smoothly.

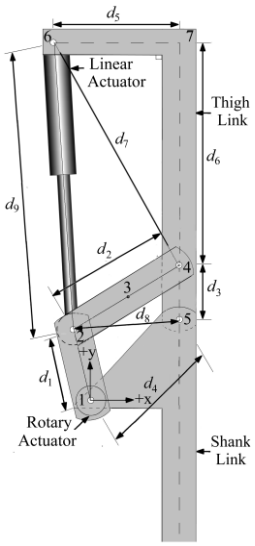

Fig. 5.1 KE with multiple actuators

Furthermore, the two rotary actuators (RA-1 and RA-2) employ a planetary geared DC motor and are connected to joint 1. These motors provide maximum rated torque at lower speeds and precise positioning. A capability is not easily achieved with conventional DC motors which lose

output power as speed decreases. The motor shaft is coaxial with joint 1 of the exoskeleton. This knee exoskeleton driven by both linear and rotary actuator ensures that the system can effectively support the user's movement from standing to sitting and back to standing, providing necessary torque angle of rotation, maintaining functionality even if one rotary actuator fails. The BG model of the KE incorporating linear and rotary actuator is depicted in Fig. 5.2 and the bond graph models of the motor with lead screw (Fig. 3.6) and linear actuator (Fig. 3.7) and the rotary actuator (Fig. 3.15) are discussed in Chapter 3 of the present work.

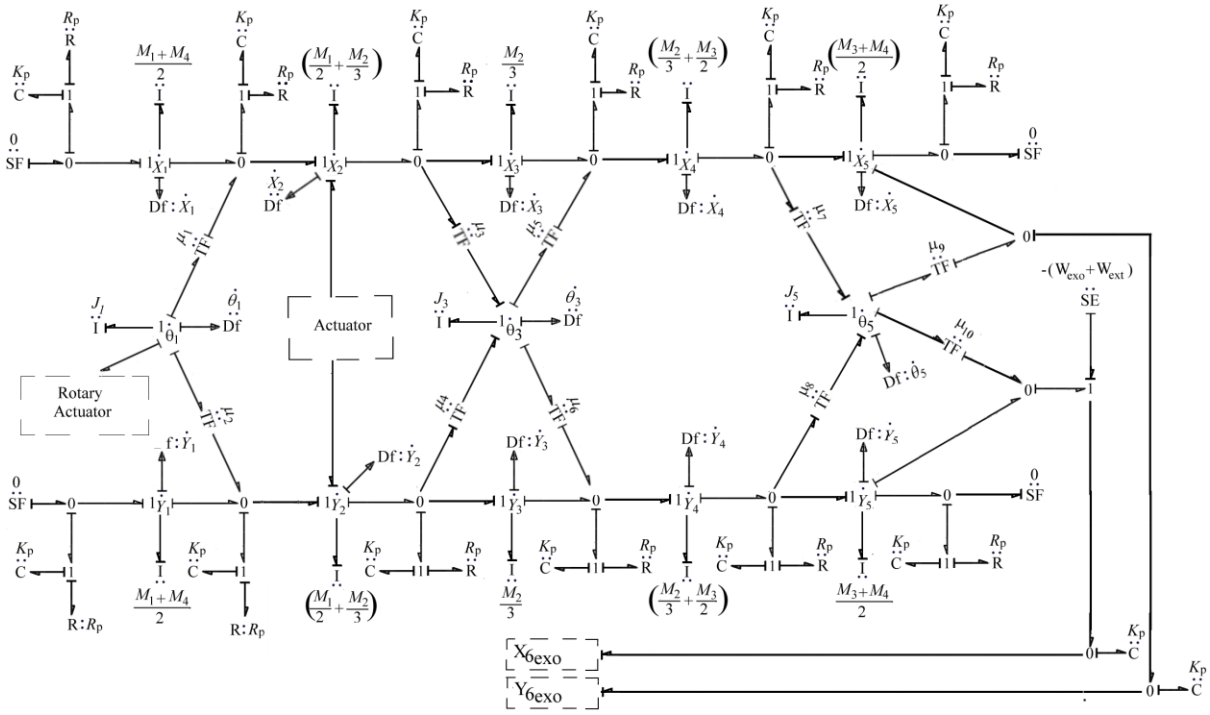

Fig. 5.2 BG model of KE driven by a linear actuator and two rotary actuators

5.3 Fault Diagnosis

A robust FDI mechanism is essential to ensure the reliability and safety of complex systems. This section outlines the development and implementation of a model-based quantitative FDI approach, leveraging analytical redundancy relations (ARRs) to detect and to isolate faults within the system. An elaborate mathematical model of the system is used for the model-based quantitative FDI because its fundamental is the comprehensive model of the system. This model serves as the basis for predicting system behaviour under various operating conditions. Operational FDI functions are

analytical in that they work with the actual process data as compared to the expected behaviour characterized by ARRs. ARRs are the mathematical expressions which describe the expected behaviour of the system based on its model. The discrepancies between actual measurements and predicted values, known as residuals, are critical for fault detection. Typically, the numbers of ARRs correspond to the numbers of sensors in the system and they ensure thorough monitoring.

Residuals, the differences between the actual and predicted values, are pivotal in the fault detection process. Hence, each structurally independent residual has different fault signature that is, each avoids the faulty component and is insensitive to other components. This distinctiveness is crucial for accurately identifying and isolating faults. For effective fault detection, ARRs must exhibit robustness. This implies that in the absence of faults, ARRs should remain insensitive, preventing false positives. Conversely, during faulty situations, ARRs should be sensitive and structured, enabling reliable fault detection. It is reasonable to have the expected value of each residual equal to zero or approximately zero during regular operations while large values are observed if fault is present.

A component-fault is monitorable if it influences each of the corresponding residual in some way. To help in fault detection a binary vector is employed and is referred to as the coherence vector. This vector shows if residuals are above or below certain value or level of normalcy or expectation. This vector indicates whether residuals deviate from their nominal values or thresholds. A non-null coherence vector (*i.e.* when at least one residual deviate significantly) signals the presence of a fault. Fault isolation is achieved when the fault signature of a faulty component is distinct from those of other components. This ensures that the non-null coherence vector can be uniquely matched to a predefined fault signature, derived from models, experiments or expert knowledge. This matching process enables the precise identification and isolation of the fault. These predetermined fault signatures are arranged in a structure referred to as fault signature matrix (FSM), which is in tabular form. The FSM is an essential model to locating and segregating faults from possible influences. In this study, the FSM is derived from the bond graph model of the system and this systematically represents the system's dynamics. Each row in the FSM corresponds to a specific fault, while each column corresponds to a residual, indicating the expected deviations for each fault.

In practice, the fault detection and isolation processes involve continuously monitoring the residuals generated by the ARRs. Upon the occurrence of a fault, the corresponding residuals

deviate from their nominal values, resulting in a non-null coherence vector. This vector is compared against the FSM to identify and isolate the fault.

In this chapter, rotary actuators are incorporated in addition to a linear actuator to enhance system's reliability. These actuators provide redundancy, ensuring continuous operation even if one actuator fails. This redundancy allows the system to maintain the necessary torque and achieve the desired angle of rotation for the thigh link during STS motion. The linear actuator, working alongside the rotary actuators, ensures robust and reliable system-performance, even in the event of actuator-failures.

5.4 Organisation and Operating Modes

The KE proposed in this work integrates two types of actuators *i.e.* linear and rotary actuators to significantly enhance mobility and support for individuals facing mobility challenges. The primary function of the linear actuator lies in providing sturdy support and precisely controlled movements, particularly crucial during STS motions. On the other hand, the secondary rotary actuator contributes additional flexibility, allowing for additional torque requirements and desired range of motions. In operational scenarios, the linear actuator independently operates. Moreover, the KE is designed with redundancy in mind: in cases where one of the rotary actuators encounters operational issues, the system seamlessly adapts by redistributing task to second rotary actuator to ensure continuous functionality. This adaptive feature plays a pivotal role in upholding consistent support and safety, which are paramount in enhancing the overall quality of life for the users. Figure 5.3 depicts the equipment availability chart.

When the fault detection and isolation (FDI) approach identifies a malfunction in a specific device, it initiates the deactivation of the associated branches connected to that device within the system. This adaptive response enables the system to adjust and continue functioning by utilizing the operational capabilities of the remaining devices.

For instance, if the rotary actuator (RA-1) fails during tasks like Sit-to-Stand (STS) motions, the knee exoskeleton (KE) can be reconfigured. This reconfiguration may involve relying solely on the linear actuator for motion control or integrating the functionality of the secondary rotary actuator (RA-2) with the primary linear actuator to achieve the required movements. This flexibility ensures that the KE exoskeleton maintains its desired functionality despite the occurrence of component failures, thereby, enhancing reliability and user-safety.

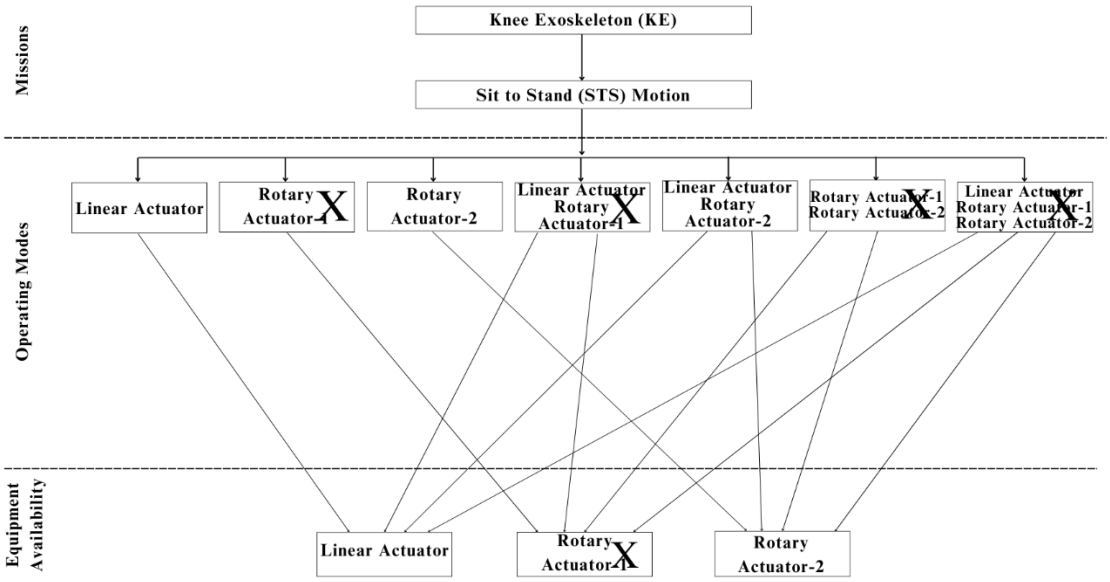

Fig. 5.3 Equipment availability chart with operating modes

5.4.1 Fault Detection

The sensors of the bond graph model are swapped into sources and are allocated the primary differential causality. Utilizing algorithms detailed in [1], ARRs are derived. Specifically, for the DC motor controlling the lead screw; the process involves dualizing four sensors into sources.

In the analysis, the ARRs for DC motor for linear actuator are expressed in Eq. (5.1–5.4). Further, the ARRs for the linear actuator are depicted in Eq. (5.5–5.14). Following this, Eq. (5.15–5.27) describe the configuration and functionality of thirteen sensors incorporated into the four-bar mechanism of the model. Moreover, ARR_{28} and ARR_{29} address the response and reliability characteristics of the rotary actuator, offering a thorough evaluation of its performance. All the ARRs are given below:

$$\textbf{ARR}_1: i_{\mathrm{m}} R_{\mathrm{m}} + \mu_{\mathrm{m}}\dot{\theta}_{\mathrm{m}} + L_{\mathrm{m}}\frac{di_m}{dt} - v = 0 \tag{5.1}$$

$$\textbf{ARR}_2: J_{\mathrm{G}}\frac{d\dot{\theta}_{\mathrm{m}}}{dt} + R_v\dot{\theta}_{\mathrm{m}} + \mu_G K_G \int\left(\mu_G\dot{\theta}_m - \dot{\theta}\right) - i_{\mathrm{m}}\,\mu_{\mathrm{m}} = 0 \tag{5.2}$$

$$\textbf{ARR3}: J_{\mathrm{L}}\frac{d\dot{\theta}}{dt} + R_{\mathrm{L}}\dot{\theta} + \mu_v K_{\mathrm{L}} \int\left(\dot{\theta}\mu_v - \dot{L}_{\mathrm{L}}\right) - K_{\mathrm{G}} \int\left(\mu_{\mathrm{G}}\dot{\theta}_m - \dot{\theta}\right) = 0 \tag{5.3}$$

ARR4: $J_{\mathrm{Ls}}\frac{d\dot{L}_L}{dt}+R_c\dot{L}_{\mathrm{L}}+K_{\mathrm{Ls}}\int\left[\dot{L}_L-\{\left(\frac{X_1-X_2}{L_{\mathrm{L}}}\right)(\dot{X}_1-\dot{X}_2)+\left(\frac{Y_1-Y_2}{L_{\mathrm{L}}}\right)(\dot{Y}_1-\dot{Y_2})\}\mu_{\mathrm{c}}\right]-K_{\mathrm{L}}\int\left(\dot{\theta}\mu_v-\dot{L}_{\mathrm{L}}\right)=0$ (5.4)

ARR5:$J_{X_1}\frac{d\dot{X}_1}{dt}-K_{\mathrm{p}}\int\left(\dot{X}_{\mathrm{c}}+\left(L_{\mathrm{cg}}\ \sin\left(\int\dot{\theta}_{\mathrm{c}}\right)\right)\dot{\theta}_{\mathrm{c}}-\dot{X}_1\right)-K_{\mathrm{p}}\int\left(\dot{x_5}+\left(-0.3928\ \cos(\int\dot{\theta}_5-1.225)\right)\dot{\theta}_5-\dot{X}_1\ \right)+\left(\frac{X_1-X_2}{L_{\mathrm{L}}}\right)\mu_{\mathrm{c}}K_{\mathrm{Ls}}\int\left[\dot{L}_L-\{\left(\frac{X_1-X_2}{L_{\mathrm{L}}}\right)(\dot{X}_1-\dot{X}_2)+\left(\frac{Y_1-Y_2}{L_{\mathrm{L}}}\right)(\dot{Y}_1-\dot{Y_2})\}\mu_{\mathrm{c}}\right]=0$ (5.5)

ARR6: $J_{Y_1}\frac{d\dot{Y}_1}{dt}-K_P\int(\dot{Y}_{\mathrm{c}}+\left(-L_{\mathrm{cg}}\ \cos\left(\int\dot{\theta}_{\mathrm{c}}\right)\right)\dot{\theta}_{\mathrm{c}}-\dot{Y}_1)-K_{\mathrm{p}}\int\left(\dot{y}_5+\left(-L_{\mathrm{cg}}\ \cos\left(\int\dot{\theta}_{\mathrm{c}}\right)\right)\dot{\theta}_5-\dot{Y}_1\right)+\left(\frac{Y_1-Y_2}{L_{\mathrm{L}}}\right)\mu_{\mathrm{c}}K_{\mathrm{Ls}}\int\left[\dot{L}_L-\{\left(\frac{X_1-X_2}{L_{\mathrm{L}}}\right)(\dot{X}_1-\dot{X}_2)+\left(\frac{Y_1-Y_2}{L_{\mathrm{L}}}\right)(\dot{Y}_1-\dot{Y_2})\}\mu_{\mathrm{c}}\right]=0$ (5.6)

ARR7:$J_{\mathrm{c}}\frac{d\dot{\theta}_{\mathrm{c}}}{dt}+K_{\mathrm{p}}\left(-L_{\mathrm{cg}}\ \cos\left(\int\dot{\theta}_{\mathrm{c}}\right)\right)\int\left(\dot{X}_{\mathrm{c}}+\left(L_{\mathrm{cg}}\ \sin\left(\int\dot{\theta}_{\mathrm{c}}\right)\right)\dot{\theta}_{\mathrm{c}}-\dot{X}_1\right)+K_{\mathrm{p}}\left(-L_{\mathrm{cg}}\ \cos\left(\int\dot{\theta}_{\mathrm{c}}\right)\right)\int\left(\dot{Y}_{\mathrm{c}}+\mu_{12}\dot{\theta}_{\mathrm{c}}-\dot{Y}_1\right)-\left(\int\dot{L}_{\mathrm{L}}-L_{\mathrm{p}}-L_{\mathrm{pg}}-\frac{d}{2}\right)\{K_{\mathrm{p}}\int\left(-\dot{X}_{\mathrm{c}}\left(-\sin\int\dot{\theta}_{\mathrm{c}}\right)-\dot{Y}_{\mathrm{c}}\left(\cos\int\dot{\theta}_{\mathrm{c}}\right)+\dot{X}_{\mathrm{p}}\left(\cos\int\dot{\theta}_{\mathrm{p}}\right)+\dot{Y}_{\mathrm{p}}\left(-\sin\int\dot{\theta}_{\mathrm{p}}\right)-\dot{\theta}_{\mathrm{c}}\left(\int\dot{L}_{\mathrm{L}}-L_{\mathrm{p}}-L_{\mathrm{pg}}-\frac{d}{2}\right)+\dot{\theta}_{\mathrm{p}}(L_{\mathrm{p}}-L_{\mathrm{pg}}+\frac{d}{2})\right)+R_{\mathrm{p}}\int\left(-\dot{X}_{\mathrm{c}}\left(-\sin\int\dot{\theta}_{\mathrm{c}}\right)-\dot{Y}_{\mathrm{c}}\left(\cos\int\dot{\theta}_{\mathrm{c}}\right)+\dot{X}_{\mathrm{p}}\left(\cos\int\dot{\theta}_{\mathrm{p}}\right)+\dot{Y}_{\mathrm{p}}\left(-\sin\int\dot{\theta}_{\mathrm{p}}\right)-\dot{\theta}_{\mathrm{c}}\left(\int\dot{L}_{\mathrm{L}}-L_{\mathrm{p}}-L_{\mathrm{pg}}-\frac{d}{2}\right)+\dot{\theta}_{\mathrm{p}}(L_{\mathrm{p}}-L_{\mathrm{pg}}+\frac{d}{2})\right)-\left(\int\dot{L}_{\mathrm{L}}-L_{\mathrm{p}}-L_{\mathrm{pg}}+\frac{d}{2}\right)\{K_{\mathrm{p}}\int(-\dot{X}_{\mathrm{c}}\left(-\sin\int\dot{\theta}_{\mathrm{c}}\right)-\dot{Y}_{\mathrm{c}}\left(\cos\int\dot{\theta}_{\mathrm{c}}\right)+\dot{X}_{\mathrm{p}}\left(\cos\int\dot{\theta}_{\mathrm{p}}\right)+\dot{Y}_{\mathrm{p}}\left(-\sin\int\dot{\theta}_{\mathrm{p}}\right)-\dot{\theta}_{\mathrm{c}}\left(\int\dot{L}_{\mathrm{L}}-L_{\mathrm{p}}-L_{\mathrm{pg}}+\frac{d}{2}\right)+\dot{\theta}_{\mathrm{p}}\left(-(L_{\mathrm{p}}-L_{\mathrm{pg}}-\frac{d}{2})\right))+R_{\mathrm{p}}(-\dot{X}_{\mathrm{c}}\left(-\sin\int\dot{\theta}_{\mathrm{c}}\right)-\dot{Y}_{\mathrm{c}}\left(\cos\int\dot{\theta}_{\mathrm{c}}\right)+\dot{X}_{\mathrm{p}}\left(\cos\int\dot{\theta}_{\mathrm{p}}\right)+\dot{Y}_{\mathrm{p}}\left(-\sin\int\dot{\theta}_{\mathrm{p}}\right)-\dot{\theta}_{\mathrm{c}}\left(\int\dot{L}_{\mathrm{L}}-L_{\mathrm{p}}-L_{\mathrm{pg}}+\frac{d}{2}\right)+\dot{\theta}_{\mathrm{p}}\left(-(L_{\mathrm{p}}-L_{\mathrm{pg}}-\frac{d}{2})\right))\}=0$ (5.7)

ARR8: $M_{X_{\mathrm{c}}}\frac{d\dot{X}_{\mathrm{c}}}{dt}+\ K_{\mathrm{p}}\int\left(\dot{X}_{\mathrm{c}}+\left(L_{\mathrm{cg}}\ \sin\left(\int\dot{\theta}_{\mathrm{c}}\right)\right)\dot{\theta}_{\mathrm{c}}-\dot{X}_1\right)-\left(-\sin\int\dot{\theta}_{\mathrm{c}}\right)\{K_{\mathrm{p}}\int\left(-\dot{X}_{\mathrm{c}}\left(-\sin\int\dot{\theta}_{\mathrm{c}}\right)-\dot{Y}_{\mathrm{c}}\left(\cos\int\dot{\theta}_{\mathrm{c}}\right)+\dot{X}_{\mathrm{p}}\left(\cos\int\dot{\theta}_{\mathrm{p}}\right)+\dot{Y}_{\mathrm{p}}\left(-\sin\int\dot{\theta}_{\mathrm{p}}\right)-\dot{\theta}_{\mathrm{c}}\left(\int\dot{L}_{\mathrm{L}}-L_{\mathrm{p}}-L_{\mathrm{pg}}-\frac{d}{2}\right)+\dot{\theta}_{\mathrm{p}}(L_{\mathrm{p}}-L_{\mathrm{pg}}+\frac{d}{2})\right)+R_{\mathrm{p}}\left(-\dot{X}_{\mathrm{c}}\left(-\sin\int\dot{\theta}_{\mathrm{c}}\right)-\dot{Y}_{\mathrm{c}}\left(\cos\int\dot{\theta}_{\mathrm{c}}\right)+\dot{X}_{\mathrm{p}}\left(\cos\int\dot{\theta}_{\mathrm{p}}\right)+\dot{Y}_{\mathrm{p}}\left(-\sin\int\dot{\theta}_{\mathrm{p}}\right)-\dot{\theta}_{\mathrm{c}}\left(\int\dot{L}_{\mathrm{L}}-L_{\mathrm{p}}-L_{\mathrm{pg}}-\frac{d}{2}\right)+\dot{\theta}_{\mathrm{p}}(L_{\mathrm{p}}-L_{\mathrm{pg}}+\frac{d}{2})\right)+K_{\mathrm{p}}\int(-\dot{X}_{\mathrm{c}}\left(-\sin\int\dot{\theta}_{\mathrm{c}}\right)-\dot{Y}_{\mathrm{c}}\left(\cos\int\dot{\theta}_{\mathrm{c}}\right)+\dot{X}_{\mathrm{p}}\left(\cos\int\dot{\theta}_{\mathrm{p}}\right)+\dot{Y}_{\mathrm{p}}\left(-\sin\int\dot{\theta}_{\mathrm{p}}\right)-\dot{\theta}_{\mathrm{c}}\left(\int\dot{L}_{\mathrm{L}}-L_{\mathrm{p}}-L_{\mathrm{pg}}+\frac{d}{2}\right)+\dot{\theta}_{\mathrm{p}}\left(-(L_{\mathrm{p}}-L_{\mathrm{pg}}-\frac{d}{2})\right)\text{`})+R_{\mathrm{p}}(-\dot{X}_{\mathrm{c}}\left(-\sin\int\dot{\theta}_{\mathrm{c}}\right)-\dot{Y}_{\mathrm{c}}\left(\cos\int\dot{\theta}_{\mathrm{c}}\right)+\dot{X}_{\mathrm{p}}\left(\cos\int\dot{\theta}_{\mathrm{p}}\right)+\dot{Y}_{\mathrm{p}}\left(-\sin\int\dot{\theta}_{\mathrm{p}}\right)-\dot{\theta}_{\mathrm{c}}\left(\int\dot{L}_{\mathrm{L}}-L_{\mathrm{p}}-L_{\mathrm{pg}}+\frac{d}{2}\right)+\dot{\theta}_{\mathrm{p}}\left(-(L_{\mathrm{p}}-L_{\mathrm{pg}}-\frac{d}{2})\right))=0$ (5.8)

ARR9: $M_{Y_c}\frac{d\dot{Y}_c}{dt} + K_p\int(\dot{Y}_c + (-L_{cg}\cos(\int\dot{\theta}_c))\dot{\theta}_c - \dot{Y}_1) -$ (5.9)
$(\cos\int\dot{\theta}_c)\{K_p\int\left(-\dot{X}_c(-\sin\int\dot{\theta}_c) - \dot{Y}_c(\cos\int\dot{\theta}_c) + \dot{X}_p(\cos\int\dot{\theta}_p) + \dot{Y}_p(-\sin\int\dot{\theta}_p) - \dot{\theta}_c\left(\int\dot{L}_L - L_p - L_{pg} - \frac{d}{2}\right) + \dot{\theta}_p(L_p - L_{pg} + \frac{d}{2})\right) + R_p\left(-\dot{X}_c(-\sin\int\dot{\theta}_c) - \dot{Y}_c(\cos\int\dot{\theta}_c) + \dot{X}_p(\cos\int\dot{\theta}_p) + \dot{Y}_p(-\sin\int\dot{\theta}_p) - \dot{\theta}_c\left(\int\dot{L}_L - L_p - L_{pg} - \frac{d}{2}\right) + \dot{\theta}_p(L_p - L_{pg} + \frac{d}{2})\right) + K_p\int(-\dot{X}_c(-\sin\int\dot{\theta}_c) - \dot{Y}_c(\cos\int\dot{\theta}_c) + \dot{X}_p(\cos\int\dot{\theta}_p) + \dot{Y}_p(-\sin\int\dot{\theta}_p) - \dot{\theta}_c\left(\int\dot{L}_L - L_p - L_{pg} + \frac{d}{2}\right) + \dot{\theta}_p\left(-(L_p - L_{pg} - \frac{d}{2})\right)\grave{}) + R_p(-\dot{X}_c(-\sin\int\dot{\theta}_c) - \dot{Y}_c(\cos\int\dot{\theta}_c) + \dot{X}_p(\cos\int\dot{\theta}_p) + \dot{Y}_p(-\sin\int\dot{\theta}_p) - \dot{\theta}_c\left(\int\dot{L}_L - L_p - L_{pg} + \frac{d}{2}\right) + \dot{\theta}_p\left(-(L_p - L_{pg} - \frac{d}{2})\right))\} = 0$

ARR10: $M_{X_p}\frac{d\dot{X}_p}{dt} + K_p\int(\dot{X}_p + \dot{\theta}_p(-L_{pg}\sin\int\dot{\theta}_p) - \dot{X}_2) +$ (5.10)
$(\cos\int\dot{\theta}_p)\{K_p\int\left(-\dot{X}_c(-\sin\int\dot{\theta}_c) - \dot{Y}_c(\cos\int\dot{\theta}_c) + \dot{X}_p(\cos\int\dot{\theta}_p) + \dot{Y}_p(-\sin\int\dot{\theta}_p) - \dot{\theta}_c\left(\int\dot{L}_L - L_p - L_{pg} - \frac{d}{2}\right) + \dot{\theta}_p(L_p - L_{pg} + \frac{d}{2})\right) + R_p\left(-\dot{X}_c(-\sin\int\dot{\theta}_c) - \dot{Y}_c(\cos\int\dot{\theta}_c) + \dot{X}_p(\cos\int\dot{\theta}_p) + \dot{Y}_p(-\sin\int\dot{\theta}_p) - \dot{\theta}_c\left(\int\dot{L}_L - L_p - L_{pg} - \frac{d}{2}\right) + \dot{\theta}_p(L_p - L_{pg} + \frac{d}{2})\right) + K_p\int(-\dot{X}_c(-\sin\int\dot{\theta}_c) - \dot{Y}_c(\cos\int\dot{\theta}_c) + \dot{X}_p(\cos\int\dot{\theta}_p) + \dot{Y}_p(-\sin\int\dot{\theta}_p) - \dot{\theta}_c\left(\int\dot{L}_L - L_p - L_{pg} + \frac{d}{2}\right) + \dot{\theta}_p\left(-(L_p - L_{pg} - \frac{d}{2})\right)\grave{}) + R_p(-\dot{X}_c(-\sin\int\dot{\theta}_c) - \dot{Y}_c(\cos\int\dot{\theta}_c) + \dot{X}_p(\cos\int\dot{\theta}_p) + \dot{Y}_p(-\sin\int\dot{\theta}_p) - \dot{\theta}_c\left(\int\dot{L}_L - L_p - L_{pg} + \frac{d}{2}\right) + \dot{\theta}_p\left(-(L_p - L_{pg} - \frac{d}{2})\right))\} = 0$

ARR11: $M_{Y_p}\frac{d\dot{Y}_p}{dt} + K_p\int(\dot{Y}_p + \dot{\theta}_p(L_{pg}\cos\int\dot{\theta}_p) - \dot{Y}_2) +$ (5.11)
$(-\sin\int\dot{\theta}_p)\{K_p\int\left(-\dot{X}_c(-\sin\int\dot{\theta}_c) - \dot{Y}_c(\cos\int\dot{\theta}_c) + \dot{X}_p(\cos\int\dot{\theta}_p) + \dot{Y}_p(-\sin\int\dot{\theta}_p) - \dot{\theta}_c\left(\int\dot{L}_L - L_p - L_{pg} - \frac{d}{2}\right) + \dot{\theta}_p(L_p - L_{pg} + \frac{d}{2})\right) + R_p\left(-\dot{X}_c(-\sin\int\dot{\theta}_c) - \dot{Y}_c(\cos\int\dot{\theta}_c) + \dot{X}_p(\cos\int\dot{\theta}_p) + \dot{Y}_p(-\sin\int\dot{\theta}_p) - \dot{\theta}_c\left(\int\dot{L}_L - L_p - L_{pg} - \frac{d}{2}\right) + \dot{\theta}_p(L_p - L_{pg} + \frac{d}{2})\right) + K_p\int(-\dot{X}_c(-\sin\int\dot{\theta}_c) - \dot{Y}_c(\cos\int\dot{\theta}_c) + \dot{X}_p(\cos\int\dot{\theta}_p) + \dot{Y}_p(-\sin\int\dot{\theta}_p) - \dot{\theta}_c\left(\int\dot{L}_L - L_p - L_{pg} + \frac{d}{2}\right) + \dot{\theta}_p\left(-(L_p - L_{pg} - \frac{d}{2})\right)\grave{}) + R_p(-\dot{X}_c(-\sin\int\dot{\theta}_c) - \dot{Y}_c(\cos\int\dot{\theta}_c) + \dot{X}_p(\cos\int\dot{\theta}_p) + \dot{Y}_p(-\sin\int\dot{\theta}_p) - \dot{\theta}_c\left(\int\dot{L}_L - L_p - L_{pg} + \frac{d}{2}\right) + \dot{\theta}_p\left(-(L_p - L_{pg} - \frac{d}{2})\right))\}$

ARR12: $J_p\frac{d\dot{\theta}_p}{dt} + (-L_{pg}\sin\int\dot{\theta}_p)K_p\int(\dot{X}_p - \dot{X}_2 + \dot{\theta}_p(-L_{pg}\sin\int\dot{\theta}_p)) +$ (5.12)
$(L_{pg}\cos\int\dot{\theta}_p)K_p\int(\dot{Y}_p - \dot{Y}_2 + \dot{\theta}_p(L_{pg}\cos\int\dot{\theta}_p)) + (L_p - L_{pg} + \frac{d}{2})\ \{K_p\int\left(-\dot{X}_c(-\sin\int\dot{\theta}_c) - \dot{Y}_c(\cos\int\dot{\theta}_c) + \dot{X}_p(\cos\int\dot{\theta}_p) + \dot{Y}_p(-\sin\int\dot{\theta}_p) + \dot{\theta}_p(L_p - L_{pg} + \frac{d}{2}) - \dot{\theta}_c\left(\int\dot{L}_L - L_p - L_{pg} - \frac{d}{2}\right)\right) + R_p\left(-\dot{X}_c(-\sin\int\dot{\theta}_c) -$

$\dot{Y}_c(\cos\int\dot{\theta}_c)+\dot{X}_p(\cos\int\dot{\theta}_p)+\dot{Y}_p(-\sin\int\dot{\theta}_p)+\dot{\theta}_p(L_p-L_{pg}+\frac{d}{2})-\dot{\theta}_c\left(\int\dot{L}_L-L_p-L_{pg}-\frac{d}{2}\right)\Big)+\left(-(L_p-L_{pg}-\frac{d}{2})\right)\{K_p\int(-\dot{X}_c(-\sin\int\dot{\theta}_c)-\dot{Y}_c(L_p-L_{pg}+\frac{d}{2})+\dot{X}_p(\cos\int\dot{\theta}_p)+\dot{Y}_p(-\sin\int\dot{\theta}_p)-\dot{\theta}_c\left(\int\dot{L}_L-L_p-L_{pg}+\frac{d}{2}\right)+\dot{\theta}_p\left(-(L_p-L_{pg}-\frac{d}{2})\right)+R_p(-\dot{X}_c(-\sin\int\dot{\theta}_c)-\dot{Y}_c(L_p-L_{pg}+\frac{d}{2})+\dot{X}_p(\cos\int\dot{\theta}_p)+\dot{Y}_p(-\sin\int\dot{\theta}_p)-\dot{\theta}_c\left(\int\dot{L}_L-L_p-L_{pg}+\frac{d}{2}\right)+\dot{\theta}_p\left(-(L_p-L_{pg}-\frac{d}{2})\right))\}=0$

ARR13: $M_{X_2}\frac{d\dot{X}_2}{dt}-K_p\int\left(\dot{X}_p-\dot{X}_2+\dot{\theta}_p(-L_{pg}\sin\int\dot{\theta}_p)\right)+K_p\int(\dot{X}_2-\dot{x}_2)-\left(\frac{X_1-X_2}{L_L}\right)\mu_c K_{Ls}\int\left[\dot{L}_L-\{\left(\frac{X_1-X_2}{L_L}\right)(\dot{X}_1-\dot{X}_2)+\left(\frac{Y_1-Y_2}{L_L}\right)(\dot{Y}_1-\dot{Y}_2)\}\mu_c\right]=0$

ARR14: $M_{Y_2}\frac{d\dot{Y}_2}{dt}-K_p\int(\dot{Y}_p-\dot{Y}_2+\dot{\theta}_p(L_{pg}\cos\int\dot{\theta}_p))+K_p\int(\dot{Y}_2-\dot{y}_2)-\left(\frac{Y_1-Y_2}{L_L}\right)\mu_c K_{Ls}\int\left[\dot{L}_L-\{\left(\frac{X_1-X_2}{L_L}\right)(\dot{X}_1-\dot{X}_2)+\left(\frac{Y_1-Y_2}{L_L}\right)(\dot{Y}_1-\dot{Y}_2)\}\mu_c\right]=0$ (5.14)

ARR15: $M_{x_1}\frac{d\dot{x}_1}{dt}-\{K_p\int(f_1-\dot{x}_1)+R_p(f_1-\dot{x}_1)\}+\{K_p\int(\dot{x}_1+\dot{\theta}_1(-L_1\sin(\int\dot{\theta}_1))-\dot{x}_2)+R_p(\dot{x}_1+\dot{\theta}_1(-L_1\sin(\int\dot{\theta}_1))-\dot{x}_2)\}=0$ (5.15)

ARR16: $M_{y_1}\frac{d\dot{y}_1}{dt}-\{K_p\int(f_2-\dot{y}_1)+R_p(f_2-\dot{y}_1)\}+\{K_p\int(\dot{y}_1+\dot{\theta}_1(L_1\cos(\int\dot{\theta}_1))-\dot{y}_2)+R_p(\dot{y}_1+\dot{\theta}_1(L_1\cos(\int\dot{\theta}_1))-\dot{y}_2)\}=0$ (5.16)

ARR17: $M_{x_2}\frac{d\dot{x}_2}{dt}-\{K_p\int(\dot{x}_1+\dot{\theta}_1(-L_1\sin(\int\dot{\theta}_1))-\dot{x}_2)+R_p(\dot{x}_1+\dot{\theta}_1(-L_1\sin(\int\dot{\theta}_1))-\dot{x}_2)\}+\{K_p\int(\dot{x}_2-\dot{\theta}_3(0.5L_2\sin(\int\dot{\theta}_3))-\dot{x}_3)+R_p(\dot{x}_2-\dot{\theta}_3(0.5L_2\sin(\int\dot{\theta}_3))-\dot{x}_3)\}-K_p\int(\dot{X}_2-\dot{x}_2)=0$ (5.17)

ARR18: $M_{y_2}\frac{d\dot{y}_2}{dt}-\{K_p\int(\dot{y}_1+\dot{\theta}_1(L_1\cos(\int\dot{\theta}_1))-\dot{y}_2)+R_p(\dot{y}_1+\dot{\theta}_1(L_1\cos(\int\dot{\theta}_1))-\dot{y}_2)\}+K_p\int(\dot{y}_2-\dot{\theta}_3(-0.5L_2\cos(\int\dot{\theta}_3))-\dot{y}_3)+R_p(\dot{y}_2-\dot{\theta}_3\left(-\frac{L_2}{2}\cos(\int\dot{\theta}_3)\right)-\dot{y}_3)-K_p\int(\dot{Y}_2-\dot{y}_2)=0$ (5.18)

ARR19: $M_{x_3}\frac{d\dot{x}_3}{dt}-\{K_p\int(\dot{x}_2-\dot{\theta}_3\left(\frac{L_2}{2}\sin(\int\dot{\theta}_3)\right)-\dot{x}_3)+R_p(\dot{x}_2-\dot{\theta}_3\left(\frac{L_2}{2}\sin(\int\dot{\theta}_3)\right)-\dot{x}_3)\}+\{K_p\int(\dot{x}_3+\dot{\theta}_3\left(-\frac{L_2}{2}\sin(\int\dot{\theta}_3)\right)-\dot{x}_4)+R_p(\dot{x}_3+\dot{\theta}_3\left(-\frac{L_2}{2}\sin(\int\dot{\theta}_3)\right)-\dot{x}_4)\}=0$ (5.19)

ARR20: $M_{y_3}\frac{d\dot{y}_3}{dt}-\{K_p\int(\dot{y}_2-\dot{\theta}_3\left(-\frac{L_2}{2}\cos(\int\dot{\theta}_3)\right)-\dot{y}_3)+R_p(\dot{y}_2-\dot{\theta}_3\left(-\frac{L_2}{2}\cos(\int\dot{\theta}_3)\right)-\dot{y}_3)\}+\{K_p\int(\dot{y}_3+\dot{\theta}_3\left(\frac{L_2}{2}\cos(\int\dot{\theta}_3)\right)-\dot{y}_4)+R_p(\dot{y}_3+\dot{\theta}_3\left(\frac{L_2}{2}\cos(\int\dot{\theta}_3)\right)-\dot{y}_4)\}=0$ (5.20)

ARR21: $M_{x_4}\frac{d\dot{x}_4}{dt}-\{K_p\int(\dot{x}_3+\dot{\theta}_3\left(-\frac{L_2}{2}\sin(\int\dot{\theta}_3)\right)-\dot{x}_4)+R_p(\dot{x}_3+\dot{\theta}_3\left(-\frac{L_2}{2}\sin(\int\dot{\theta}_3)\right)-\dot{x}_4)\}+\{K_p\int(\dot{x}_4-\dot{\theta}_5(-L_3\sin(\int\dot{\theta}_5))-\dot{x}_5)+R_p(\dot{x}_4-\dot{\theta}_5(-L_3\sin(\int\dot{\theta}_5))-\dot{x}_5)\}=0$ (5.21)

ARR22: $M_{y_4}\frac{d\dot{y}_4}{dt}-\{K_{\mathrm{p}}\int(\dot{y}_3+\dot{\theta}_3\left(\frac{L_2}{2}\cos(\int\dot{\theta}_3)\right)-\dot{y}_4)+R_{\mathrm{p}}(\dot{y}_3+\dot{\theta}_3\left(\frac{L_2}{2}\cos(\int\dot{\theta}_3)\right)-\dot{y}_4)\}+\{K_{\mathrm{p}}\int(\dot{y}_4-\dot{\theta}_5\left(L_3\cos(\int\dot{\theta}_5)\right)-\dot{y}_5)+R_{\mathrm{p}}(\dot{y}_4-\dot{\theta}_5\left(L_3\cos(\int\dot{\theta}_5)\right)-\dot{y}_5)\}=0$ (5.22)

ARR23 : $M_{x_5}\frac{d\dot{x}_5}{dt}-\{K_{\mathrm{p}}\int(\dot{x}_4-\dot{\theta}_5\left(-L_3\sin(\int\dot{\theta}_5)\right)-\dot{x}_5)+R_{\mathrm{p}}(\dot{x}_4-\dot{\theta}_5\left(-L_3\sin(\int\dot{\theta}_5)\right)-\dot{x}_5)\}+\{K_{\mathrm{p}}\int(\dot{x}_5+\dot{\theta}_5\left(-0.3928\ \cos(\int\dot{\theta}_5-1.225)\right)-\dot{X}_1)+R_{\mathrm{p}}(\dot{x}_5+\dot{\theta}_5\left(-0.3928\ \cos(\int\dot{\theta}_5-1.225)\right)-\dot{X}_1)\}+\{K_{\mathrm{p}}\int(\dot{x}_5-f_3)+R_{\mathrm{p}}(\dot{x}_5-f_3)\}=0$ (5.23)

ARR24: $M_{\mathrm{y}_5}\frac{d\dot{y}_5}{dt}-\{K_{\mathrm{p}}\int(\dot{y}_4-\dot{\theta}_5\left(L_3\cos(\int\dot{\theta}_5)\right)-\dot{y}_5)+R_{\mathrm{p}}(\dot{y}_4-\dot{\theta}_5\left(L_3\cos(\int\dot{\theta}_5)\right)-\dot{y}_5)\}+\{K_{\mathrm{p}}\int(\dot{y}_5+\dot{\theta}_5\left(-0.3928\ \sin(\int\dot{\theta}_5-1.225)\right)-\dot{Y}_1)+R_{\mathrm{p}}(\dot{y}_5+\dot{\theta}_5\left(-0.3928\ \sin(\int\dot{\theta}_5-1.225)\right)-\dot{Y}_1)-e_1\}+\{K_{\mathrm{p}}\int(\dot{y}_5-f_4)+R_{\mathrm{p}}(\dot{y}_5-f_4)\}=0$ (5.24)

ARR25: $J_1\frac{d\dot{\theta}_1}{dt}+\left(-L_1\sin(\int\dot{\theta}_1)\right)\{K_{\mathrm{p}}\int(\dot{x}_1+\dot{\theta}_1\left(-L_1\sin(\int\dot{\theta}_1)\right)-\dot{x}_2)+R_{\mathrm{p}}(\dot{x}_1+\dot{\theta}_1\left(-L_1\sin(\int\dot{\theta}_1)\right)-\dot{x}_2)\}+\left(L_1\cos(\int\dot{\theta}_1)\right)\{K_{\mathrm{p}}\int(\dot{y}_1+\dot{\theta}_1\left(-L_1\sin(\int\dot{\theta}_1)\right)-\dot{y}_2)+R_{\mathrm{p}}(\dot{y}_1+\dot{\theta}_1\left(-L_1\sin(\int\dot{\theta}_1)\right)-\dot{y}_2)\}-\mu_{\mathrm{C}}K_{\mathrm{t}}\int(\dot{\theta}_{mr}g-\dot{\theta}_1\mu_{\mathrm{C}})=0$ (5.25)

ARR26: $J_3\frac{d\dot{\theta}_3}{dt}-\{K_{\mathrm{p}}\int(\dot{x}_2-\dot{\theta}_3\left(\frac{L_2}{2}\sin(\int\dot{\theta}_3)\right)-\dot{x}_3)+R_{\mathrm{p}}(\dot{x}_2-\dot{\theta}_3\left(\frac{L_2}{2}\sin(\int\dot{\theta}_3)\right)-\dot{x}_3)\}+\{K_{\mathrm{p}}\int(\dot{x}_3+\dot{\theta}_3\left(-\frac{L_2}{2}\sin(\int\dot{\theta}_3)\right)-\dot{x}_4)+R_{\mathrm{p}}(\dot{x}_3+\dot{\theta}_3\left(-\frac{L_2}{2}\sin(\int\dot{\theta}_3)\right)-\dot{x}_4)\}-\{K_{\mathrm{p}}\int(\dot{y}_2-\dot{\theta}_3\left(-\frac{L_2}{2}\cos(\int\dot{\theta}_3)\right)-\dot{y}_3)+R_{\mathrm{p}}(\dot{y}_2-\dot{\theta}_3\left(-\frac{L_2}{2}\cos(\int\dot{\theta}_3)\right)-\dot{y}_3)\}+\{K_{\mathrm{p}}\int(\dot{y}_3+\dot{\theta}_3\left(\frac{L_2}{2}\cos(\int\dot{\theta}_3)\right)-\dot{y}_4)+R_{\mathrm{p}}(\dot{y}_3+\dot{\theta}_3\left(\frac{L_2}{2}\cos(\int\dot{\theta}_3)\right)-\dot{y}_4)\}=0$ (5.26)

ARR27: $J_5\frac{d\dot{\theta}_5}{dt}+R_{\mathrm{P}}\dot{\theta}_5-\left(-L_3\sin(\int\dot{\theta}_5)\right)\{K_{\mathrm{p}}\int(\dot{x}_4-\dot{\theta}_5\left(-L_3\sin(\int\dot{\theta}_5)\right)-\dot{x}_5)+R_{\mathrm{p}}(\dot{x}_4-\dot{\theta}_5\left(-L_3\sin(\int\dot{\theta}_5)\right)-\dot{x}_5)\}-\left(L_3\cos(\int\dot{\theta}_5)\right)\{K_{\mathrm{p}}\int(\dot{y}_4-\dot{\theta}_5\left(L_3\cos(\int\dot{\theta}_5)\right)-\dot{y}_5)+R_{\mathrm{p}}(\dot{y}_4-\dot{\theta}_5\left(L_3\cos(\int\dot{\theta}_5)\right)-\dot{y}_5)\}+\left(-0.3928\ \cos(\int\dot{\theta}_5-1.225)\right)\{K_{\mathrm{p}}\int(\dot{x}_5+\dot{\theta}_5\left(-0.3928\ \cos(\int\dot{\theta}_5-1.225)\right)-\dot{X}_1)+R_{\mathrm{p}}(\dot{x}_5+\dot{\theta}_5\left(-0.3928\ \cos(\int\dot{\theta}_5-1.225)\right)-\dot{X}_1)\}+\left(-0.3928\ \sin(\int\dot{\theta}_5-1.225)\right)\{K_{\mathrm{p}}\int(\dot{y}_5+\dot{\theta}_5\left(-0.3928\ \sin(\int\dot{\theta}_5-1.225)\right)-\dot{Y}_1)+R_{\mathrm{p}}(\dot{y}_5+\dot{\theta}_5\left(-0.3928\ \sin(\int\dot{\theta}_5-1.225)\right)-\dot{Y}_1)-e_1\}=0$ (5.27)

ARR28: $L_{\mathrm{mr}}\frac{di_{\mathrm{mr}}}{dt}+i_{\mathrm{mr}}R_{\mathrm{mr}}+\mu_{\mathrm{mr}}\dot{\theta}_{\mathrm{mr}}-v_{mr}=0$ (5.28)

ARR29: $J_{\mathrm{Gr}}\frac{d\dot{\theta}_{\mathrm{mr}}}{dt}+R_{\mathrm{vr}}\dot{\theta}_{\mathrm{mr}}-i_{\mathrm{mr}}\mu_{\mathrm{mr}}+g\{K_{\mathrm{p}}\int(g\dot{\theta}_{\mathrm{mr}}-\dot{\theta}_1\mu_{\mathrm{C}})\}=0$ (5.29)

These ARRs and sensor-configurations play a key role in accurately monitoring and controlling the dynamic behaviour of the KE system. In an ideal operational state, the evaluation of algebraic residual relations (ARRs) yields an outcome of zero on the left-hand side (LHS). However, when real-world measurements are applied to assess these ARRs, the result obtained is referred to as a residual. Ideally, this residual remains at zero when no faults are present but deviates from zero in the presence of faults. For this purpose, various types of noises and biases related to the modelling error, involving inaccuracies in the estimation of parameters involved in the model, noise from the sensor etc, it is assumed that the residuary deviates only when it is beyond a pre-defined static or adaptive standard. This method of addressing uncertainties is commonly known as a passive approach.

5.4.2 Structural Analysis of ARR and Fault Signature Matrix

Structural analysis of the ARRs is crucial in generating a fault signature matrix (FSM), illustrated in Table 1. This matrix details how variations in parameters of different components influence specific residuals. The analysis confirms that faults in any component lead to visible changes in at least one residual, thereby, ensuring the monitorability of all component faults. Moreover, each component's fault signature which defines how a fault impacts certain residuals while leaving others unaffected, is unique. This distinctiveness facilitates the isolation of faults in all listed components.

In this work the calculation of ARRs uses the bond graph modelling software known as SYMBOLS Shakti. In addition to cognitive support with derivation of the ARRs in the symbolic form, the FDIPad toolbox of this software also generates the FSM in an automated manner. Further, it enables effective modelling of fault isolation performance given various changes in the structure of the instrumentation system including the position of sensors and actuators. It also makes the design of analytical redundancy based approaches stronger and more efficient in the complex systems thus improving the fault detection and isolation techniques. Additionally, it allows for optimization of fault isolation performance through adjustments in instrumentation architecture, such as sensor and actuator-placements. This integrated approach enhances the robustness and effectiveness of fault detection and isolation strategies in the complex systems.

In the real-time monitoring system for the knee exoskeleton (KE), actual measurements obtained from the KE are used to estimate the residuals. The KE of the bond graph model of the KE is simulated in order to obtain artificial data; the simulation uses a continuous time integrator (a 4th order Runge-Kutta). The obtained outputs at regular time instances and given to a residual evaluator developed in MATLAB.

It is important to note that SYMBOLS Shakti software supports residual evaluation but lacks compatibility with data acquisition systems. As such, MATLAB is used for residual evaluation, fault isolation with reference to the FSM, reconfiguration decisions (for mode shift) and decision support system operations of the knee exoskeleton.

5.5 Operating Scenarios

This section discusses the operating scenarios in which the knee exoskeleton (KE) performs stand-to-sit (STS) motions over a period of 5.15 s. The motion starts from the standing position when the length of linear actuator is maximum and moving to the sitting position when linear actuator is at minimum position. The entire operation cycle is divided into three phases *i.e.* the first, a fault-free scenario from 0 to 2 s, the second stage, fault simulation from 2 to 4 s and the third; reconfiguration takes place from 4 to 5.15 s.

5.5.1 Fault Free Scenario

In a specific fault scenario context during 0–2 s, the knee exoskeleton system initially operates smoothly without any faults. Both the linear and rotary actuators collaborate seamlessly to facilitate the stand-to-sit (STS) motion within the critical timeframe of 0–2 s. In this scenario, the knee exoskeleton demonstrated the integrated performance of both linear and rotary actuators in achieving the desired STS motion.

Table 1: Fault signature matrix of the KE (FSM)

Components	**Residuals**																														**Mo**	**I_O**
	r_1	**r_2**	**r_3**	**r_4**	**r_5**	**r_6**	**r_7**	**r_8**	**r_9**	**r_{10}**	**r_{11}**	**r_{12}**	**r_{13}**	**r_{14}**	**r_{15}**	**r_{16}**	**r_{17}**	**r_{18}**	**r_{19}**	**r_{20}**	**r_{21}**	**r_{22}**	**r_{23}**	**r_{24}**	**r_{25}**	**r_{26}**	**r_{27}**	**r_{28}**	**r_{29}**		
DC motor of Linear actuator	**1**	**1**	**1**	0	0	0	0	0	0	0	0	0	0	0	0	0	0	0	0	0	0	0	0	0	0	0	0	0	0	0	1	1
Gear mounted on shaft	0	**1**	**1**	**1**	0	0	0	0	0	0	0	0	0	0	0	0	0	0	0	0	0	0	0	0	0	0	0	0	0	0	1	1
Lead screw	0	0	0	**1**	**1**	**1**	**1**	**1**	**1**	**1**	**1**	**1**	**1**	**1**	0	0	0	0	0	0	0	0	0	0	0	0	0	0	0	0	1	1
Cylinder end of the slider	0	0	0	0	**1**	**1**	**1**	**1**	**1**	**1**	**1**	**1**	0	0	0	0	0	0	0	0	0	0	0	0	0	0	0	0	0	0	1	1
Piston end of the slider	0	0	0	0	0	0	**1**	**1**	**1**	**1**	**1**	**1**	**1**	**1**	0	0	0	0	0	0	0	0	0	0	0	0	0	0	0	0	1	1
Link -1 (d1)	0	0	0	0	0	0	0	0	0	0	0	0	0	0	**1**	**1**	**1**	**1**	0	0	0	0	0	0	**1**	**1**	0	0	0	0	1	1
Link -2 (d_2)	0	0	0	0	0	0	0	0	0	0	0	0	0	0	0	0	**1**	**1**	**1**	**1**	**1**	**1**	0	0	**1**	**1**	0	0	0	0	1	1
Link -3 (d_3)	0	0	0	0	0	0	0	0	0	0	0	0	0	0	0	0	0	0	0	**1**	**1**	**1**	**1**	0	**1**	**1**	0	0	0	0	1	1
Link -2 (d_4)	0	0	0	0	0	0	0	0	0	0	0	0	0	0	**1**	**1**	**1**	**1**	**1**	**1**	**1**	**1**	**1**	**1**	**1**	**1**	**1**	0	0	0	1	1
Rotary actuator (RA-1)	0	0	0	0	0	0	0	0	0	0	0	0	1	1	**1**	**1**	**0**	**0**	**0**	**0**	**0**	**0**	**0**	**0**	**1**	**0**	**0**	1	1	1	1	1
Rotary actuator (RA-2)	0	0	0	0	0	0	0	0	0	0	0	0	0	0	**0**	**0**	**0**	**0**	**0**	**0**	**0**	**0**	**0**	**0**	**0**	**0**	**0**	1	1	1	1	1

The analytical redundancy relation (ARR) values in Fig. 5.4–5.7 which show a no-fault situation, are consistently near zero on all the graphs. The system is fault-free, as shown by the exact alignment between the actual measurements and the model predictions. In these cases, there are no differences between the predicted and actual behaviour of the system, hence, the ARR values stay close to zero. Thus, ARR's aim is to identify discrepancies between expected and actual data which means when there are no errors, there are no deviations. Due to this consistency, the residuals *i.e.* differences between actual and anticipated values are zero, proving that the behaviour of the system closely follows the model. As a result, there is zero analytical redundancy which is utilized to find possible errors. Figure 5.4 depicts ARR values for DC motor of the linear actuator with no fault scenario between 0–5 s.

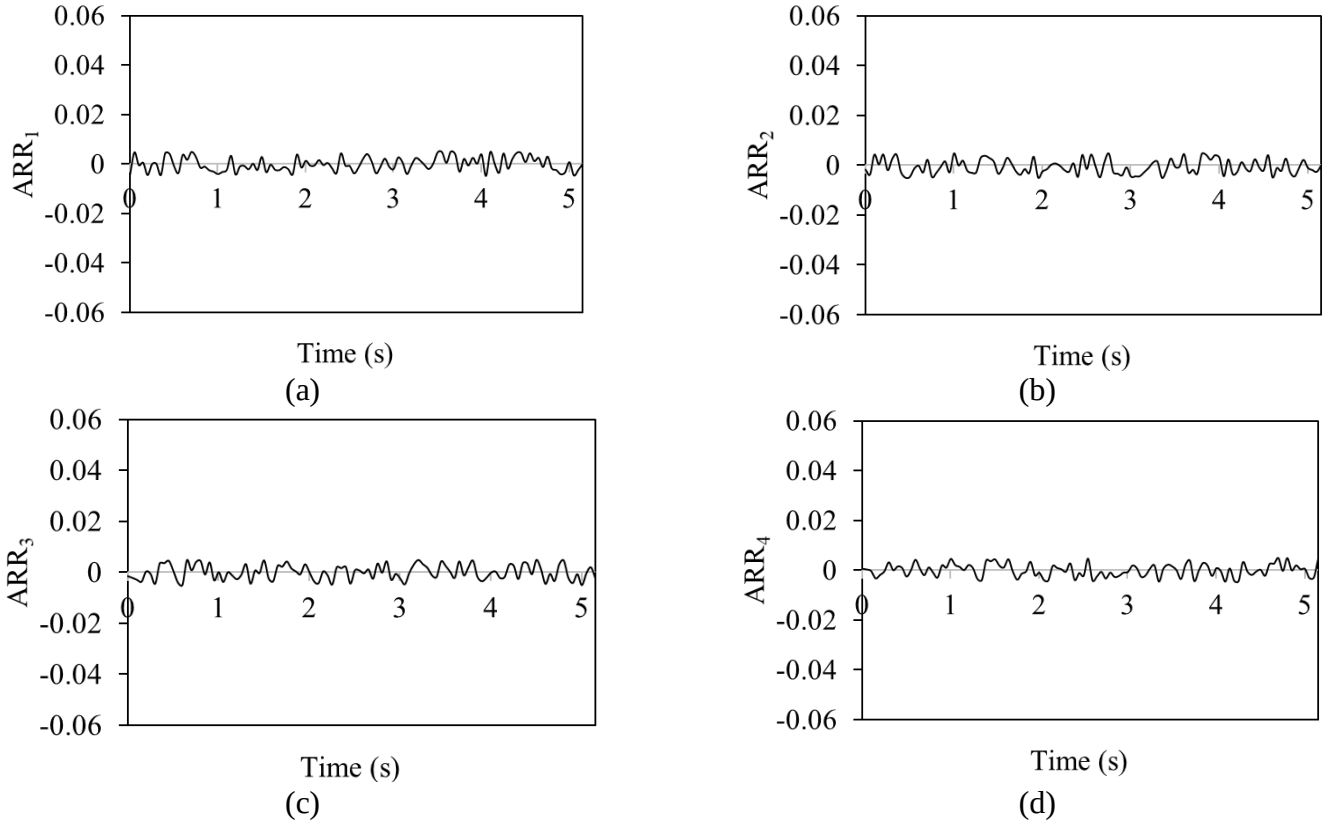

Fig. 5.4 ARRs for DC motor of the linear actuator with no fault condition

Figure 5.5 illustrate the values corresponding to analytical redundancy relations (ARR) for the linear actuator under a no-fault scenario from 0 to 5 seconds. All the ARRs were not given here due to similarity in nature.

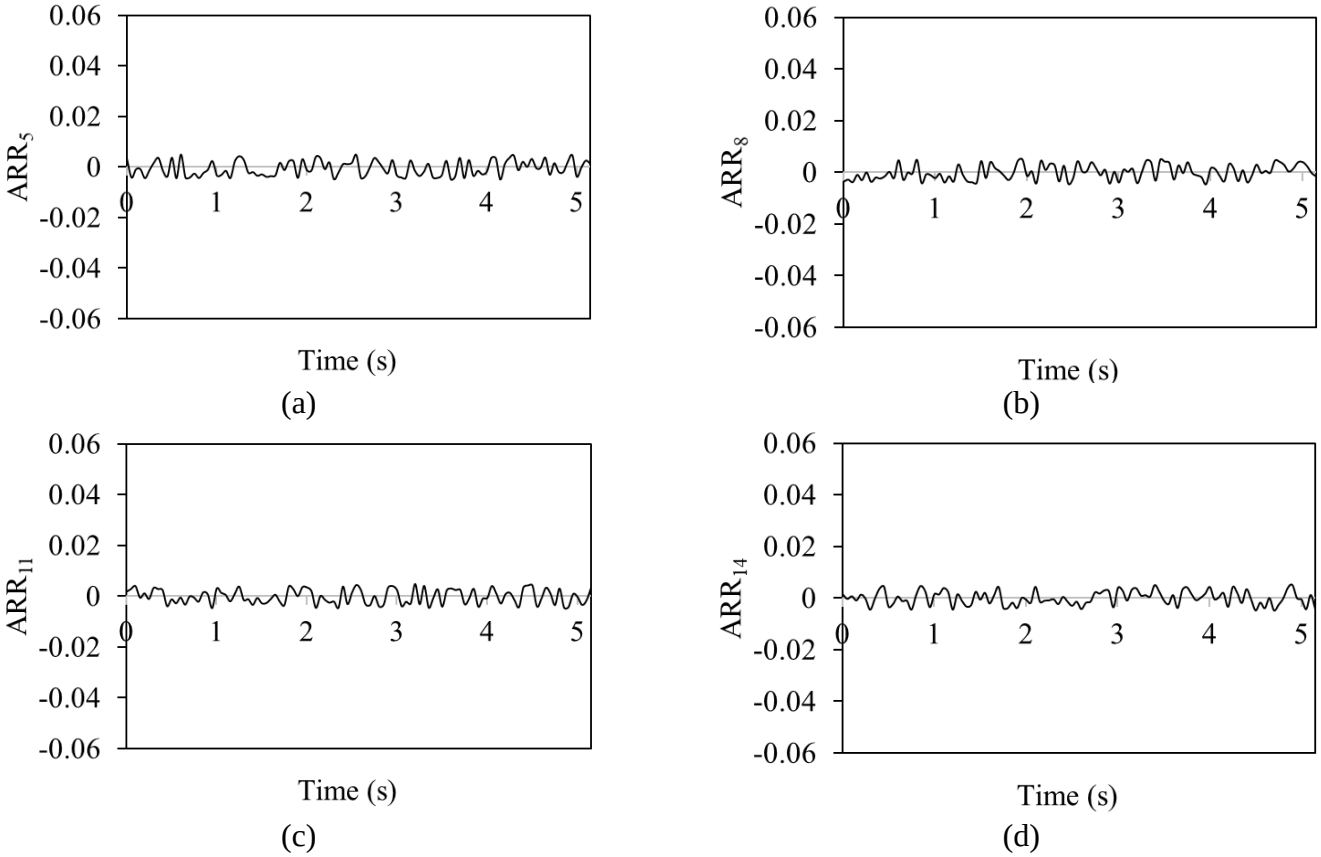

Fig. 5.5 ARR for the linear actuator under a no-fault scenario from 0 to 2 seconds

The analytical redundancy relations (ARR) for the four-bar mechanism under a no-fault scenario are shown in Fig. 5.6 during the time interval of 0–5 s. These graphs depict how the ARR values constantly stay near to zero, demonstrating the precise agreement between the model's predictions and the measured data. This consistent near-zero ARR shows that the four-bar mechanism is operating without any faults during the specified period 0–5 s.

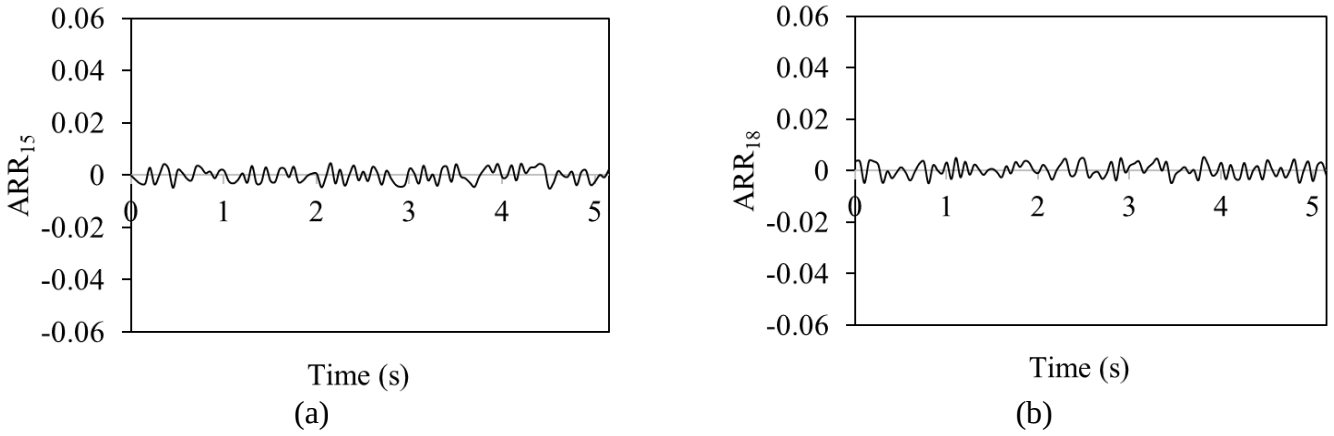

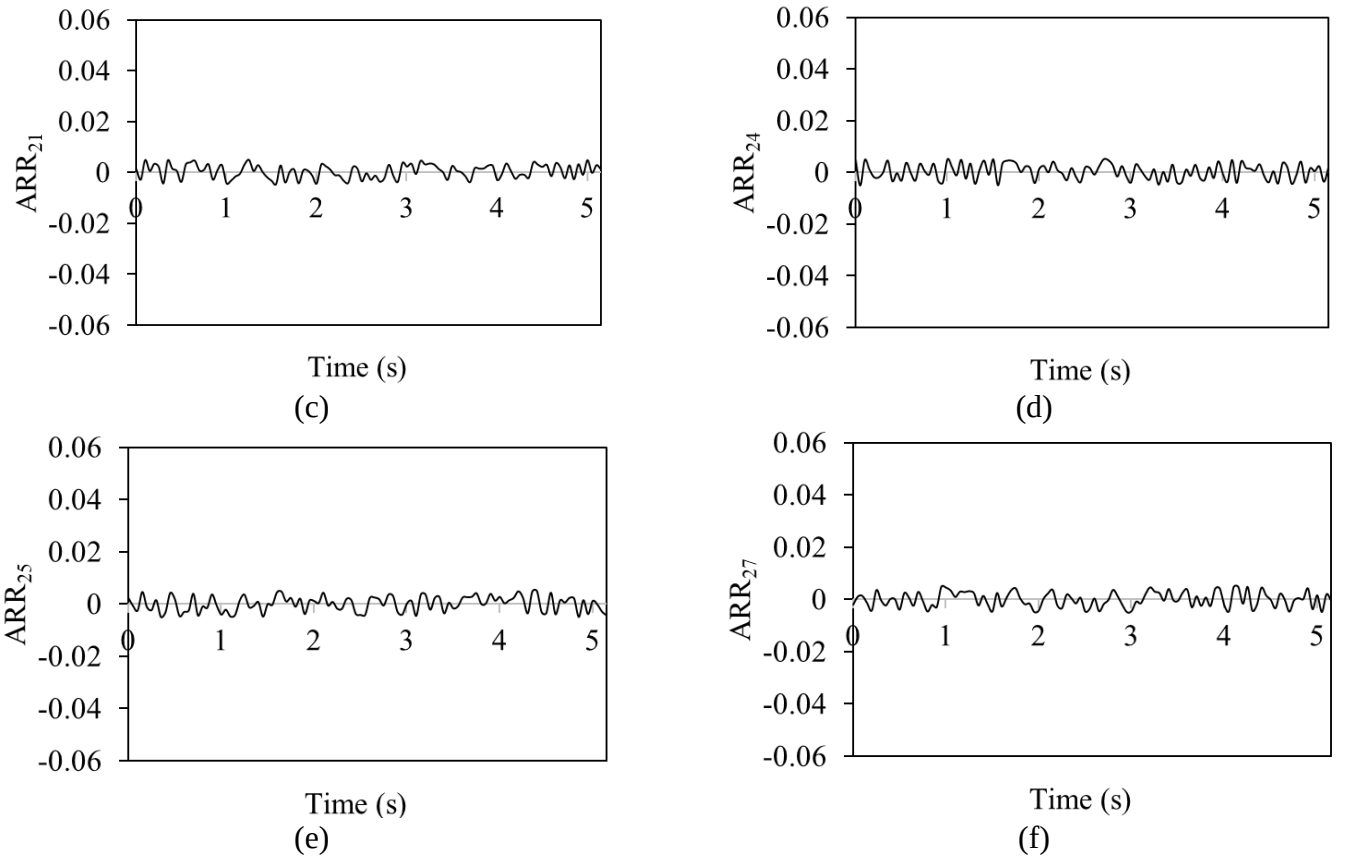

Fig. 5.6 ARR for the four-bar mechanism showing fault-free operation

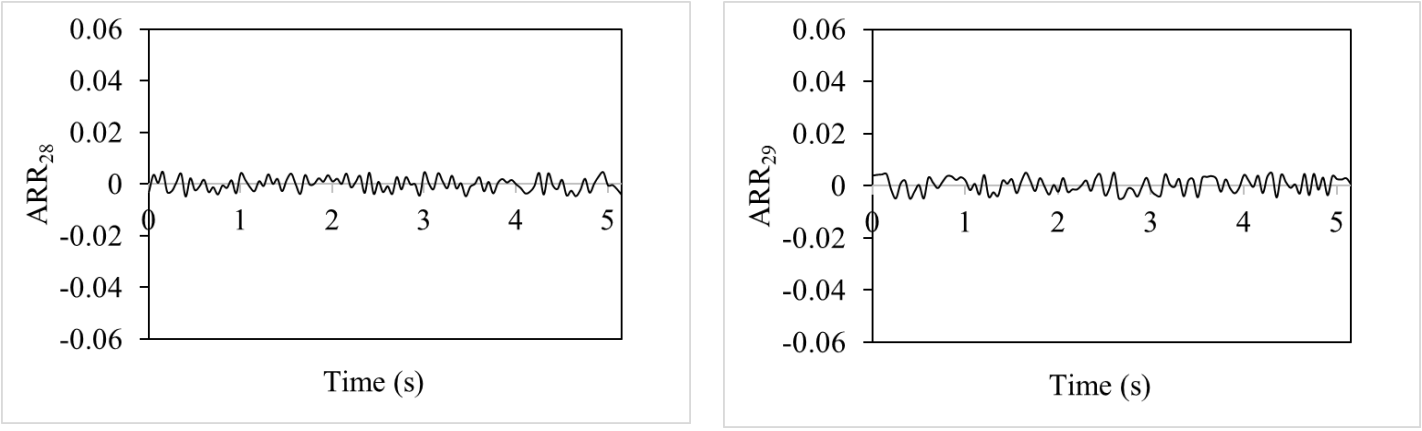

Fig. 5.7 ARR for the rotary actuator (0–5 seconds) showing fault-free operation

To conclude, during the 0 to 5 s interval, the knee exoskeleton system functions smoothly and without faults, demonstrating the seamless integration of both linear and rotary actuators in

executing the stand-to-sit (STS) motion. The system's performance during this period exemplifies the effective collaboration of its components to achieve the desired motion.

The Analytical Redundancy Relations (ARR) values presented in Fig. 5.4–5.7 consistently remain near zero, indicating a fault-free operation. This alignment between actual measurements and model predictions signifies that the system's behaviour adheres closely to the expected performance, with no observed discrepancies. The near-zero ARR values confirm that there are no deviations from the model, highlighting the absence of faults within the system.

5.5.2 Fault Simulation

For the scenario (2–4 seconds), the fault is induced deliberately at the 2 second mark, the power supply to the rotary actuator (RA-1) is intentionally disconnected, however, the linear actuator is still operational. Hence, this serves as a controlled fault scenario aimed at testing the system's response and resilience under the faulty conditions.

Analytical redundancy relations (ARR) values are continuously close to zero, as shown in Fig. 5.8. These ARR belongs to the DC motor for linear actuator. This observation is crucial since it shows that the DC motor for linear actuator keeps working regularly even after the rotary actuator stops operating. The near zero ARR numbers highlight how, even in the case of one actuator (rotary) being inactive, the system's performance is in line with the model's predictions. The ARR value indicates that system-functionality and expected behaviour can be maintained only by the linear actuator's performance. The contribution of the linear actuator to the entire system is demonstrated by the ARR values which remain relatively constant even when the rotary actuator is not in use. This demonstrates the system's fault tolerance and dependability.

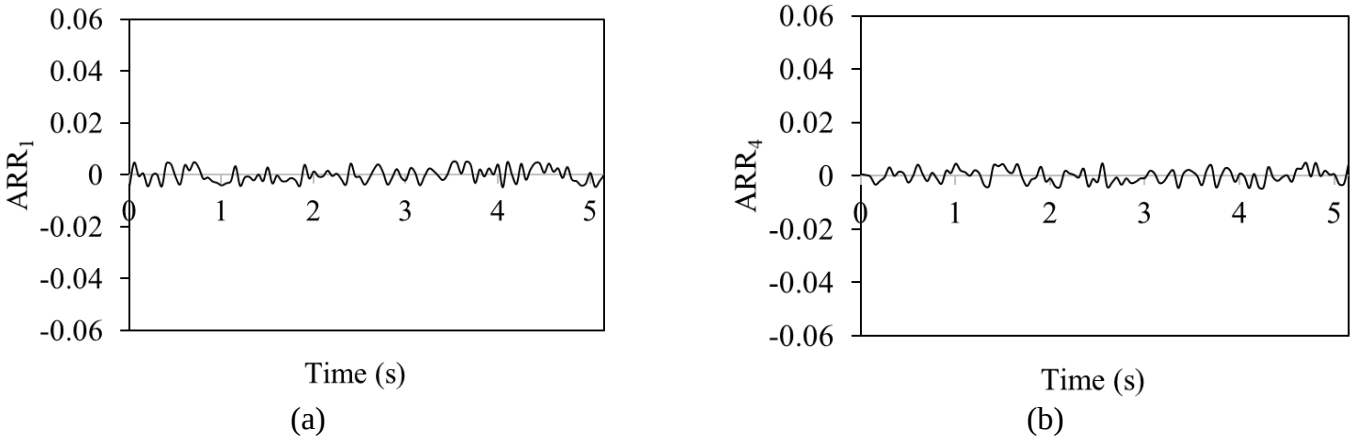

Fig. 5.8 ARR values for the DC motor for linear actuator during fault scenario

The ARR values for the linear actuator in the fault induced scenario are shown in Fig. 5.9.

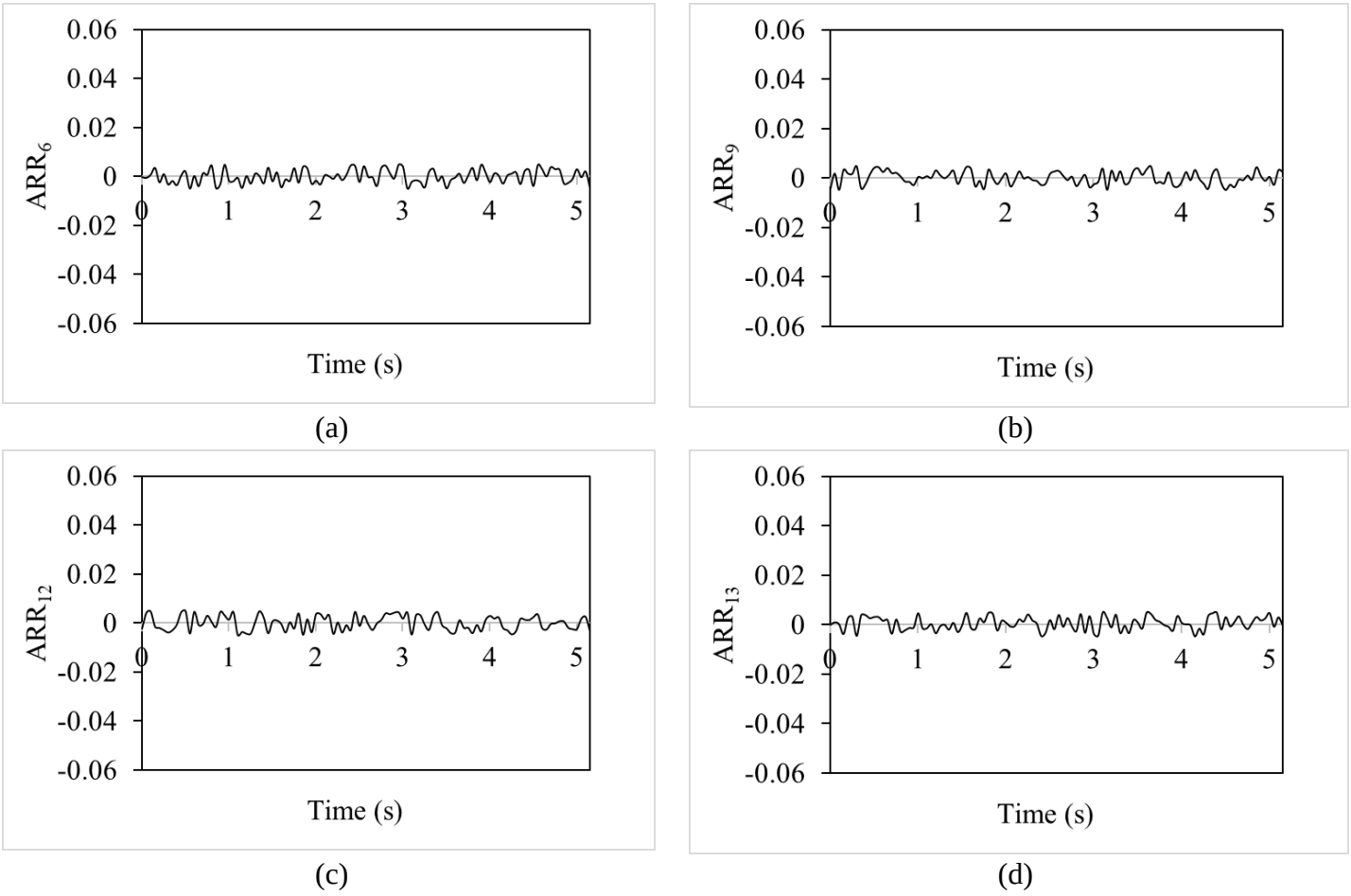

Figure 5.9 ARR for the linear actuator during fault induced scenario (2–4 s)

Figure 5.10 show ARR values for the four-bar mechanism from 2 to 4 seconds and these are non-zero due to a fault mode scenario. These figures reveal that although, the linear actuator remains operational, the rotary actuator is faulty. The non-zero ARR values highlight the discrepancies between actual performance and model predictions, demonstrating the impact of the rotary actuator's failure on the system. Despite the linear actuator's continued functionality, the fault in the rotary actuator leads to deviations in ARR values for four- bar mechanism, emphasizing the system's sensitivity to faults and the importance of both actuators for maintaining proper system performance.

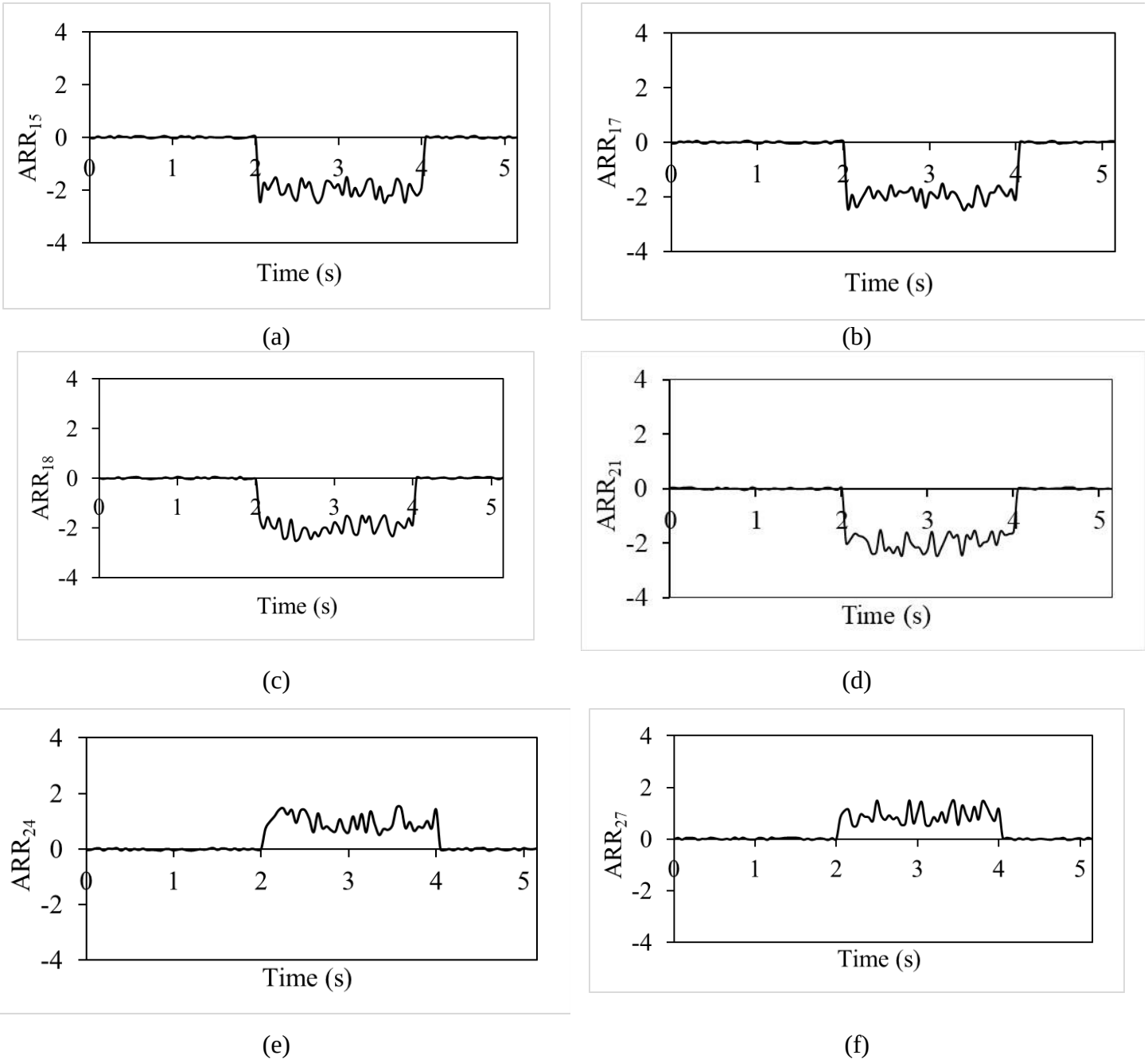

Fig. 5.10 ARR for the four-bar mechanism (2–4 seconds) during fault induced scenario

The ARR values for rotary actuator RA-1 from 2 to 4 seconds are shown in Fig. 5.11. The non-zero numbers show that an externally generated defect is causing RA-1 to malfunction. These figures reveal that the performance of RA-1 deviates from expectations, which impacts the overall system functionality, as reflected by the non-zero ARR values.

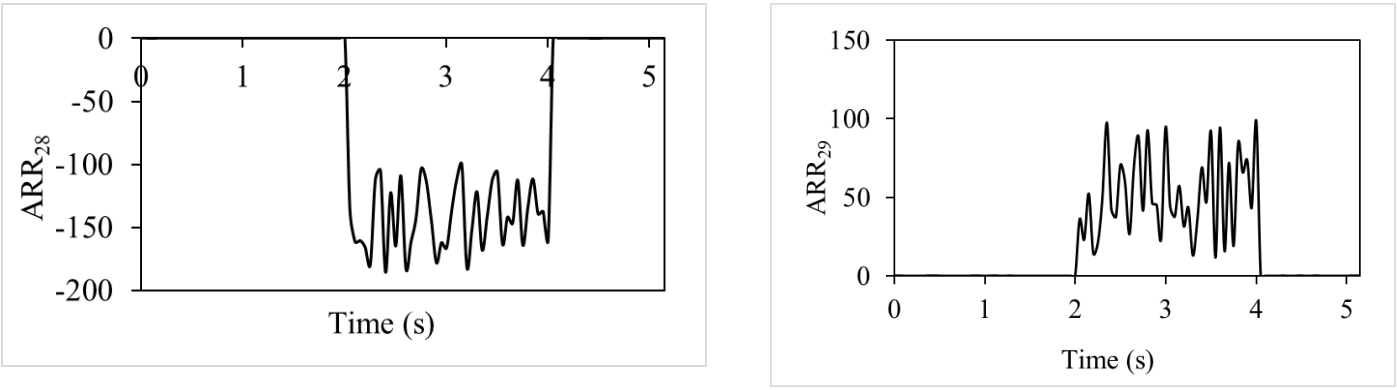

(a) (b)

Fig. 5.11: ARR for the rotary actuator (2–4 seconds) during fault induced scenario

5.5.3 Fault Isolation & Reconfiguration

For the scenario from time 4.0 –5.15 seconds, by the 4-second mark, the fault reconfiguration process is successfully completed and the power supply to the rotary actuator (RA-2) is provided. This actuation enables the knee exoskeleton to resume its intended function and complete the stand-to-sit (STS) motion as originally intended. Figures 5.5–5.11 show that the ARR values are near zero during this period, indicating that the system returns to normal operation and maintains expected performance during the stand-to-sit motion.

6. Conclusions

In this chapter, advancements and challenges associated with knee exoskeleton systems were examined, with a particular focus on fault management capabilities. The analysis reveals the impact of fault scenarios and the effectiveness of FDI technique in maintaining system functionality and reliability.

During the initial no-fault period (0 to 2 seconds), the knee exoskeleton is operated optimally with ARR values remaining close to zero. This period is represented in normal operation, where both linear and rotary actuators worked seamlessly. The absence of faults ensured stable and predictable performance, providing baseline for comparison with subsequent fault-induced and reconfiguration phases.

In the fault-induced period (2 to 4 seconds), a fault scenario was introduced by disconnecting the rotary actuator by turning off the power supply. This fault was detected by the system, as indicated by significant deviations in ARR values from the baseline. Despite the fault, the linear

actuator continued to function, demonstrating partial resilience but also highlighting the need for effective fault management strategies.

During the reconfiguration period (4 to 5.15 seconds), backup actuators was turned on to restore normal operation. Successful reconfiguration was evident from ARR values returning to near-zero levels, indicating that the impact of the fault was mitigated and stable performance was resumed. This phase demonstrated the effectiveness of reconfiguration strategies in addressing actuator faults and maintaining exoskeleton functionality, illustrating the system's robustness and fault tolerance.

Overall, this chapter emphasizes that the proposed knee exoskeleton with the integration of backup actuators and the application of analytical redundancy relations (ARRs) have proven effective in enhancing system-reliability. The successful handling of fault scenarios and the return to normal operation after reconfiguration highlight fault management capabilities thus enabling KE to perform the desired STS motions.

Chapter 6

Optimisation of Design Parameters of the Knee Exoskeleton

6.1 Introduction

The proposed knee exoskeleton (KE) is suitable to assist the user to carry out activities of daily living specifically for STS motion. STS motions are essential for several daily tasks of an individual. The effectiveness of such exoskeletons is largely deapendent on their design characteristics which must be improved to maximize their utility and user-comfort. The parameters can be optimised by utilizing suitable optimisation technique and understanding the kinematic properties of the KE.

Several optimisation strategies have been utilized in the design of robotics. Conventional methods such as linear and quadratic programming have been employed for problems with well-defined constraints. [99] However, these methods may not be useful for the complex and nonlinear character of real-world challenges, requiring the implementation of more advanced techniques. Metaheuristic algorithms, such as Genetic Algorithms (GA) and Particle Swarm Optimisation (PSO) have been widely applied to the mechanical system's optimisation due to their ability to handle complex and nonlinear objective functions and constraints. GAs are known for their robustness and ability to explore large search spaces, while PSO is valued for its simplicity and efficiency in finding out of optimal solutions[100,101].

Interior Point Methods (IPMs) have gained prominence because they effectively address large-scale optimisation problems with nonlinear constraints[102]. IPMs utilized in solvers such as MATLAB's fmincon, offer exceptional global optimisation capabilities and robustness in handling both equality and inequality constraints. Recently, researchers have applied these techniques to optimise knee exoskeleton design parameters. For example, Particle Swarm Optimisation (PSO) is used to optimise robotic systems, showcasing its effectiveness with complex design parameters[103]. Ant Colony Optimisation (ACO) was utilised for robotic arm configurations, providing valuable insights into optimisation strategies for mechanical systems[104].

Despite these advancements, challenges persist in achieving optimal design parameters due to the complexity of exoskeleton-dynamics and the need for precise control over design variables. This chapter focusses upon enhancing the comfort and functionality of the user using the KE by

optimising its design parameters within defined constraints. IPM technique is used to optimise the design parameters of the four-bar mechanism-based KE.

6.2 Optimisation of Design Parameters of KE for Stand-Sit-Stand (STS) Motion

The STS motion cycle which is crucial for the knee exoskeleton's functionality, involves complex interactions between various components. Figure 3.1 depicts the motion cycle. Initially, the thigh is positioned at an angle (α_3) of 1.7° from the shank's axis in the clockwise direction. During sitting, the thigh rotates through an angle (α_2) of 83.3° in the counter-clockwise direction. In the sitting posture, the thigh maintains an angle (α_1) of 6.7° relative to the negative *x*-axis. The total angle (θ) of rotation of the thigh link is approximately 85°. The aim of the optimisation is to maximize this angle to enhance user-comfort during the STS activity.

Objective Function

The objective optimisation of the KE is to increase the angle of rotation for improving the exoskeleton's performance during the STS motion. The objective function is expressed as:

$$\text{Minimise } -\theta\,(X) \text{ subject to } g_i\ (X) \leq 0 \text{ for } i = 1, 2, ..., 9$$

Where:

- $X = \{d_1, d_2, d_3, d_4, d_5, d_6\}$ are the design variables (link lengths).
- The constraints $g_i(X)$ are the mechanical and kinematic limits described in Eq. (6.1– 6.8), ensuring the functional integrity of the four-bar mechanism.

6.3 Modelling and Optimisation Approach

In the context of optimising the design parameters of the knee exoskeleton, a detailed modelling approach is essential. This involves understanding the relationships between the kinematic parameters and their influence on the joint angles.

6.3.1 Dependence of Joint Angle on Kinematic Parameters

The joint angle θ is influenced by various design variables, including the length of the thigh link and the components of the four-bar mechanism. The kinematic model of the exoskeleton must account for these variables to determine their effect on the joint angle.

6.3.2 Design Variables and Objective Function

The design variables for this optimisation problem are the lengths of the links in the four-bar mechanism: $X = \{d_1, d_2, d_3, d_4, d_5, d_6\}$.

6.3.3 Constraints Formulation

In the present work, the design parameters of the knee exoskeleton and several constraints are established based on mechanical design requirements and kinematic relationships. Each constraint is justified through considerations of mechanical feasibility, stability and functionality.

The constraint represented by Eq. 6.1 ensures that the sum of the lengths of components d_3 and d_4 does not exceed the sum of d_2 and d_1 as per Grashof's law. This is essential to prevent mechanical interference and ensures that the four-bar mechanism operates within its kinematic limits. In a four-bar linkage system, the lengths of adjacent links must be appropriately balanced to avoid over-constraining the mechanism, which could otherwise lead to interference or incorrect motion profiles. This maintained constraint is crucial for preserving the functional integrity and effective range of motion of the exoskeleton.

$$g_1(X) = d_3 + d_4 - d_2 - d_1 \leq 0, \tag{6.1}$$

$$g_2(X) = d_3 - d_2 \leq 0, \tag{6.2}$$

$$g_3(X) = d_3 - d_1 \leq 0, \tag{6.3}$$

$$g_4(X) = d_3 - d_4 \leq 0, \tag{6.4}$$

$$g_5(X) = d_2 - d_4 \leq 0, \tag{6.5}$$

$$g_6(X) = d_1 - d_4 \leq 0, \tag{6.6}$$

$$g_7(X) = d_5 - d_6 \leq 0, \tag{6.7}$$

$$g_8(X) = d_4 - d_6 \leq 0, \tag{6.8}$$

where $d_9 = d_{\min} = 244$ mm.

By adhering to these constraints, the design parameters of the proposed KE meet the necessary mechanical and functional requirements during STS motions.

6.3.4 Solution Method: Interior Point Method in MATLAB

The Interior Point Method (IPM) is employed in this work for solving the optimisation problem due to its efficiency in handling large-scale, nonlinear problems with both equality and inequality constraints. The fmincon function in MATLAB is used to implement the IPM which is based on the primal-dual approach. This method updates the primal variables (design parameters) and dual variables (Lagrange multipliers) simultaneously, providing a robust solution to the optimisation problem.[105] The general formularization of fmincon is stated as: Minimize $f(x)$ $subject\ to: c(x) \leq 0, ceq(x) = 0, lb \leq x \leq ub$.[106]

The lengths of two bars (d_2 and d_3) of the four-bar mechanism are assumed. The lengths of the other two bars (d_1 and d_4) of the four-bar mechanism are designed based on the actuator length (d_9) in the compressed state (0.242 m) and the expanded position (0.379 m), the lengths d_5 and d_6 of the KE frame and initial angle are $\theta_i = (90° - \alpha_3)$ and final angle $\theta_f = (90° + \alpha_2)$ of rotation of the link d_3. The lengths of the link d_1 and d_4 are calculated using the relations: $\psi_1 = \tan^{-1}\frac{d_5}{d_6}, \psi_2 = \cos^{-1}\left(\frac{d_7^2+d_2^2-d_9^2}{2d_7d_2}\right), d_7 = ({d_5}^2 + {d_6}^2)^{\frac{1}{2}}, d_8 = ({d_2}^2 + {d_3}^2 - 2d_2d_3\cos(180 - \psi_1 - \psi_2))^{\frac{1}{2}}, \phi_1 = \cos^{-1}\left(\frac{{d_8}^2+{d_3}^2-{d_2}^2}{2d_8d_3}\right), \phi_2 = \cos^{-1}\left(\frac{{d_8}^2+{d_4}^2-{d_1}^2}{2d_8d_4}\right)$ $\phi_3 = \tan^{-1}\left(\frac{x_5-x_1}{y_5-y_1}\right)$ and $\theta = (180 + \alpha_3) - (\phi_1 + \phi_2 + \phi_3)$.

The above equations are essential for determining the optimal configuration of the knee exoskeleton which ensures that the design parameters satisfy the necessary mechanical and functional requirements while maximizing the angle of thigh rotation during the Stand-Sit-Stand (STS) motion. IPM is well-suited for the intricate optimisation problem of the knee exoskeleton due to its global coverage, robustness and capacity to address infeasible and unbounded problems.

6.4 Simulation and Analysis

The simulation and analysis of the current problem are done by applying the IPM to optimise the design parameters of the four-bar mechanism-based knee exoskeleton and evaluating the results to assess the effectiveness of the optimisation.

6.4.1 Utilization of fmincon for Optimisation

The **fmincon** function in MATLAB which is designed to solve nonlinear constrained optimisation problems plays a pivotal role in this study. This function is greatly useful when solving problems containing both equality and inequality constraints as applied to the knee exoskeleton mechanical setup in this case. The Interior Point Method (IPM) implemented within **fmincon** leverages the primal-dual interior point approach which is well-regarded for its efficiency in solving large-scale optimisation problems[107].

The **fmincon** algorithm iteratively refines the design parameters by solving a sequence of subproblems that approximate the original problem. It does this by updating both primal variables (design parameters) and dual variables (associated with the constraints) in a manner that maintains feasibility and optimality throughout the optimisation process[108]. This approach is particularly advantageous for mechanical design-optimisation because it accommodates complex, nonlinear constraints and provides a global optimisation framework that reduces the likelihood of converging to local optima[109].

In this study, **fmincon** is employed to optimise the design parameters of the knee exoskeleton, focusing on maximizing the angle of thigh rotation during the Stand-Sit-Stand (STS) motion.

6.4.2 Advantages of Interior Point Method in Optimisation

The Interior Point Method (IPM) have several advantages in addressing optimisation problems, particularly those involving nonlinear constraints and large-scale variables. Its implementation through fmincon offers an effective approach for solving complex design challenges such as optimising the design parameters of the current KE.

One significant advantage of IPM is its efficiency in solving large-scale problems. The technique operates by iteratively improving the solution by maintaining the constraints. Unlike conventional optimisation techniques which can get trapped in local optima, IPM demonstrates robustness in navigating toward global optima, thereby reducing the likelihood of converging to suboptimal solutions.

6.5 Results and Discussions

This section discussed the outcome of the optimisation process which is further aimed to enhance user-comfort and functionality by maximizing the angle of rotation of the thigh link.

6.5.1 Simulation Results and Optimum Design Parameters

Table 6.1 presents an overview of the design parameters before and after the optimisation process. The link lengths underwent considerable modifications during optimisation process. The length of the link d_1 got increased by 0.607 mm and this improved the integration of this component within the overall design. In contrast, d_2 and d_4 got significantly reduced by 63.736 mm and 65.609 mm, respectively. This led to optimising the placement of actuators.

Similarly, d_3 and the frame components (d_5 and d_6) got adjusted. The length of the d_3 link was slightly decreased by 2.525 mm, contributing to improve the kinematic accuracy. The frame length adjustments were more substantial, with reductions of 6.05 mm and 38.13 mm for d_5 and d_6, respectively. These changes were aimed at enhancing the stability and functionality of the KE.

The most desirable and significant outcome is the increase in the total angle of rotation ($\alpha_3+\alpha_2+\alpha_4$), which was improved from 85° to 105°. This means that the user can now flex its shank with additional 20° of rotational motion, thereby improving the flexibility and comfort of the user wearing the KE during STS transitions.

Table 6.1 Comparison of initial and optimised design parameters

Design Aspect	Initial Value	Optimised Value	Difference	Description
Link Length d_1	0.050 m	0.0506 m	+0.0006 m	Minor adjustment improves component integration and performance
Link Length d_2	0.115 m	0.0513 m	-0.0637 m	Reduction optimises actuator integration
Link Length d_3	0.053 m	0.0505 m	-0.0025 m	Adjusted to enhance kinematic accuracy
Link Length d_4	0.117 m	0.0514 m	-0.0656 m	Enhanced movement optimisation and fit
Link Length d_5	0.116 m	0.1099 m	-0.0060 m	Adjusted length improves mechanical stability and reduces interference

Link Length d_6	0.310 m	0.2719 m	-0.0381 m	Reduced length enhances fit and functionality
Total Rotation Angle ($\alpha_3+\alpha_2+\alpha_4$)	85°	105°	+20°	Enhanced angle significantly improves STS motion and user comfort

6.5.2 Comparison of the Pre and Post Optimisation Observations

Figure 6.1(a) depicts the STS motion with the initial design parameters, while Fig. 6.1(b) shows the enhanced motion resulting from the optimisation. The post-optimisation analysis reveals a notable increase in the total angle of rotation which now stands at approximately 105°, compared to the initial angle of 85°. This additional 20° of angle of rotation enhances the functionality and comfort of the exoskeleton, as it improves the ease and efficiency of STS transitions by effectively addressing the design constraints, resulting in a more user-friendly knee exoskeleton.

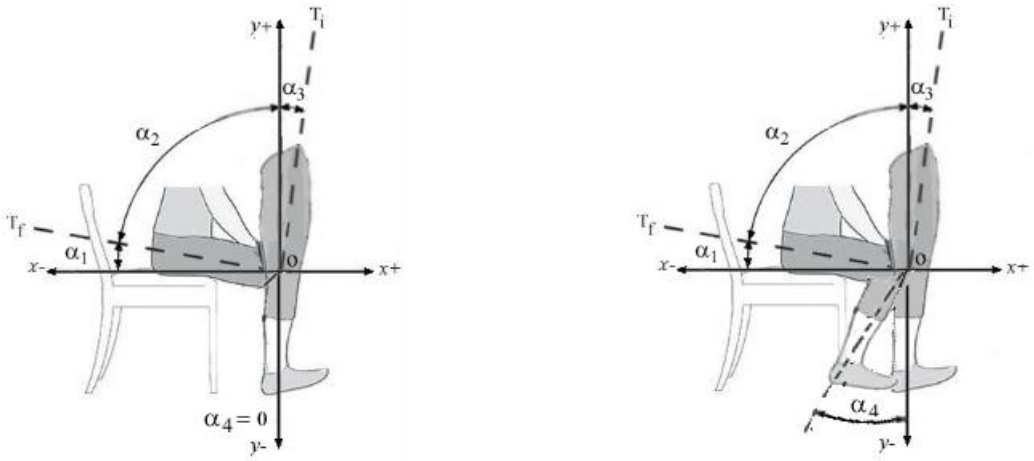

(a) (b)

Fig. 6.1 STS motion cycles before and after the optimisation

6.6 Conclusions

This chapter has comprehensively addressed the optimisation of design parameters for the knee exoskeleton, focusing on enhancing the Stand-Sit-Stand (STS) motion. By employing the Interior Point Method (IPM) within MATLAB's **fmincon** function, improvements have been achieved in the angle of thigh rotation and this is crucial for user-comfort and functionality.

The optimisation process is successfully maximized for the total rotation-angle from 85° to 105°, representing a notable enhancement of 20°. The results demonstrate that the optimised parameters lead to improved comfort to the users of the knee exoskeleton during STS transitions. The utilization of the IPM method offered a robust resolution to the current optimisation problem.

The optimization framework presented in this chapter can be extended to include user-specific customization by integrating anthropometric data, such as variations in thigh length, knee range of motion, and body weight, into the kinematic and dynamic models. This adaptation would ensure the system's applicability across a broader demographic, addressing individual differences in physical attributes. Additionally, the system could be tested under varying activity levels, such as different speeds or workloads, to ensure its adaptability and comfort. As a future scope, further simulations and experimental studies could validate these user-specific modifications, thereby enhancing the system's usability.

Chapter 7

Conclusions and Future Scope of Work

This work attempts the implementations of the design, modelling and fabrication of the proposed knee exoskeleton with a focus on a four-bar mechanism operated with linear and rotary actuators. It has been the primary focus of this study to counter the issues experienced by persons with knee-disorders especially while performing STS motions which are significant in daily operations. Due to this, people with low levels of knee-function cannot generate the amount of torque needed to perform these motions. Current assistive devices and technologies fall short of meeting this requirement and hence, giving the reason for the development of an advanced and fault-tolerant knee exoskeleton to assist in reducing the effort needed for performing STS motions and improving the mobility of the user.

The four-bar mechanism was chosen among the other types of the mechanisms incorporated in the exoskeleton's structure due to the need in the stable mechanical characteristics and possibility to control the movement of the knee joint. It is the linear actuator that delivers the right measure of force to generate torque in the four-bar mechanism to help the user with the STS transition. With regards to physical ergonomics, one of the key objectives of design was to minimize the amount of effort which the user had to put in and, as both theoretical and experimental results show, the effort is reduced approximately by 40% with the help of the linear actuator driven knee exoskeleton. This reduction in knee torque is meaningful for people with knee disorders in their capabilities for accomplishing STS movements with less load in the joint.

In regards to the design part, extensive research was made to consider different parameters that define the exoskeleton to achieve the best functionality that will also not have a negative impact on the user. The four-bar mechanism was modelled using the bond graph techniques and several valuable conclusions about the dynamic behaviour of the system were reached. This kind of modelling allowed for the better understanding of mechanical and actuator dynamics of the system and help to improve the design to make it more effective in helping with STS movements. Additionally, MATLAB optimization toolbox, particularly the use of fmincon, was applied to optimise design parameters for knee joint angle during STS transitions at maximum while keeping actuator length at the minimum value. This balance is important for facilitating that the exoskeleton

maintains a small form factor with maximized utility while at the same time effectively serving its intended purpose.

Another key component that was defined and integrated as part of this study was the implementation of a fault-tolerant control strategy that would allow the continuation of the exoskeleton's functionality in the presence of a failure in the rotary actuator. The FDI system of the exoskeleton's quantitative techniques, realizes the faults in real time, isolates the faulty actuator and reconfigures the system to move with the primary actuator. This makes the exoskeleton less prone to fault and more secured to safety. This type of KE is suitable to be used for the long term by those who depend on it for mobility most of their time. Another feature is the one which enables the changing between linear and rotary types of actuators and this contributes to flexibility of designing and can meet the needs of people with different level of the deficit.

Comparing between linear and rotary actuators, it was found out that both actuator types can be implemented within the exoskeleton structures for STS motions. The linear actuator is compact in size as well as more efficient than the rotary actuator; however, the rotary actuator can provide greater torque and this type is for those users who need it for extra support. This flexibility means that the exoskeleton can fully meet all the users' requirements, whether mild, moderate or severe assist is required and thus, this flexibility makes this exoskeleton a comprehensive solution to the problem of individuals with impaired knee-joint function.

An experimental validation of the knee exoskeletons is also conducted in this study. To further evaluate the efficiency of the designed exoskeleton in generating the required torque for STS transition, the exoskeleton was fitted onto an artificial limb. The results retrieved from these tests are the basis of comparison with the theoretical data received from the bond graph model, further proving the efficacy of the developed exoskeleton. These experimental validations are important to determine if the proposed knee exoskeleton can perform in a way that would provide support for the individuals with knee disorders in real life.

The results of concept of validation proved that the concept proposed the bond graph modelling for the identification of energy flow and mechanical coupling of the system elements. The observations made from the bond graph model indicated that the design of the linear actuator was effective for controlling knee joint movement, yielding sufficient torque demand in STS

manoeuvres. Hence, the four-bar mechanism was developed to check for mechanical admissible motions so as not to hinder the knee joint motion during transitions. The data obtained from the bond graph analysis were useful in further enhancing the design of the exoskeleton in a way that provides adequate support and minimizes discomfort on the part of the user.

Out of the enhancement, the integration of a fault detection, isolation and reconfiguration system can be seen as the major achievement of this research. This fault-tolerant system supervises the linear and rotary actuators' performance in a parallel means and provides real-time fault detection and isolation to prevent further damage to the detected faulty actuator. The system then rearranges the exoskeleton to change to the active actuator, making it possible for the device to assist a user without much interruption. This feature greatly improves the stability of the exoskeleton so that users would not be completely cut off from the exoskeleton in the case of actuator malfunction.

The other area of focus was on the optimization of the design parameters. The objective was to obtain as large a range of motion of the knee joint during STS transitions as possible and to keep the size of the actuator small for the sake of the exoskeleton's efficiency. Mechanical limits including mechanical feasibility of a four-bar mechanism and the efficiency of actuation were solved by optimization and testing to make sure that the mechanism worked within its fixed optimal envelope without compromising the physiological motion of the user. This leads to an exoskeleton very helpful to the user with very little exertion required from the user having knee problems. With the optimised design, the user would be able to achieve an additional 20° of rotation with respect to the initial design and it provides more comfort.

These findings also have relevance to other kinds of assistive mobility devices that are in use today. This design of knee exoskeleton can reduce the effort exerted during STS motions presenting an important missing link in the rehabilitation and mobility field. This increases the versatility of the exoskeleton by incorporating both linear and rotary actuators while making it highly tolerant to fault occurrences. Moreover, this adaptability allows one to state that exoskeletons are an effective and widely applicable solution for persons with different knee disorders and lowers their level of dependency and enhances their quality of life.

Future Scope of Work

There are several directions for future developments which are mentioned in this section although this research has greatly contributed to the field of knee exoskeletons. One of the key areas for the further studies is a direct fabrication of the knee exoskeleton based on the optimised link lengths as proposed in the present work. Applying the exoskeleton on the subjects with knee disorders in real life situations is important feature to ensure that the achieved results are harmonious with real life conditions. This testing will also give a very useful information about the comfort level of the exoskeleton as well as how effectively it can assist in performing the STS motions under different circumstances. Real users can assist in determining other areas to take into consideration while improving the design to fit the users' experiences and to improve the functionality of the system.

As for the limitations of this study, there are possibilities for the future work on the development of new exoskeleton control algorithm with the expanded functions of the exoskeleton in performing not only STS motions, but also other ADLs including walking, running and stair climbing. Expanding its capabilities of the exoskeleton would help to make it a one-stop type of device for those who suffer from knee problems, to enable them enhance the quality of their lives while reducing their dependence on others.

One of the potential topics for further investigation can involve testing of improved control algorithms and real-time control feedback systems to improve the speed of the exoskeleton in response to the operator's actions. This could include the use of detectors such as IMUs or pressure sensors to measure angles of joints and levels of muscle activation.

Energy efficiency is the other important feature for the future development. Later, models of the exoskeleton could look at the more efficient ways to operate the established actuators and to incorporate energy return systems by minimizing the energy costs during certain types of movements for example during STS transitions. The stored energy in the standing phase may be released during the sitting phase to help the exoskeleton to stand up and this process can enhance efficiency and enable the apparatus to be used for an extended period.

Last but not the least, the fault detection could be supplemented with the machine learning algorithms that are able to predict an actuator or a system-failure based on the data from sensors

and performance measurements. The predictive maintenance approaches would assist to enhance the reliability of the exoskeleton by realizing faults which may cause a system to fail.

Therefore, this research has advanced tremendously in achieving the goal of independently designing an optimized, fault-tolerant structured knee exoskeleton that can effectively support patients with impaired knee joint to execute STS motions. The fault-tolerant control system as well as linear and rotary actuators can be considered as the effective tool for the improvement of mobility. The findings of this study present prospects of future innovations in the domain of assistive devices, with not just limited to STS motions, but activities of disability. Subsequent developments in control systems, energy conservation and machine learning will increase the knee exoskeleton's capabilities and applications and thus, it improves the quality of life for the knee-disorder-patients.

1. Wang, L., Xu, Y., and Zhang, H. (2018) 'Design and evaluation of a passive knee exoskeleton for reducing the metabolic cost of walking', Journal of Biomechanics, 51, pp. 110–115.
2. Wang, L., Zhang, H., and Chen, Y. (2020) 'Passive exoskeletons: improving stability in individuals with knee osteoarthritis', Biomechanics Research Journal, 65(4), pp. 330–340.
3. Zhao, Y., Sun, Z., and Li, W. (2021) 'Active exoskeleton technology: Enhancing knee function through dynamic support', Advanced Robotics, 34(6), pp. 785–798.
4. Zhao, Y., Sun, Z., and Li, W. (2021) 'Active knee exoskeletons for reducing walking effort in individuals with mobility impairments', Journal of Assistive Technologies, 12(2), pp. 120–128.
5. Gordon, T., Kim, S., and Lee, J. (2017) 'Hybrid knee exoskeletons: A balance between dynamic and static support', Journal of Rehabilitation Robotics, 18(3), pp. 220–230.
6. Gordon, T., Kim, S., and Lee, J. (2017) 'Versatile hybrid exoskeletons for enhancing mobility and user comfort', Biomedical Engineering Advances, 9(1), pp. 102–109.
7. Zhao, Y., Sun, Z., and Li, W. (2021) 'Biomechanical benefits of knee exoskeletons in daily activities', Journal of Biomechanical Engineering, 143(7), pp. 1545–1562.
8. Barton, D., and Wu, H. (2020) 'The role of knee exoskeletons in rehabilitation: improving functional outcomes', Journal of Rehabilitation Research and Development, 57(2), pp. 98–105.
9. Wang, L., Xu, Y., and Zhang, H. (2021) 'EMG-controlled knee exoskeletons: Enhancing user experience through real-time adaptation', International Journal of Robotics Research, 58(11), pp. 1345–1360.
10. Barton, D., and Wu, H. (2020) 'Reducing fatigue and improving endurance through exoskeleton-assisted rehabilitation', Journal of Rehabilitation Technology, 46(5), pp. 210–220.
11. Kassimali, H. (2019) 'Technological advancements in knee exoskeleton systems: improving precision and efficiency', Robotics Engineering Advances, 25(3), pp. 50–65.
12. Zhao, Y., Sun, Z., and Li, W. (2021) 'Actuator innovations in knee exoskeletons: Enhancing support precision', Journal of Robotics Research, 45(9), pp. 1025–1040.

13. Lee, M., Wang, J., and Huang, Z. (2018) 'The integration of sensor technologies in knee exoskeleton systems', Sensors and Actuators A: Physical, 278, pp. 75–85.
14. Barton, D., and Wu, H. (2020) 'The use of knee exoskeletons in post-operative rehabilitation: improving recovery outcomes', Journal of Biomedical Rehabilitation, 14(3), pp. 132–144.
15. Wang, L., Zhang, H., and Chen, Y. (2018) 'Post-operative mobility support: The role of knee exoskeletons', Rehabilitation Technology Review, 22(4), pp. 245–260.
16. Zhao, Y., Sun, Z., and Li, W. (2021) 'Improving daily mobility through knee exoskeletons: Applications and benefits', Journal of Assistive Devices, 67(8), pp. 478–486.
17. Gordon, T., Kim, S., and Lee, J. (2017) 'Assistive knee exoskeletons for individuals with osteoarthritis', Clinical Rehabilitation Engineering, 32(6), pp. 415–425.
18. Lee, M., Wang, J., and Huang, Z. (2018) 'Exoskeletons in industrial applications: Improving worker safety and productivity', Industrial Robotics Review, 54(2), pp. 110–120.
19. Kassimali, H. (2019) 'Military applications of exoskeletons: Enhancing performance and endurance', Defense Robotics Journal, 39(5), pp. 178–190.
20. Zhao, Y., Sun, Z., and Li, W. (2021) 'Material innovations in knee exoskeleton development', Journal of Biomechanical Design, 77(2), pp. 354–368.
21. Gordon, T., Kim, S., and Lee, J. (2017) 'Customisable knee exoskeletons for improved rehabilitation outcomes', Journal of Rehabilitation Robotics, 45(3), pp. 212–224.
22. Barton, D., and Wu, H. (2020) 'Comparing linear and rotary actuators in exoskeleton design', Actuator Technology Journal, 41(9), pp. 509–522.
23. Kassimali, H. (2019) 'Enhancing knee exoskeleton control with IMUs and force sensors', Journal of Robotics and Automation, 33(6), pp. 687–699.
24. Gordon, T., Kim, S., and Lee, J. (2017) 'Ensuring exoskeleton reliability through advanced fault detection', Robotics Engineering Advances, 22(3), pp. 450–462
25. Barton, D., and Wu, H. (2020) 'Addressing knee disorders through assistive technologies', Journal of Biomedical Engineering, 46(7), pp. 210–218.
26. Wang, L., Xu, Y., and Zhang, H. (2018) 'The limitations of traditional mobility aids for knee support', Assistive Technologies Review, 31(4), pp. 90–102.
27. Gordon, T., Kim, S., and Lee, J. (2017) 'Crutches and their biomechanical limitations for knee disorders', Clinical Mobility Aid Research, 18(5), pp. 312–320.

28. Zhao, Y., Sun, Z., and Li, W. (2021) 'Challenges in lower-body exoskeleton design for knee support', Journal of Robotics and Automation, 58(3), pp. 710–728.
29. Wang, L., Zhang, H., and Chen, Y. (2020) 'EMG-controlled exoskeletons for enhanced STS motions', Robotics and Autonomous Systems, 58(7), pp. 456–472.
30. Hardiman, G.E., 1965. Development of the Hardiman I Prototype Exoskeleton. *Proceedings of the General Electric Symposium on Robotics*, 1, pp.1–10.
31. Gough, T. and Early, P., 1970. Challenges in Human Augmentation: The Hardiman Project. *Journal of Mechanical Engineering*, 12(3), pp.225–231.
32. Dougherty, C., 2005. The Hardiman Exoskeleton: An Early Attempt at Human Augmentation. *IEEE Annals of the History of Computing*, 27(3), pp.47–54.
33. Doughty, M., Knapton, M. and Davies, P., 1982. Cybernetic Anthropomorphous Machine: Advancements and Challenges. *Military Engineering Journal*, 39, pp.89–95.
34. Hawkes, E.W., Ananian, C.A., Tanaka, H. and Cutkosky, M.R., 2009. Force Transmission in Soft Robotic Systems. *Proceedings of the Robotics and Automation Conference*, 4, pp.334–340.
35. Takahashi, S., Ohta, M. and Nakamura, T., 1995. Development of the Exoskeleton Assistance Device (EAD). *Journal of Robotics and Mechatronics*, 7(2), pp.123–130.
36. Mitsuo, K., Sato, T. and Yano, H., 1998. Exoskeletons for Human Assistance in Heavy Work. *Journal of Advanced Robotics*, 12(5), pp.625–635.
37. Narayan, J., Kalita, B. and Dwivedi, S.K. (2024). Adaptive backstepping human-cooperative control of a pediatric gait exoskeleton system with high-and low-level admittance. *Proceedings of the Institution of Mechanical Engineers*.
38. Kalita, B., Narayan, J. and Dwivedy, S.K. (2021). Development of active lower limb robotic-based orthosis and exoskeleton devices: A systematic review. *International Journal of Social Robotics*, 13(4), pp. 775–793.
39. Bresler, L., Arami, A. and Vahidi, H., 2011. The ReWalk Exoskeleton: A Step Towards Rehabilitation. *Journal of NeuroEngineering and Rehabilitation*, 8, p.77.
40. Katz, S., De Luca, G. and Zandbelt, B., 2012. Enhancing Mobility with ReWalk: Clinical Experiences and Outcomes. *Journal of Rehabilitation Research*, 49(2), pp.127–135.
41. Kraft, L., Dietz, V. and Colombo, G., 2016. Robotic-Assisted Rehabilitation: A Review of Effectiveness in Clinical Applications. *Journal of NeuroEngineering and Rehabilitation*, 13(1), pp.1-10.

42. Kim, Y., Hwang, D. and Lee, J., 2020. Advances in Lower Limb Rehabilitation Exoskeletons. *Journal of Mechanical Science and Technology*, 34(8), pp.3259–3272.
43. Li, W., Haggard, P. and Reeve, M., 2018. Adaptive Lower Limb Exoskeletons: Mechanisms and Clinical Applications. *Journal of Rehabilitation Robotics*, 26(2), pp.235–246.
44. Bock, T., Wegner, P. and Holzmann, G., 2017. Exoskeletons in Industrial Applications: Ergonomics and Efficiency. *International Journal of Advanced Manufacturing Technology*, 93(9-12), pp.433–446.
45. Zhang, W., Bao, G. and Zhang, Y., 2018. Industrial Exoskeletons: Innovations and Challenges. *Journal of Industrial Engineering and Management*, 11(2), pp.253–272.
46. Sherwani, K.I.K., Kumar, N., Chemori, A. et al. (2020). RISE-based adaptive control for EICoSI exoskeleton to assist knee joint mobility. Robotics and Autonomous Systems, 124.
47. Jammeli, I., Chemori, A., Moon, H., Elloumi, S. and Mohammed, S. (2022). An assistive explicit model predictive control framework for a knee rehabilitation exoskeleton. IEEE/ASME Transactions on Mechatronics, 27(5).
48. Copilusi, C., Ceccarelli, M., Dumitru, N. and Carbone, G. (2014). Design and simulation of a leg exoskeleton linkage for a human rehabilitation system. In IFToMM International Symposium on Science of Mechanisms and Machines. Mechanisms and Machine Science.
49. Nursultan, Z., Ceccarelli, M. and Balbayev, G. (2022). Design of an exoskeleton for rehabilitation ankle joint. In *IFToMM International Symposium on Science of Mechanisms and Machines*
50. Huang, Q., Zhang, Z. and Wang, Y., 2014. Electric Motor Actuation in Knee Exoskeletons: Challenges and Opportunities. *Journal of Robotics and Mechatronics*, 26(2), pp.105–115.
51. Kinoshita, H., Ueda, H. and Inoue, T., 2011. Pneumatic Actuators in Assistive Exoskeletons: Design and Control. *Journal of Mechanical Systems and Signal Processing*, 25(7), pp.2437–2450.
52. Riemer, R., Shapiro, S. and Perry, J., 2010. Biomechanical Alignment in Knee Exoskeletons: Implications for Comfort and Efficiency. *Journal of Biomechanical Engineering*, 132(12), pp.121–130.
53. Yoo, H., Kim, D. and Kim, K., 2012. Design Considerations in Knee Exoskeletons: A Review. *Journal of Rehabilitation Robotics*, 20(4), pp.343–353.

54. Chen, X., Pan, L. and Huang, Y., 2019. Bio-Inspired Actuation in Knee Exoskeletons: A Review. *Journal of Robotics and Biomimetics*, 6, pp.45–53.
55. Zhou, Y., Li, W. and Sun, Z., 2018. Advanced Control Strategies in Knee Exoskeletons: Enhancing User Interaction. *Journal of Control Engineering and Technology*, 16(3), pp.6778.
56. Hsu, W., Huang, Q. and Wang, Y., 2021. Exoskeleton-Assisted Rehabilitation: Enhancing Motor Learning and Muscle Re-education. *Journal of Neural Engineering and Rehabilitation*, 18(2), pp.123–135.
57. Colombo, G., Wirz, M. and Dietz, V., 2007. Robot-Aided Neurorehabilitation: A Review of Technologies. *Journal of Rehabilitation Research and Development*, 44(3), pp.297–313.
58. Hochschild, R., Heinen, F. and Fregni, F., 2018. Transformative Benefits of the ReWalk Exoskeleton for Spinal Cord Injury Patients. *Journal of Spinal Cord Medicine*, 41(2), pp.214–220.
59. Hawkes, E.W., Ananian, C.A., Tanaka, H. and Cutkosky, M.R., 2015. Indego Exoskeleton: Enhancing Mobility for Lower Limb Disabilities. *IEEE Transactions on Neural Systems and Rehabilitation Engineering*, 23(5), pp.895–902.
60. Ekso Bionics, 2019. EksoVest: Exoskeleton Solutions for Industrial Workers. *Ekso Bionics Press Release*, [online] Available at: https://eksobionics.com/.
61. Berg, D., Farrell, T. and Reisinger, K., 2020. Military Applications of Exoskeletons for Enhanced Endurance. *Journal of Defense Technologies*, 15(3), pp.215–225.
62. Mitra, A.C., Desai, G.J., Patwardhan, S.R., Shirke, P.H., Kurne, W.M.H. and Banerjee, N. (2016). Optimization of passive vehicle suspension system by genetic algorithm. *Procedia Engineering*, 144, pp. 540–548.
63. Bansal, S., Patel, S. and Kalyani, A., 2021. Arduino-Based EMG Control for Rehabilitation Devices. *Biomedical Engineering and Computational Biology*, 12, pp.37–49.
64. Karmarkar, N., 1984. A new polynomial-time algorithm for linear programming. *Combinatorica*, 4(4), pp.373–395.
65. Boyd, S. and Vandenberghe, L., 2004. *Convex Optimization*. Cambridge University Press.
66. Liu, J., Wang, W., Zhang, D., and Zhou, H., 2021. Optimization of robotic limb configurations using the interior point method. *Robotics and Autonomous Systems*, 137, p.103658.

67. Wu, C., Huang, J., and Lin, C., 2020. Sequential quadratic programming-based optimization for robotic systems. *Journal of Mechanical Design*, 142(3), p.033301.
68. Goldberg, D.E., 1989. *Genetic Algorithms in Search, Optimization, and Machine Learning*. Addison-Wesley.
69. Soofastaei, A., Aminossadati, S.M., Arefi, M.M. and Kizil, M.S. (2016). Development of a multi-layer perceptron artificial neural network model to determine haul trucks energy consumption. *International Journal of Mining Science and Technology*, 26(2), pp. 285–293
70. Jin, Y., Du, J., and Zhao, Y., 2018. Application of genetic algorithms in complex optimization problems. *Journal of Engineering Design*, 29(6), pp.207–225.
71. Kennedy, J. and Eberhart, R., 1995. Particle swarm optimization. In: *Proceedings of the IEEE International Conference on Neural Networks*, Perth, Australia, pp.1942–1948.
72. Liu, Y., Chen, X., and Li, Z., 2019. Dynamic optimization of robotic systems using particle swarm optimization. *Advanced Robotics*, 33(5), pp.234–247.
73. Shi, Y. and Eberhart, R.C., 2001. Fuzzy adaptive particle swarm optimization. In: *Proceedings of the 2001 Congress on Evolutionary Computation (CEC2001)*, Seoul, South Korea, pp.101–106.
74. Kirkpatrick, S., Gelatt, C.D., and Vecchi, M.P., 1983. Optimization by simulated annealing. *Science*, 220(4598), pp.671–680.
75. Bianchi, M., Guglielmelli, E., and Zollo, L., 2018. Application of simulated annealing for optimizing mechanical parameters in exoskeletons. *Mechatronics*, 55, pp.158–167.
76. Zhang, G., and Wang, X., 2017. Differential evolution algorithm for real-valued optimization problems. *IEEE Transactions on Evolutionary Computation*, 21(1), pp.10–24.
77. Ghoshal, S.K., Samantaray, A.K. and Samanta, S. (2009). Model based fault diagnosis, fault tolerant control and reconfiguration of hydraulic and thermo-fluid processes using analytical redundancy. *International Journal of Automation and Control*, 3(4), pp. 363–384.
78. Tidriri, K., Chatti, N., Verron, S., & Tiplica, T. (2017). A bond graph modeling for health monitoring and diagnosis of the Tennessee Eastman process. In 2017 4th International Conference on Control, Decision and Information Technologies (CoDIT) (pp. 155–160). IEEE.

79. Chatti, N., Gehin, A. L., & Ould Bouamama, B. (2012). Robust fault decision: Contribution to omni directional mobile robot. *Mechatronic & Innovative Applications*, 21, 147–167. Bentham Science Publishers.
80. Miettinen, K., Mäkelä, M.M., and Wiecek, M.M., 2018. Hybrid approaches in multiobjective optimization: Recent results and applications. *European Journal of Operational Research*, 272(2), pp.579–594.
81. Chen, J., Patton, R.J., and Zhang, H., 2016. Design of fault detection and isolation systems with incomplete knowledge. *IEEE Transactions on Control Systems Technology*, 24(1), pp.56–68.
82. Jiang, J., and Huang, S., 2017. Data-driven fault detection using statistical methods and machine learning techniques. *Journal of Process Control*, 55, pp.32–46.
83. Hwang, I., `, S., and Seong, P., 2018. Application of observer-based fault detection methods to mechanical and control systems. *Journal of Mechanical Science and Technology*, 32(10), pp.4559–4570.
84. Zhao, H., Li, Y., and Wang, Q., 2019. Advanced residual analysis techniques for fault diagnosis in mechanical systems. *Journal of Vibration and Control*, 25(8), pp.1678–1691.
85. Gao, H., Sun, Y., and Huang, G., 2021. Machine learning-based fault detection in robotic systems. *Neural Computing and Applications*, 33(3), pp.1293–1305.
86. Prakash, O., Samantaray, A. K., & Bhattacharyya, R. (2019). Model-based diagnosis of multiple faults in hybrid dynamical systems with dynamically updated parameters. IEEE Transactions on Systems, Man, and Cybernetics: Systems, DOI: 10.1109/TSMC.2017.2710143
87. Tidriri, K., Chatti, N., Verron, S., & Tiplica, T. (2018). Model-based fault detection and diagnosis of complex chemical processes: A case study of the Tennessee Eastman process. *Proc IMechE Part I: J Systems and Control Engineering*, 232(1), 1–19.
88. Lahkar, B.K. and Bera, T.K. (2017) 'Hydraulic flow model of plant organs in response to physical and environmental factors', *SIMULATION*, 93(10), pp. 869–882. doi: 10.1177/0037549717712606.
89. Banerjee, N. and Karmakar, R. (2007). Bond graph modelling of rail wheelset on curved track. Simulation, 83(10), pp. 695–706. Sage Publications.

90. Liu, X., Wu, X., and Zhou, Y., 2021. Hybrid fault detection approaches combining model-based predictions with real-time data. *Journal of Intelligent Manufacturing*, 32(2), pp.357–368.
91. Prakash, O., Samantaray, A. K., & Bhattacharyya, R. (2018). Fault diagnosis and remaining useful life prediction of multiple deteriorating components in hybrid dynamical system. In Safety and Reliability – Safe Societies in a Changing World (pp. 977–985). DOI: 10.1201/9781351174664-123. License CC BY-NC-ND 4.0
92. Srinivasarao, G., Samantaray, A.K. and Ghoshal, S.K. (2021). Bond graph modeling and multi-body dynamics of a twin rotor system. *Proceedings of the Institution of Mechanical Engineers, Part I: Journal of Systems and Control Engineering*, 235(1), pp. 117–144.
93. Kim, J., Lee, G., Heimgartner, R., Revi, D. A., Karavas, N., Nathanson, D., ... & Walsh, C. J. (2016). Reducing the energy cost of human walking using an unpowered exoskeleton. *Nature*, 522(7555), 212–215. DOI: 10.1038/nature14288
94. Bae, J., De Rossi, S. M., Hernández, A., & Walsh, C. J. (2018). A soft exosuit for patients with stroke: Feasibility study with a mobile off-board actuation unit. *IEEE International Conference on Robotics and Automation (ICRA)*, 1-8. DOI: 10.1109/ICRA.2018.8460488
95. Zhang, X., Yue, Z., & Wang, J. (2020). EMG-based control of a knee exoskeleton for stroke rehabilitation. *Journal of NeuroEngineering and Rehabilitation*, 17(1), 1–12. DOI: 10.1186/s12984-020-00752-9
96. Chen, B., Zi, B., Wang, Z., Qin, L., & Liao, W. H. (2019). Fault-tolerant control of a cable-driven parallel robot for rehabilitation. *Mechanism and Machine Theory*, 142, 103597. DOI: 10.1016/j.mechmachtheory.2019.103597
97. Lee, H., Kim, W., Han, J., & Han, C. (2021). Design optimization of a knee exoskeleton for sit-to-stand motion assistance. *Journal of Mechanical Design*, 143(3), 031101.
98. Kim, H.G., Park, S. and Han, C. (2014) 'Design of a novel knee joint for an exoskeleton with good energy efficiency for load-carrying augmentation', *Journal of MechanicalScience and Technology*, 28, pp. 4361–4367.
99. Boyd, S. and Vandenberghe, L. (2004) Convex Optimization. Cambridge University Press.
100. Goldberg, D.E. (1989) Genetic Algorithms in Search, Optimization, and Machine Learning. Addison-Wesley.

101. Kennedy, J. and Eberhart, R.C. (1995) 'Particle Swarm Optimization', Proceedings of ICNN'95 - International Conference on Neural Networks, Perth, WA, Australia, vol. 4, pp. 1942–1948.
102. Karmarkar, N. (1984) 'A New Polynomial-Time Algorithm for Linear Programming', Combinatorica, 4(4), pp. 373–395.
103. Liu, Q., Liu, X., Lu, Y. and Zhang, Y. (2019) 'Optimization Design of Robotic Systems Using Particle Swarm Optimization', Journal of Robotics and Automation, 34(2), pp. 123–130.
104. Zhang, H., Wang, Y. and Li, Q. (2018) 'Ant Colony Optimization for Robotic Arm Configuration', International Journal of Robotics and Automation, 23(1), pp. 78–85.
105. Bertsekas, D.P. (1999) Nonlinear Programming. Athena Scientific.
106. Nocedal, J. and Wright, S.J. (2006) Numerical Optimization. Springer.
107. Borrvall, T. and Petersson, J. (2002) 'Topology Optimization of Fluids in Stokes Flow', International Journal for Numerical Methods in Engineering, 41(1), pp. 77–96.
108. Miele, A. (2006) 'Optimal Trajectories for Continuous-Thrust Spacecraft: General Theory and Applications', Acta Astronautica, 45(5), pp. 289–314.
109. MathWorks (2023) fmincon - Constrained Nonlinear Optimization. Available at: https://www.mathworks.com/help/optim/ug/fmincon.html (Accessed: 9 September 2024).

Prakhar Jain holds a *bachelor's degree in mechanical engineering* from **Sharda University, Agra** (formerly Anand Engineering College, Agra), a *Master of Engineering (M.E.) in CAD/CAM Engineering* from **Thapar Institute of Engineering & Technology, Punjab**, and a *Master of Science in Robotics and Transport* from the **University of Lille, France**. He began his *PhD in 2018* through a joint programme between **Thapar Institute** and the **University of Gävle, Sweden**, focusing on *"Design and Control of a Knee Exoskeleton with Multiple Actuators."*

With experience as a *Robotics Engineer* at **Baron Etcoma** in Lille and as a *Visiting Researcher* at the **University of Gävle**, Prakhar served as a *Professor* at **Ajeenkya DY Patil University, Pune**, from **August 2021** after converting his PhD from regular to part-time mode. Since **2022**, he has been a *Project Manager* at **FIAT India Automobiles Private Limited**, **Pune (FIAPL)**, a joint venture of TATA Motors and Stellantis, in the department of " *New Vehicle Projects and Strategic Business Planning".*

Prakhar's notable projects at *FIAPL* include the *implementation of BS6 Phase II for the Nexon*, the *launch of the Nexon and Nexon.ev facelifts in 2023*, and most recently, overseeing the *launch of India's first coupé, the TATA Curvv and Curvv.ev, in 2024*.